UNIVERSITETET I AGDER

# Active Power Filters in Zero Energy Buildings

ASBJØRN RYSSTAD

SUPERVISOR
Professor Dr. Mohan Lal Kolhe

**University of Agder, 2017**
Faculty of Engineering and Science
Department of Engineering Science

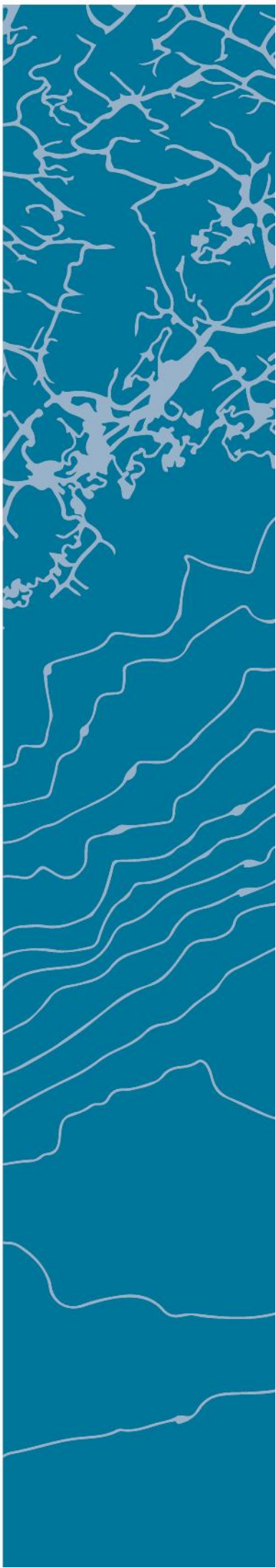

**Abstract**

With an increasing focus on the environment and moving from fossil to renewable energy, there has and is an increasing interest in zero energy buildings. Zero energy buildings often utilize local intermittent renewable energies such as wind and solar energy, and are going to play an important role in the smart grid development with their distributed generation and energy storage etc. In Southern Norway, the smart village Skarpnes is utilizing building integrated photovoltaic systems and is developed for studying zero energy buildings and its impact on electricity demand and power quality.

Power electronic based equipment such as uninterruptible power supplies, adjustable speed drives, personal computers and more have all enhanced our daily lives by providing an efficient and reliable way of utilizing the electrical energy. Because of their non-linear behaviour, they are responsible for harmonic currents causing additional losses and harmful effects.

In this thesis, a shunt active power filter based on the instantaneous power theory used for power quality improvement is studied. This involves harmonic current, reactive power and neutral current compensation, where load data is obtained from the smart village Skarpnes project. Investigating the operation of the shunt active power filter during import and export of power, during load changes and operation during distorted and unbalanced utility voltage.

Based on simulations using MATLAB/Simulink the three-phase, four-wire shunt active power filter is able to compensate the harmonic currents, reactive power and neutral current. The total harmonic distortion in the source current after compensation is below limits proposed by the Institute of Electrical and Electronics Engineers Standard 519-2014 for all test cases.

## Preface

This thesis has been submitted in partial fulfilment of the degree of Master of Science in Renewable Energy at the University of Agder, Grimstad, Norway. The thesis' main objective was to study the use of shunt active power filters in zero energy buildings. The work has been conducted under the supervision of Professor Dr. Mohan Lal Kolhe at the Faculty of Engineering and Science, Department of Engineering Science, University of Agder.

My sincere gratitude goes to Professor Dr. Mohan Lal Kolhe for his expertise, continuous support and availability throughout the process of the master thesis in spite of a busy schedule. My special thanks also goes to Dr. Timothy C. Lommason at Teknova AS for granting me access to recorded measurements from the project *Electricity Usage in Smart Village Skarpnes* supported by the Norwegian Research Council.

Asbjørn Rysstad
University of Agder
Grimstad, Norway
May 2017

# Contents

# List of Figures

# List of Tables

# Acronyms

| | |
|---|---|
| **AC** | Alternating Current |
| **DC** | Direct Current |
| **PCC** | Point of Common Coupling |
| **THD** | Total Harmonic Distortion |
| **TDD** | Total Demand Distortion |
| **RMS** | Root Mean Square |
| **IEEE** | Institute of Electrical and Electronics Engineers |
| **APF** | Active Power Filter |
| **BIPV** | Building Integrated Photovoltaic |
| **KCL** | Kirchhoff's Current Law |
| **UPQC** | Unified Power Quality Conditioner |
| **PWM** | Pulse Width Modulation |
| **VSC** | Voltage Source Converter |
| **CSC** | Current Source Converter |
| **PF** | Power Factor |
| **LPF** | Low-Pass Filter |
| **PLL** | Phase Locked Loop |
| **SRF** | Synchronous Reference Frame |
| **HCC** | Hysteresis Current Controller |
| **HB** | Hysteresis Band |

Chapter 1

# Introduction

## 1.1 Background

Today, a large portion of our electrical energy utilization involves power electronics. Power electronic based equipment such as uninterruptible power supplies, adjustable speed drives, personal computers and more have all enhanced our daily lives by providing an efficient and reliable way of utilizing the electrical energy [1]. The equipment mentioned draw non-sinusoidal currents, commonly referred to as harmonic currents, these currents are usually unwanted and affect the power system in a negative manner. Figure 1.1 shows a non-linear load connected to the point of common coupling (PCC)[1], notice how the harmonic currents have contributed with distorting the voltage waveform at the PCC. A distorted voltage waveform will most likely affect other loads connected at the PCC, both linear and non-linear, in a negative manner.

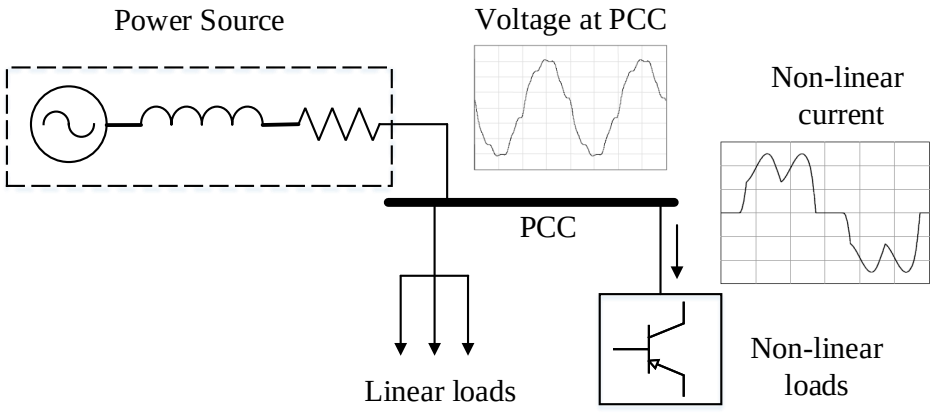


Figure 1.1: Definition of point of common coupling [3].

[1]PCC is defined as the closest point of the customer to the power system where another customer could be supplied from [2].

Harmonic currents do increase the root mean square ($rms$) value of the line current causing additional losses, extra heating and loading, and may also cause failure in power system equipment such as power factor correction capacitors [4]. In spite of of providing an efficient way of utilizing the electrical energy, power electronic devices causes power quality issues and therefore a conflict exists.

Many countries have developed their own standards to limit the effect of harmonics in the power system, but standards such as IEEE Std 519 and EN61000-3-4 by IEC are often referred to. In general, customers are responsible for limiting harmonic currents injected to the power system, while the utility is responsible for voltage distortion at PCC at distribution level [5]. How much harmonic content or distortion is in a voltage or current waveform can be expressed with Total Harmonic Distortion (THD) as

$$THD_I = \frac{\sqrt{\sum_{h=2}^{\infty} I_{h,rms}^2}}{I_{1,rms}} \tag{1.1}$$

$$THD_V = \frac{\sqrt{\sum_{h=2}^{\infty} V_{h,rms}^2}}{V_{1,rms}} \tag{1.2}$$

Sometimes, under light load conditions, $THD_I$ might reveal high distortions. However due to light load conditions i.e. small currents, the harmonic currents will most likely not influence the voltage at the PCC. Therefore, to provide a more suitable definition under light load, IEEE Std 519-2014 defines the term Total Demand Distortion (TDD) as

$$TDD_I = \frac{\sqrt{\sum_{h=2}^{\infty} I_{h,rms}^2}}{I_{L,rms}} \tag{1.3}$$

Where $I_L$ is the rated $rms$ value of the load current at fundamental frequency, operating at rated values $THD_I$ is equal to $TDD_I$. IEEE Std 519-2014 defines TDD and individual harmonic current limits for customers having different utilization capacities, by using the short circuit ratio ($I_{SC}/I_L$), where $I_{SC}$ is the available short circuit current at the PCC and $I_L$ is the rated demand current of the loads connected at the PCC. Table 1.1 shows different limits for different short circuit ratios, a lower short circuit ratio indicates a high source impedance or in other words a weaker distribution system and therefore the harmonic currents will have a greater impact than in a system with higher short circuit ratio. This can be demonstrated using Ohm's law

$$V_h = Z_h \times I_h \tag{1.4}$$

A higher value of $Z_h$ will cause greater voltage distortion for the same amount of harmonic currents injected. Instead of injecting harmonic currents in the system, customers should mitigate their own harmonics by using e.q. various filtering techniques explained later in the thesis.

Table 1.1: IEEE Std 519-2014 Harmonic Current Limits (120 V - 69 kV)

| $I_{sc}/I_L$ | $< 11$ | $11 \leq h < 17$ | $17 \leq h < 23$ | $23 \leq h < 35$ | $35 \leq h \leq 50$ | TDD (%) |
|---|---|---|---|---|---|---|
| $< 20$ | 4.0 | 2.0 | 1.5 | 0.6 | 0.3 | 5.0 |
| $20 < 50$ | 7.0 | 3.5 | 2.5 | 1.0 | 0.5 | 8.0 |
| $50 < 100$ | 10.0 | 4.5 | 4.0 | 1.5 | 0.7 | 12.0 |
| $100 < 1000$ | 12.0 | 5.5 | 5.0 | 2.0 | 1.0 | 15.0 |
| $> 1000$ | 15.0 | 7.0 | 6.0 | 2.5 | 1.4 | 20.0 |

Similarly, IEEE Std 519-2014 also propose voltage distortion limits as shown in Table 1.2.

Table 1.2: IEEE Std 519-2014 Harmonic Voltage Limits

| Bus Voltage at PCC | Individual Voltage Distortion (%) | Total Voltage Distortion (%) |
|---|---|---|
| V $\leq$ 1.0 kV | 5.0 | 8.0 |
| 1kV<69 kV | 3.0 | 5.0 |
| 69-161 kV | 1.5 | 2.5 |
| $>$ 161 kV | 1.0 | 1.5 |

Nowadays, active power filters (APFs) have become a viable and available solution for improving various power quality issues [6]. The basic principle is shown in Figure 1.2, where a shunt APF/compensator behaves as a three-phase controlled current source injecting the inverse of the harmonic currents originated from the non-linear load resulting in sinusoidal supply currents.

### 1.1.1 Electricity Usage in Smart Village Skarpnes

Electricity Usage in Smart Village Skarpnes is a project owned by Agder Energi Nett AS, in collaboration with Teknova AS, Eltek AS and University of Agder with support from the Norwegian Research Council under grant 226139. Where one of the goal is to examine how the distribution network can be designed and operated in an efficient manner when more zero energy buildings are connected to the grid [8].

Skarpnes is a residential area just outside of Arendal, the area consist of several houses of near-zero energy standards[2]. Each house is equipped with an advanced power quality analyzer from Elspec with high time resolution, offering the possibility to study harmonics, waveforms etc. Additionally Scanmatic AS has installed measurement devices that take measurements of each circuit inside each house, but with a lower time resolution. The distribution transformer supplying Skarpnes is also equipped with a power quality analyzer from Elspec with high time resolution.

[2]A zero energy building is a building with zero net energy consumption [9].

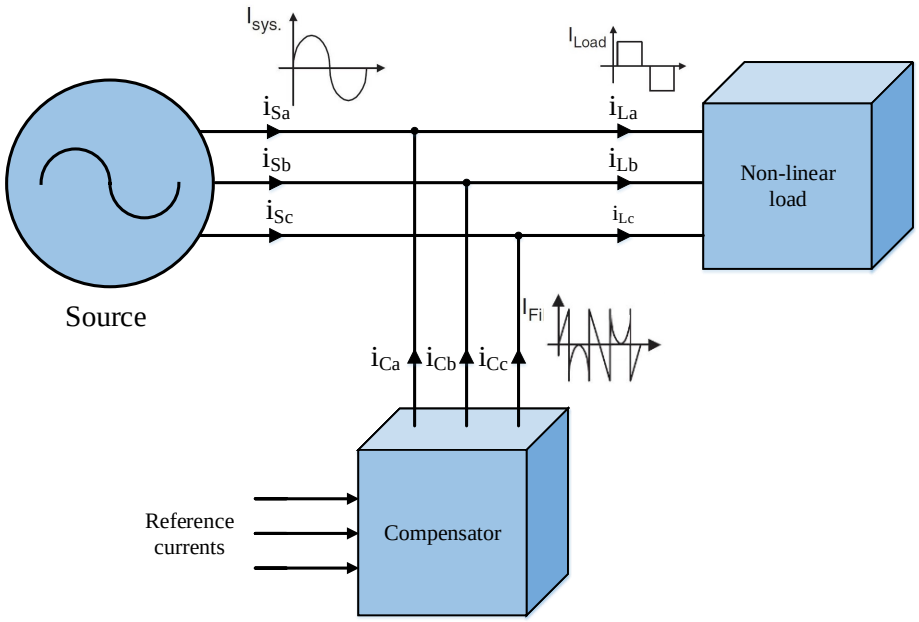


Figure 1.2: Basic principle of shunt current compensation [7].

With these measurements, utility companies like Agder Energi Nett AS would like to understand how zero energy buildings affect the power quality, and how the load profile will change based on the installed on-site generation of electricity, energy storage and ground heated water.

## 1.2 Objectives

The main objective is to investigate the use of a shunt active power filter used for power quality improvement with focus on harmonic currents, reactive power and neutral current compensation in zero energy buildings. The main objective can further be divided into different smaller objectives and are as follows:

- After installing the shunt APF in the zero energy building is the total harmonic distortion within limits proposed by IEEE Std 519?
- How does the shunt APF handle transients and currents shifted 180 electrical degrees with respect to the voltage because of exporting energy production from the building integrated photovoltaic (BIPV) system?
- Study the effect when a shunt APF is connected to a weaker grid i.e. greater system impedance.

## 1.3 Scope of Work

The scope of work is based on the objectives and are:

- Overview of power quality issues focusing on harmonics, understanding the impact of non-linear equipment connected to the grid and harmonic currents, reactive power and neutral current compensation.
- Overview of electrical power definitions under sinusoidal and non-sinusoidal conditions.
- Understanding how the instantaneous power theory can be used as a control algorithm in shunt APFs, both during sinusoidal and non-sinusoidal utility voltage.
- Development of a simulation model of a shunt APF using Skarpnes data as load profile using MATLAB/Simulink.

## 1.4 Limitations

In the simulation model, parameters such as sampling frequency and physical limitations i.e. maximum switching frequency etc. are not being considered.

## 1.5 Thesis Outline

Below is a short description for each chapter in this thesis.

- **Chapter 1** gives a brief introduction to power quality, explaining a few common terms, as well as an introduction to the Skarpnes project, Electricity Usage in Smart Village Skarpnes. At last the objectives, scope of work and limitations for this thesis are mentioned.
- **Chapter 2** gives the reader insight of what power quality is and what problems are associated with it, as well as presenting a few common solutions for power quality improvement.
- **Chapter 3** gives the reader insight in different power theory definitions for single-phase as well as three-phase systems. Power definitions by Budeanu and Fryze are presented, as well as the instantaneous power theory.
- **Chapter 4** gives the reader insight in how a shunt active power filter is implemented using the instantaneous *p-q* theory as the control algorithm for current reference generation.
- **Chapter 5** shows how the simulation model is built in MATLAB/Simulink based on knowledge from Chapter 4.
- **Chapter 6** shows the simulation results and are then discussed after each section.

- **Chapter 7** presents a conclusion based on Chapter 6 and suggestions for future work is presented.
- **Appendix A** gives a quick overview of the data acquisition system at Skarpnes.
- **Appendix B** load parameters used in the MATLAB/Simulink model are displayed.
- **Appendix C** various simulation results not shown in Chapter 6 are displayed.

Chapter 2

# Theoretical Background

This chapter provides general knowledge regarding power quality, mathematical tools used in power quality analysis and various solutions for improving it. Power quality is a term used to describe the quality of the power delivered by the power system. When electrical devices are exposed to poor power quality they may experience loss of performance and their lifetime may become shorter [10], therefore maintaining good power quality in the distribution network is important. Power quality is becoming an important topic as the increase of power electronic devices that are beeing connected to the grid as a result of more intermittent renewable energy sources, zero energy buldings, electric vehicles etc. [11].

## 2.1 Power Quality Issues

There are several type of events that affect the power quality, some are defined in IEEE 1159 [12] as:

**Voltage unbalance**: The voltage is unbalanced or not symmetric when the three waveforms have unequal magnitudes and/or not shifted 120 degrees with respect to each other. It is defined as the ratio of the negative sequence to the positive sequence component. Positive and negative sequences are explained in Section 2.3. Voltage unbalances may be caused by unbalanced loads or generation faults.

**Voltage sag**: When the *rms* value of the voltage waveform drops 10% or more below the nominal voltage for a period from half a cycle to a few seconds. Events lasting longer are referred to as undervoltage. Voltage sags are typically caused by an abrupt increase in load (short circuits, motors etc.).

**Voltage swell**: When the *rms* value of the voltage waveform increases 10% or more above the nominal voltage for a period from half a cycle to a few seconds. Events lasting longer are referred to as overvoltage. Voltage swells are typically caused by an abrupt reduction in load.

**Frequency variations** are deviation from its nominal operating value. The voltage waveforms are supposed to have a specific frequency, in Norway 50 Hz, and any deviation from that value are referred to as frequency variations. At any instant, the frequency depends on the balance between power produced and power demand ($P_{produced} - P_{demand} \neq 0 \rightarrow \Delta f$).

**Waveform distortion**: When a current or voltage waveform deviates from a sinusoidal shape in steady state it is said to be distorted. Non-linear loads may cause distorted waveforms. Fourier analysis provides a mathematical tool for describing distorted waveforms, explained in the next section.

## 2.2 Harmonics

Fourier showed that any periodic function that satisfy $f(t) = f(t+T)$ where $T$ is the time period of the function can be described as a sum of sinusoidal functions, this can mathematically be written as

$$f(t) = F_0 + \sum_{h=1}^{\infty} f_h(t) = F_0 + \sum_{h=1}^{\infty} \{a_h \cos(h\omega t) + b_h \sin(h\omega t)\} \tag{2.1}$$

where

$$F_0 = \frac{1}{2\pi} \int_0^{2\pi} f(t)dt \tag{2.2}$$

$$a_h = \frac{1}{\pi} \int_0^{2\pi} f(t) \cos(h\omega t)dt \qquad \text{for } h = 1, 2, \ldots, \infty \tag{2.3}$$

$$b_h = \frac{1}{\pi} \int_0^{2\pi} f(t) \sin(h\omega t)dt \qquad \text{for } h = 1, 2, \ldots, \infty \tag{2.4}$$

Most waveforms in the power system possesses half-wave symmetry i.e. $f(t+\pi) = -f(t)$, as a result the Fourier series of such waveforms contain only odd integer values of $h$ and no DC component. Even order harmonics may exist but are much rarer and are caused by for example arc furnances, cyclonconverters and half-wave rectifiers [13]. Even harmonics can cause the undesired dc component and unequal positive and negative peak values [14]. Even harmonics are limited to 25% of the odd harmonic limits in Table 1.1.

### 2.2.1 Causes and Effects

Often the cause of harmonics currents are the end-user loads, utility equipment such as transformers are also responsible for harmonic currents with their magnetizing currents, but due to their low magnitude compared full load current, the end-user loads are usually the main source of harmonic pollution. Because of the needed step of a DC/AC converter, BIPVs are a source of harmonic pollution and actions should be taken to reduce it. High harmonic distortion may cause unwanted effects such as transformer, power factor correction capacitor, motor or generator heating and interference with voice communication circuits. [4].

## 2.3 Symmetrical Components

Symmetrical components is a mathematical method of expressing a set of $n$ unbalanced phasors as a set of $n$ balanced sets of phasors, where each balanced phasor set includes positive, negative and zero sequence phasors [15]. The positive sequence has the rotational sequence *abc*, the negative sequence has the rotational sequence *acb* and for the zero sequence all phases are co-phasal, illustrated in Figure 2.1. For a three-phase unbalanced system one would require three sets of positive, negative and zero sequence phasors, one set for each phase. Mathematically this can be represented as

$$V_{abc} = \begin{bmatrix} V_a \\ V_b \\ V_c \end{bmatrix} = \begin{bmatrix} V_{a,0} \\ V_{b,0} \\ V_{c,0} \end{bmatrix} + \begin{bmatrix} V_{a,+} \\ V_{b,+} \\ V_{c,+} \end{bmatrix} + \begin{bmatrix} V_{a,-} \\ V_{b,-} \\ V_{c,-} \end{bmatrix} \tag{2.5}$$

where

$$\begin{bmatrix} V_0 \\ V_+ \\ V_- \end{bmatrix} = \frac{1}{3} \begin{bmatrix} 1 & 1 & 1 \\ 1 & \alpha & \alpha^2 \\ 1 & \alpha^2 & \alpha \end{bmatrix} \begin{bmatrix} V_a \\ V_b \\ V_c \end{bmatrix} \tag{2.6}$$

where $\alpha = e^{\frac{2}{3}\pi i}$, shifting a vector by an angle of 120 degrees counter clockwise. Using symmetrical components one can analyse unbalanced systems the same way as analyzing balanced systems and treat the problem as a superposition of the three symmetrical components [16].

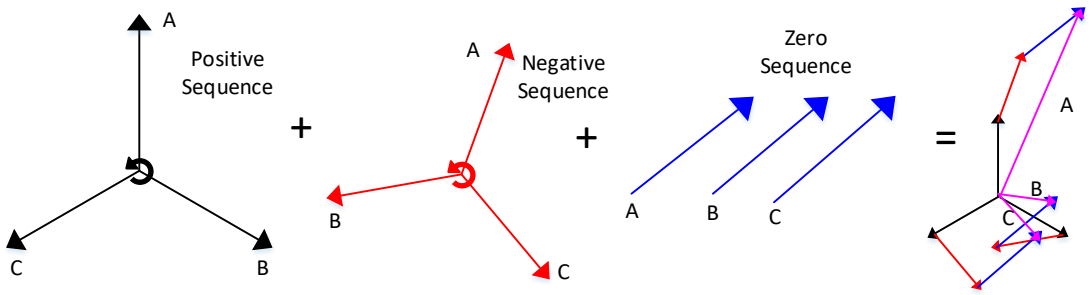


Figure 2.1: Symmetrical components.

## 2.4 Positive, Negative and Zero Sequence Harmonics

The fundamental currents in a balanced three-phase system are shifted 120 degrees with respect to each other and may be written as

$$\begin{aligned} i_a(t) &= i(t) \\ i_b(t) &= i(t - \frac{2\pi}{3}) \\ i_c(t) &= i(t + \frac{2\pi}{3}) \end{aligned} \tag{2.7}$$

For balanced harmonics, where $h$ is the harmonic number, may be written as

$$\begin{aligned} i_{a,h} &= I_h \cos(h \times 2\pi ft + \phi_h) \\ i_{b,h} &= I_h \cos(h \times 2\pi ft - h \times \frac{2\pi}{3} + \phi_h) \\ i_{c,h} &= I_h \cos(h \times 2\pi ft + h \times \frac{2\pi}{3} + \phi_h) \end{aligned} \tag{2.8}$$

Looking at the third harmonic

$$\begin{aligned} i_{a,3} &= I_3 \cos(3 \times 2\pi ft + \phi_3) \\ i_{b,3} &= I_3 \cos(3 \times 2\pi ft - 3 \times \frac{2\pi}{3} + \phi_3) = I_3 cos(3 \times 2\pi ft + \phi_3) \\ i_{c,3} &= I_3 \cos(3 \times 2\pi ft + 3 \times \frac{2\pi}{3} + \phi_3) = I_3 cos(3 \times 2\pi ft + \phi_3) \end{aligned} \tag{2.9}$$

It is clear that $i_{a,3} = i_{b,3} = i_{c,3}$ and are thus often referred to as zero sequence harmonics. Looking at the fifth harmonic

$$\begin{aligned} i_{a,5} &= I_5 \cos(5 \times 2\pi ft + \phi_5) \\ i_{b,5} &= I_5 \cos(5 \times 2\pi ft - 5 \times \frac{2\pi}{3} + \phi_5) = I_5 \cos(5 \times 2\pi ft + \frac{2\pi}{3} + \phi_5) \\ i_{c,5} &= I_5 \cos(5 \times 2\pi ft + 5 \times \frac{2\pi}{3} + \phi_5) = I_5 \cos(5 \times 2\pi ft - \frac{2\pi}{3} + \phi_5) \end{aligned} \tag{2.10}$$

Showing the fifth harmonic has a negative rotational sequence ($acb$). Looking at the seventh harmonic

$$\begin{aligned} i_{a,7} &= I_7 \cos(7 \times 2\pi ft + \phi_7) \\ i_{b,7} &= I_7 \cos(7 \times 2\pi ft - 7 \times \frac{2\pi}{3} + \phi_7) = I_7 \cos(7 \times 2\pi ft - \frac{2\pi}{3} + \phi_7) \\ i_{c,7} &= I_7 \cos(7 \times 2\pi ft + 7 \times \frac{2\pi}{3} + \phi_7) = I_7 \cos(7 \times 2\pi ft + \frac{2\pi}{3} + \phi_7) \end{aligned} \tag{2.11}$$

Showing the seventh harmonic has a positive rotational sequence ($abc$), furthermore it can be proven that the following pattern in Table 2.1 is valid and is repeated further when the harmonic currents are balanced [17]. If unbalanced, each harmonic order may have a positive, negative and zero sequence component.

Table 2.1: Harmonic Sequences.

| Harmonic | 2 | 3 | 4 | 5 | 6 | 7 |
|---|---|---|---|---|---|---|
| Sequence | Negative | Zero | Positive | Negative | Zero | Positive |

### 2.4.1 Triplen Harmonics

Triplen harmonics are defined as the multiples of the third harmonic (3rd, 6th, 9th etc.) [18]. The triplen harmonics are of particular concern because their co-phasal nature (shown in Section 2.4). Using Kirchhoff's current law (KCL) and if ($i_{3a} = i_{3b} = i_{3c}$) the following can be written

$$i_{3n} = i_{3a} + i_{3b} + i_{3c} = 3i_{3a} \tag{2.12}$$

As a result, the neutral conductor may carry large currents at multiples of three times the fundamental frequency, which it would not do in a balanced three-phase system without zero sequence harmonics. Therefore the neutral conductor must be sized with this in mind or actions to reduce the neutral current should be considered.

## 2.5 Clarke and Park Transformation

The Clarke and Park transformation also known as the $\alpha\beta 0$ and $dq0$ transformation respectively, are mathematical transformations used to simplify the analysis of three-phase systems. The transformations transform the three-phase system from an abc reference frame to a stationary $\alpha\beta 0$ or a rotating $dq0$ reference frame, illustrated in Figure 2.2. The power invariant transformation from abc to $\alpha\beta 0$ is given by

$$\begin{bmatrix} u_0 \\ u_\alpha \\ u_\beta \end{bmatrix} = \sqrt{\frac{2}{3}} \begin{bmatrix} \frac{1}{\sqrt{2}} & \frac{1}{\sqrt{2}} & \frac{1}{\sqrt{2}} \\ 1 & -\frac{1}{2} & -\frac{1}{2} \\ 0 & \frac{\sqrt{3}}{2} & -\frac{\sqrt{3}}{2} \end{bmatrix} \begin{bmatrix} u_a \\ u_b \\ u_c \end{bmatrix} \tag{2.13}$$

and the inverse transformation is given by

$$\begin{bmatrix} u_a \\ u_b \\ u_c \end{bmatrix} = \sqrt{\frac{2}{3}} \begin{bmatrix} \frac{1}{\sqrt{2}} & 1 & 0 \\ \frac{1}{\sqrt{2}} & -\frac{1}{2} & \frac{\sqrt{3}}{2} \\ \frac{1}{\sqrt{2}} & -\frac{1}{2} & -\frac{\sqrt{3}}{2} \end{bmatrix} \begin{bmatrix} u_0 \\ u_\alpha \\ u_\beta \end{bmatrix} \tag{2.14}$$

The transformation from $abc$ to $dq0$ is given by

$$\begin{bmatrix} u_d \\ u_q \\ u_0 \end{bmatrix} = \frac{2}{3} \begin{bmatrix} \cos(\omega_s t) & \cos(\omega_s t - 120°) & \cos(\omega_s t + 120°) \\ -\sin(\omega_s t) & -\sin(\omega_s t - 120°) & -\sin(\omega_s t + 120°) \\ 1/2 & 1/2 & 1/2 \end{bmatrix} \begin{bmatrix} u_a \\ u_b \\ u_c \end{bmatrix} \tag{2.15}$$

and the inverse transformation is given by

$$\begin{bmatrix} u_a \\ u_b \\ u_c \end{bmatrix} = \begin{bmatrix} \cos(\omega_s t) & -\sin(\omega_s t) & 1 \\ \cos(\omega_s t - 120°) & -\sin(\omega_s t - 120°) & 1 \\ \cos(\omega_s t + 120°) & -\sin(\omega_s t + 120°) & 1 \end{bmatrix} \begin{bmatrix} u_d \\ u_q \\ u_0 \end{bmatrix} \tag{2.16}$$

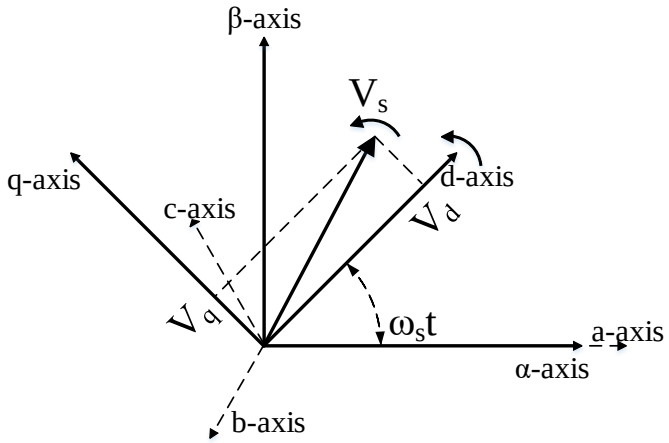


Figure 2.2: Clarke and Park transformation.

Both the Clarke and Park transformation are widely used in various electrical engineering applications such as power conditioning devices, field-oriented control of induction machinery etc.

## 2.6 Harmonic Mitigation Techniques

Harmonic currents should be limited to limit the voltage distortion, as well as reducing losses e.q. eddy current losses which are proportional to the square of the frequency [19].

There are several harmonic mitigation techniques, common filtering techniques are passive and active power filters. Delta/star distribution transformers can be used to *trap* the zero-sequence third harmonic as they will circulate inside the delta windings, this will prevent them for polluting the power system further up. Avoiding long cables (greater impedance) to harmonic polluting loads may also help, but not always possible.

### 2.6.1 Passive Filters

Passive filters can either be connected in series or in shunt with respect to the load. Series filters must be sized for the full load current, while the shunt filters can be sized for the harmonic currents only. Passive filters are tuned for specific harmonic frequencies, and are therefore more commonly connected to individual loads. The basic principle of a shunt filter is shown in Figure 2.3b, it provides a low impedance path for the tuned frequency and at the same time act as a high impedance path for other frequencies. Undesirable resonance events may occur between the installed filter and the system impedance [20], therefore the implementation of passive filters should be done with care.

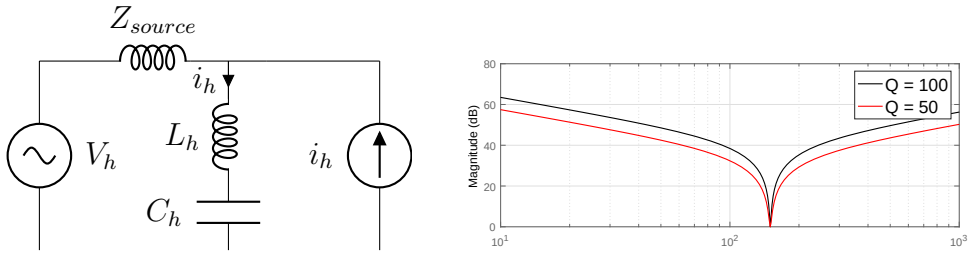


(a) Passive single-tuned shunt filter. (b) Impedance versus frequency.

Figure 2.3: Passive filter.

### 2.6.2 Active Power Filters

Active power filters can be series connected, shunt connected or a combination of both.

**Shunt Active Power Filters**
From Figure 2.4, the source current is equal to the load current before connecting the shunt APF and can be written as

$$i_s = i_L = i_f + i_h \tag{2.17}$$

where $i_s$ and $i_L$ are the source and load current respectively, the load current can be decomposed to a fundamental current $i_f$ and harmonic currents $i_h$. Identifying the harmonic currents from the load, the shunt APF can be controlled in such a way to inject the inverse of the harmonic currents at the PCC, resulting in sinusoidal source currents

$$i_s = i_f + i_h - i_{filter} = i_f \tag{2.18}$$

Essentially the filter act as a controllable current source injecting currents at the PCC.

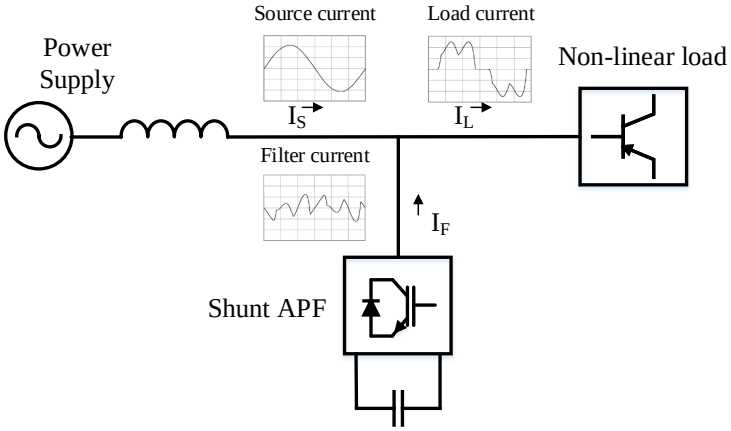


Figure 2.4: Shunt active power filter.

**Series Active Power Filters**
The series APF act as a controlled voltage source illustrated in Figure 2.5. The series APF is mainly used to compensate for utility problems such as voltage disturbances (sags, swells etc.), voltage unbalances and/or voltage distortion [21]. To compensate for harmonic currents a shunt passive filter must be connected as shown in Figure 2.5, providing a low impedance path [22].

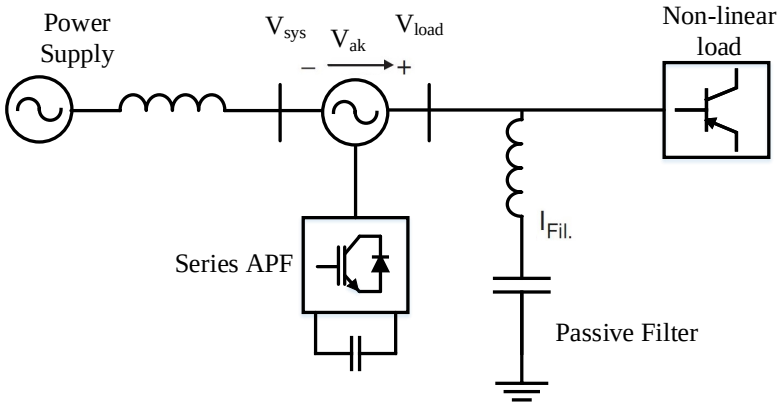


Figure 2.5: Series active power filter.

**Unified Power Quality Conditioner**
Combining the functionalites of both the shunt- and series APF, two systems can be connected back to back sharing the same DC bus [23]. The combination of shunt- and series APFs shown in Figure 2.6 is often referred to as unified power quality conditioner (UPQC).

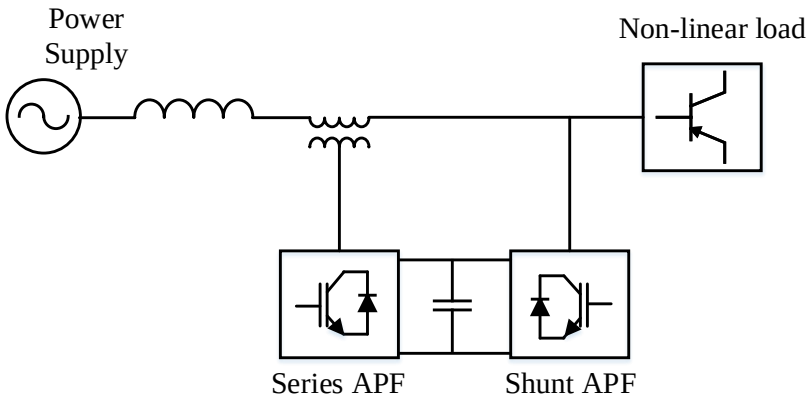


Figure 2.6: Series and shunt active power filter combination.

**Converter Topologies**
For the implementation of a shunt APF, different converter topologies may be used. Figure 2.7 shows two three-phase, three-wire power converters. Figure 2.7a shows a pulse width modulation (PWM) voltage source converter (VSC) with a capacitor as energy storage element. Figure 2.7b shows a PWM current source converter (CSC) with an inductor as energy storage element.

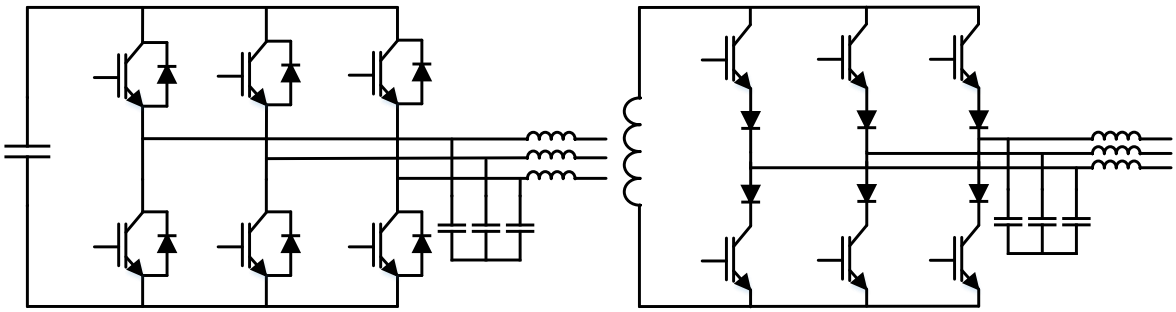


Figure 2.7: Converter topologies: (a) Voltage source converter (b) Current source converter.

An analysis of benefits and drawbacks of VSCs and CSCs for APFs is done in [24, 25], but generally VSCs are preferred due to efficiency, size and reliability [25].

In residential areas, office buildings etc. with single-phase, non-linear loads supplied by a three-phase, four-wire system, power electronic topologies as shown in Figure 2.8 are used to be able to compensate zero-sequence currents. A comparison between different three-phase, four-wire topologies is given in [26].

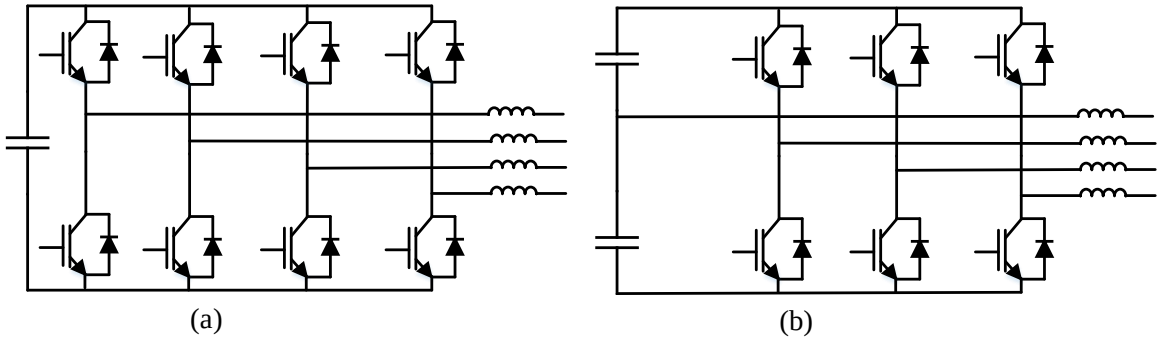


Figure 2.8: Converter topologies: (a) Four leg converter (b) Three leg, split capacitor converter.

### 2.6.3 Line Reactors

Line reactors may help with high frequency harmonic attenuation by being placed in front of for example a variable frequency drive. From Equation 2.19, the line reactors reactance is proportional to the frequency, $f$.

$$X_L = 2\pi f L \tag{2.19}$$

For harmonic attenuation purposes one typically apply no more than 5% impedance to the input of the drive. Adding 5% impedance, the current THD can be reduced to around 30-40% down from 70-100% [27, 28].

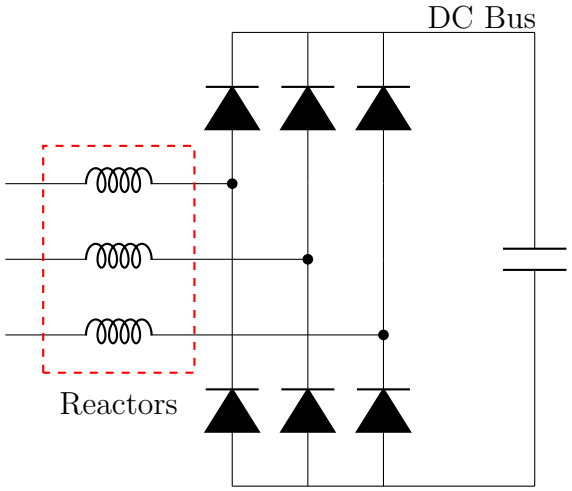


Figure 2.9: Line reactors in front of a three-phase rectifier.

Chapter 3

# Power Theory Definitions

Power definitions under sinusoidal operating conditions are well established and accepted worldwide, but under non-sinusoidal operating conditions several and different power theories are in use [7].

## 3.1 Definitions Under Sinusoidal Balanced Conditions

This section presents power definitions for systems operating under sinusoidal and balanced conditions.

### 3.1.1 Single-Phase Power Theory

The voltage and current in a single-phase system can be written as

$$v(t) = \sqrt{2}V\sin(\omega t) \tag{3.1}$$
$$i(t) = \sqrt{2}I\sin(\omega t - \phi) \tag{3.2}$$

where $V$ and $I$ are the *rms* value of the voltage and current waveforms respectively . The instantaneous power is given by

$$p(t) = v(t)i(t) = 2VI\sin(\omega t)\sin(\omega t - \phi) = VI\cos(\phi) - VI\cos(2\omega t - \phi) \tag{3.3}$$

Equation 3.3 has two components, an average and an oscillating component. Further decomposing and re-arrangement of Equation 3.3 gives

$$p(t) = \underbrace{VI\cos(\phi)[1 - \cos(2\omega t)]}_{\text{Term 1}} - \underbrace{VI\sin(\phi)\sin(2\omega t)}_{\text{Term 2}} \tag{3.4}$$

Based on Equation 3.4 the instantaneous power has two terms and are described as:

- **Term 1** has an average value equal to $VI\cos(\phi)$ and an oscillating component with a frequency twice of the fundamental and represents an unidirectional power flow.

- **Term 2** has only an oscillating component with a frequency twice of the fundamental with a peak value of $VI\sin(\phi)$, and has an average value of zero and represents a bidirectional power flow. Term 2 is absent if the voltage and current waveforms are in phase i.e. $\phi = 0$.

Based on Equation 3.4, three constant powers are conventionally represented as:
Active power, P is defined as the average value of *Term 1*

$$P = VI\cos(\phi) \tag{3.5}$$

Reactive power, Q is defined as the peak value of *Term 2*

$$Q = VI\sin(\phi) \tag{3.6}$$

Apparent Power, S is defined as

$$S = VI \tag{3.7}$$

The apparent power is often referred to as the maxium reachable active power at unity power factor (PF) [29]. The PF is defined as the ratio of the active power to the apparent power

$$\mathrm{PF} = \frac{P}{S} \tag{3.8}$$

and is a term used to describe the utilization of the power system when supplying energy.

### 3.1.2 Three-Phase Power Theory

Looking at a balanced sinusoidal three-phase system, the voltages and currents can be written as

$$\begin{aligned} v_a(t) &= \sqrt{2}V\sin(\omega t) \\ v_b(t) &= \sqrt{2}V\sin(\omega t - \frac{2\pi}{3}) \\ v_c(t) &= \sqrt{2}V\sin(\omega t + \frac{2\pi}{3}) \end{aligned} \tag{3.9}$$

and

$$\begin{aligned} i_a(t) &= \sqrt{2}I\sin(\omega t + \phi) \\ i_b(t) &= \sqrt{2}I\sin(\omega t + \phi - \frac{2\pi}{3}) \\ i_c(t) &= \sqrt{2}I\sin(\omega t + \phi + \frac{2\pi}{3}) \end{aligned} \tag{3.10}$$

With or without a neutral conductor, the three-phase instantaneous power is given by

$$p_3(t) = v_a(t)i_a(t) + v_b(t)i_b(t) + v_c(t)i_c(t) \tag{3.11}$$

Substituting Equations 3.9 and 3.10 in Equation 3.11 gives

$$\begin{aligned} p_a(t) &= VI\cos(\phi)[1-\cos(2\omega t)] - VI\sin(\phi)\sin(2\omega t) \\ p_b(t) &= VI\cos(\phi)[1-\cos(2\omega t - \frac{2\pi}{3})] - VI\sin(\phi)\sin(2\omega t - \frac{2\pi}{3}) \\ p_c(t) &= VI\cos(\phi)[1-\cos(2\omega t + \frac{2\pi}{3})] - VI\sin(\phi)\sin(2\omega t + \frac{2\pi}{3}) \end{aligned} \tag{3.12}$$

Adding the three instantaneous powers gives

$$p_3(t) = p_a(t) + p_b(t) + p_c(t) = 3VI\cos(\phi) = 3P \tag{3.13}$$

From Equation 3.13 the three-phase instantaneous power is constant and have no oscillating component like the instantaneous power in a single-phase system. The three-phase active power, $P_3$ is given as the average value of $p_3(t)$

$$P_3 = 3VI\cos(\phi) \tag{3.14}$$

The three-phase reactive power, $Q_3$ is given by the sum of the peak value of the terms with zero average from Equation 3.12

$$Q_3 = 3VI\sin(\phi) \tag{3.15}$$

The three-phase apparent power, $S$ is given by

$$S_3 = 3VI \tag{3.16}$$

## 3.2 Definitions Under Non-Sinusoidal Conditions

Under non-sinusoidal conditions the power definitions are not unique. An example is the extension of apparent power to polyphase systems, it has at least three different definitions, which yields the same results under balanced sinusoidal conditions but yield different results if one of the conditions above are not met [30]. Two sets of individual power definitions by Budeanu and Fryze gained popularity after their publication.

### 3.2.1 Power Definitions by Budeanu

Budeanu proposed in 1927 [31] a set power definitions that can be used in analysis of the power system under non-sinusoidal conditions in the frequency domain.

Budeanu defined the the active power $P$ and reactive power $Q$ as a superposition of active and reactive powers of all harmonics

$$P = \sum_{h=1}^{\infty} P_h = \sum_{h=1}^{\infty} V_h I_h \cos(\phi_h) \tag{3.17}$$

$$Q = \sum_{h=1}^{\infty} Q_h = \sum_{h=1}^{\infty} V_h I_h \sin(\phi_h) \tag{3.18}$$

where $V$ and $I$ are the $rms$ values of the voltage and current waveforms and are calculated as

$$V = \sqrt{\frac{1}{T}\int_0^T v^2(t)dt} = \sqrt{\sum_{n=1}^{\infty} V_h^2} \tag{3.19}$$

$$I = \sqrt{\frac{1}{T}\int_0^T i^2(t)dt} = \sqrt{\sum_{n=1}^{\infty} I_h^2} \tag{3.20}$$

where $T$ is the fundamental waveform period. Budeanu concluded that in circuits with distorted voltages and/or currents there was another power, Budeanu referred to it as the distortion power, $D$.

$$D^2 = S^2 - P^2 - Q^2 \tag{3.21}$$

The reactive and distortion power proposed by Budeanu lack clear physical meaning and are just mathematical expressions, and their values does not provide the required information which could be used to design compensating circuits [32].

### 3.2.2 Power Definitions by Fryze

Fryze proposed in 1930 [33] a set of power definitions under non-sinusoidal conditions in the time domain. Fryze decomposed the source current into an active and a reactive component.

The active power is given as the average value of the instantaneous power, $p(t)$

$$P_w = \frac{1}{T}\int_0^T p(t)dt = \frac{1}{T}\int_0^T v(t)i(t)dt = V_w I = V I_w \tag{3.22}$$

where $V$ and $I$ are the voltage and current $rms$ values and $V_w$ and $I_w$ are the active voltage and current. Other parameters were defined as:
Apparent power, $P_s$

$$P_s = VI \tag{3.23}$$

Active power factor, $\lambda$

$$\lambda = \frac{P_w}{P_s} \tag{3.24}$$

Reactive power factor, $\lambda_q$

$$\lambda_q = \sqrt{1 - \lambda^2} \tag{3.25}$$

Reactive power, $P_q$

$$P_q = \sqrt{P_s^2 - P_w^2} = V_q I = V I_q \tag{3.26}$$

where $V_q$ and $I_q$ are the reactive voltage and current and are defined as

$$V_q = \lambda q V \tag{3.27}$$

$$I_q = \lambda_q I \tag{3.28}$$

and the active voltage and current as

$$V_w = \lambda V \tag{3.29}$$
$$I_w = \lambda I \tag{3.30}$$

The power definitions proposed by Fryze do not need to decompose the waveforms using Fourier series, but requires the calculation of $rms$ values and hence not valid during transients. The idea of decomposing the current into an active and reactive component offers the opportunity to compensate for undesired currents.

## 3.3 The Instantaneous Power Theory

The instantaneous power theory, commonly referred to as the $p$-$q$ theory, was proposed by Akagi et al. [34] and is based on a set of instantaneous powers defined in the time domain. It can be applied to three-phase systems with or without a neutral wire, with no restrictions to the voltage or current waveforms and is valid during transients and in steady state operating conditions [7]. The instantaneous power theory first transforms the voltage and current waveforms from the $abc$ reference frame to the $\alpha\beta 0$ reference frame, using the Clarke transformation and defines the instantaneous powers there. Unlike traditional theories where one treat the three-phase system as three single-phase systems, the $p$-$q$ theory deals with all three phases at the same time and treat it as one system [7].

The instantaneous zero sequence power $p_0$, real/active power $p$ and imaginary/reactive power $q$ are defined as

$$\begin{bmatrix} p_0 \\ p \\ q \end{bmatrix} = \begin{bmatrix} v_0 & 0 & 0 \\ 0 & v_\alpha & v_\beta \\ 0 & v_\beta & -v_\alpha \end{bmatrix} \begin{bmatrix} i_0 \\ i_\alpha \\ i_\beta \end{bmatrix} \tag{3.31}$$

The three-phase instantaneous active power is equal to the sum of $p$ and $p_0$

$$p_3(t) = v_a i_a + v_b i_b + v_c i_c = v_\alpha i_\alpha + v_\beta i_\beta + v_0 i_0 = p + p_0 \tag{3.32}$$

The three instantaneous powers above can each be decomposed to an average and an oscillating part as done below [35].

1. Instantaneous zero sequence power ($p_0$)

$$p_0 = \bar{p}_0 + \tilde{p}_0 \tag{3.33}$$

$\bar{p}_0$: Average value of the instantaneous zero sequence power. It corresponds to the energy per unit of time that is transferred from the source to the load by the zero sequence voltage and current.
$\tilde{p}_0$: Oscillating part of the instantaneous zero sequence power, meaning the energy per unit of time that is oscillating between the source and load by the zero sequence voltage and/or current.

2. Instantaneous real power ($p$)

$$p = \bar{p} + \tilde{p} \tag{3.34}$$

$\bar{p}$: Average value of the instantaneous real power, corresponding to the energy per unit of time transferred from the source to the load.
$\tilde{p}$: Oscillating part of the instantaneous real power, meaning the energy per unit of time that is oscillating between the source and load and does not result in any energy transfer from the source to the load.

3. Instantaneous imaginary power ($q$)

$$q = \bar{q} + \tilde{q} \tag{3.35}$$

The imaginary power $q$ represents the energy per unit of time that is beeing exchanged between the phases of the system, meaning the imaginary power does not contribute to energy transfer between the source and load at any time [7].
$\bar{q}$: Average value of the instantaneous imaginary power, corresponding to the conventional three-phase reactive power.
$\tilde{q}$: Oscillating part of the instantaneous imaginary power.

Figure 3.1 shows a graphical representation of the three instantaneous power terms.

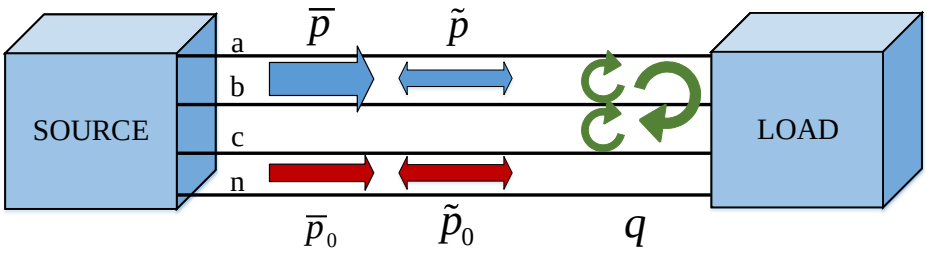


Figure 3.1: Instantaneous powers in a three phase, four wire system [7].

The zero sequence power has the same characteristics as the instantaneous power in a single-phase circuit, it has an average value, $\bar{p}_0$. The average value $\bar{p}_0$ do contribute with energy transfer, but it cannot produce constant power alone, because $p_0$ always consists of $\bar{p}_0$ together with $\tilde{p}_0$ [7].

Below are expressions for the three instantaneous powers $p_0$, $p$ and $q$.

Average powers

$$\bar{p_0} = \sum_{h=1}^{\infty} 3V_{0h}I_{0h}\cos(\phi_{0h} - \delta_{0h}) \tag{3.36}$$

$$\bar{p} = \sum_{h=1}^{\infty} 3V_{+h}I_{+h}\cos(\phi_{+h} - \delta_{+h}) + \sum_{h=1}^{\infty} 3V_{-h}I_{-h}\cos(\phi_{-h} - \delta_{-h}) \tag{3.37}$$

$$\bar{q} = \sum_{h=1}^{\infty} 3V_{+h}I_{+h}\sin(\phi_{+h} - \delta_{+h}) - \sum_{h=1}^{\infty} 3V_{-h}I_{-h}\sin(\phi_{-h} - \delta_{-h}) \tag{3.38}$$

Oscillating powers

$$\begin{aligned}\tilde{p}_0 = &\sum_{\substack{m=1\\m\neq h}}^{\infty}\left[\sum_{h=1}^{\infty} 3V_{0m}I_{0h}\cos((\omega_m-\omega_h)t+\phi_{0m}-\delta_{0m})\right]\\ &+\sum_{m=1}^{\infty}\left[\sum_{h=1}^{\infty} -3V_{0m}I_{0h}\cos((\omega_m+\omega_h)t+\phi_{0m}+\delta_{0m})\right]\end{aligned} \tag{3.39}$$

$$\begin{aligned}\tilde{p} = &\sum_{\substack{m=1\\m\neq h}}^{\infty}\left[\sum_{h=1}^{\infty} 3V_{+m}I_{+h}\cos((\omega_m-\omega_h)t+\phi_{+m}-\delta_{+h})\right]\\ &+\sum_{\substack{m=1\\m\neq h}}^{\infty}\left[\sum_{h=1}^{\infty} 3V_{-m}I_{-h}\cos((\omega_m-\omega_h)t+\phi_{-m}-\delta_{-h})\right]\\ &+\sum_{m=1}^{\infty}\left[\sum_{h=1}^{\infty} -3V_{+m}I_{-h}\cos((\omega_m+\omega_h)t+\phi_{+m}+\delta_{-h})\right]\\ &+\sum_{m=1}^{\infty}\left[\sum_{h=1}^{\infty} -3V_{-m}I_{+h}\cos((\omega_m+\omega_h)t+\phi_{-m}+\delta_{+h})\right]\end{aligned} \tag{3.40}$$

$$\begin{aligned}\tilde{q} = &\sum_{\substack{m=1\\m\neq h}}^{\infty}\left[\sum_{h=1}^{\infty} 3V_{+m}I_{+h}\sin((\omega_m-\omega_h)t+\phi_{+m}-\delta_{+h})\right]\\ &+\sum_{\substack{m=1\\m\neq h}}^{\infty}\left[\sum_{h=1}^{\infty} -3V_{-m}I_{-h}\sin((\omega_m-\omega_h)t+\phi_{-m}-\delta_{-h})\right]\\ &+\sum_{m=1}^{\infty}\left[\sum_{h=1}^{\infty} -3V_{+m}I_{-h}\sin((\omega_m+\omega_h)t+\phi_{+m}+\delta_{-h})\right]\\ &+\sum_{m=1}^{\infty}\left[\sum_{h=1}^{\infty} -3V_{-m}I_{+h}\sin((\omega_m+\omega_h)t+\phi_{-m}+\delta_{+h})\right]\end{aligned} \tag{3.41}$$

From Equations 3.36 to 3.41 it is evident that only the product of voltage and current at the same frequency and rotational sequence yields average power, while the product of voltage and current at different frequencies and rotational sequences yields oscillating powers.

### 3.3.1 Using the p-q Theory for Shunt Compensation

The *p-q* theory is often used in power condition devices [36, 37, 38], Figure 3.2 shows a general overview of the control algorithm when used for shunt compensation. After calculating the instantaneous powers, a selection of powers to be compensated based on the compensation goal is decided. Various powers compensation combinations are:

- Compensation of the load imaginary power $q$, resulting in zero imaginary source power.

- Compensation of the average load imaginary power $\bar{q}$, resulting in oscillating imaginary source power.
- Compensation of the oscillating active power $\tilde{p}$, resulting in the source reactive power to be equal to the load reactive power, while the source only supplies constant active power.
- Compensation of both the oscillating powers $\tilde{p}$ and $\tilde{q}$ resulting in sinusoidal source currents, if the voltages are sinusoidal. The average powers $\bar{p}$ and $\bar{q}$ are still supplied by the source, not compensating for $\bar{q}$ makes the displacement power factor less than unity.
- Compensating the oscillating power $p$, the zero sequence power $p_0$ and both the average and oscillating powers of $q$, all the undesirable currents are in theory being eliminated. Togheter the non-linear load and the compensator act as a linear resistive load [7], assuming balanced and sinusoidal supply voltages.

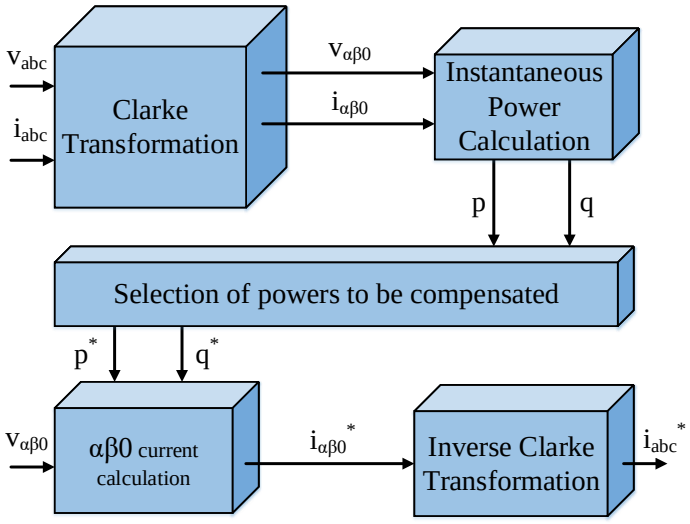


Figure 3.2: Control method based on the instantaneous $p$-$q$ theory.

If the utility voltage is distorted and/or unbalanced, the p-q theory can not satisify the three "optimal" compensation strategies given below, but only one [7], therefore a choice must be made between:

- Draw constant instantaneous power from the source.
- Draw sinusoidal currents from the source.
- Draw the minimum $rms$ value of the source current that transfer the same amount of energy to the load with minimum losses along the transmission line.

The sinusoidal current strategy should be the best alternative to control a shunt APF according to [39].

Chapter 4

# Shunt Active Power Filter

Passive filters have been among the popular solutions for reducing the effect of harmonic pollution, however under varying load conditions they are not optimal as they are tuned for specific frequencies. Shunt APFs have proven to offer a good solution for reducing the harmonic pollution caused by non-linear loads [37, 40], as well as reactive power and neutral current compensation. This chapter will focus on how the instantaneous *p-q* theory can be used as a control algorithm for shunt APFs. An overview including the control algorithm is shown in Figure 4.1.

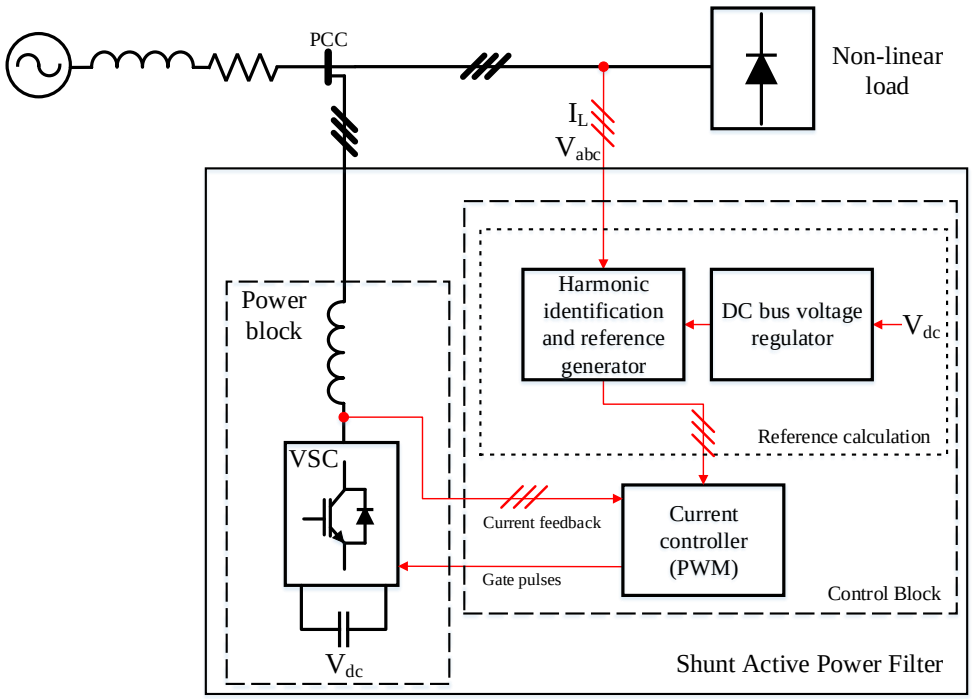


Figure 4.1: Control block schematic of shunt active power filter [3].

## 4.1 Instantaneous Power Theory

The instantaneous p-q theory is a popular theory used as the control algorithm for shunt APFs, undesirable powers can conveniently be selected and compensated. The transformation from $v_{abc}$ to $v_{\alpha\beta 0}$ is given by the Clarke transformation

$$\begin{bmatrix} v_0 \\ v_\alpha \\ v_\beta \end{bmatrix} = \sqrt{\frac{2}{3}} \begin{bmatrix} \frac{1}{\sqrt{2}} & \frac{1}{\sqrt{2}} & \frac{1}{\sqrt{2}} \\ 1 & -\frac{1}{2} & -\frac{1}{2} \\ 0 & \frac{\sqrt{3}}{2} & -\frac{\sqrt{3}}{2} \end{bmatrix} \begin{bmatrix} v_a \\ v_b \\ v_c \end{bmatrix} \tag{4.1}$$

and the inverse transformation is given by

$$\begin{bmatrix} v_a \\ v_b \\ v_c \end{bmatrix} = \sqrt{\frac{2}{3}} \begin{bmatrix} \frac{1}{\sqrt{2}} & 1 & 0 \\ \frac{1}{\sqrt{2}} & -\frac{1}{2} & \frac{\sqrt{3}}{2} \\ \frac{1}{\sqrt{2}} & -\frac{1}{2} & -\frac{\sqrt{3}}{2} \end{bmatrix} \begin{bmatrix} v_0 \\ v_\alpha \\ v_\beta \end{bmatrix} \tag{4.2}$$

Similarly, for the three-phase line currents the Clarke transformation is given by

$$\begin{bmatrix} i_0 \\ i_\alpha \\ i_\beta \end{bmatrix} = \sqrt{\frac{2}{3}} \begin{bmatrix} \frac{1}{\sqrt{2}} & \frac{1}{\sqrt{2}} & \frac{1}{\sqrt{2}} \\ 1 & -\frac{1}{2} & -\frac{1}{2} \\ 0 & \frac{\sqrt{3}}{2} & -\frac{\sqrt{3}}{2} \end{bmatrix} \begin{bmatrix} i_a \\ i_b \\ i_c \end{bmatrix} \tag{4.3}$$

and the inverse transformation is given by

$$\begin{bmatrix} i_a \\ i_b \\ i_c \end{bmatrix} = \sqrt{\frac{2}{3}} \begin{bmatrix} \frac{1}{\sqrt{2}} & 1 & 0 \\ \frac{1}{\sqrt{2}} & -\frac{1}{2} & \frac{\sqrt{3}}{2} \\ \frac{1}{\sqrt{2}} & -\frac{1}{2} & -\frac{\sqrt{3}}{2} \end{bmatrix} \begin{bmatrix} i_0 \\ i_\alpha \\ i_\beta \end{bmatrix} \tag{4.4}$$

Recalling from Chapter 3, Section 3.3 that the instantaneous zero sequence power $p_0$, the instantaneous real/active power $p$ and the instantaneous imaginary/reactive power $q$ are defined from the instantaneous phase voltages and line currents in the $\alpha\beta 0$ coordinate frame as

$$\begin{bmatrix} p_0 \\ p \\ q \end{bmatrix} = \begin{bmatrix} v_0 & 0 & 0 \\ 0 & v_\alpha & v_\beta \\ 0 & v_\beta & -v_\alpha \end{bmatrix} \begin{bmatrix} i_0 \\ i_\alpha \\ i_\beta \end{bmatrix} \tag{4.5}$$

The powers $p_0$, $p$ and $q$ could further be decomposed and expressed as

$$p_0 = \bar{p}_0 + \tilde{p}_0 \tag{4.6}$$
$$p = \bar{p} + \tilde{p} \tag{4.7}$$
$$q = \bar{q} + \tilde{q} \tag{4.8}$$

Shown in Section 3 the product of harmonic current and voltage only result in average power if voltage at the same harmonic frequency and rotational sequence is present, otherwise the result is oscillating power. Assuming that the compensation goal is to compensate undesired currents and obtain sinusoidal source currents, the reference compensation

powers become

$$p_0^* = -\bar{p}_0 - \tilde{p}_0 \tag{4.9}$$
$$p^* = -\tilde{p} + p_{loss} \tag{4.10}$$
$$q^* = -\bar{q} - \tilde{q} \tag{4.11}$$

Notice the reference power, $p^* = -\tilde{p} + p_{loss}$ has the term $p_{loss}$ included. Because of the regulation of the DC bus voltage and losses in the VSC, the VSC requires some power from the grid [41]. A DC voltage controller is used for calculating $p_{loss}$. If losses are more than what is supplied to the VSC the DC link voltage would fall, and rise if the losses are less than what is supplied. For proper operation the DC voltage should be maintained at a fixed reference value by a controller, the controller does not need to have a fast response [42]. Using a PI controller as in Figure 4.2, the term $p_{loss}$ is given by

$$p_{loss} = K_p(V_{ref} - V_{dc}) + K_i \int (V_{ref} - V_{dc})dt \tag{4.12}$$

The reference currents are calculated from Equation 4.5 solving for $i_{\alpha\beta 0}$ and gives

$$\begin{bmatrix} i_0^* \\ i_\alpha^* \\ i_\beta^* \end{bmatrix} = \frac{1}{v_0(v_\alpha^2 + v_\beta^2)} \begin{bmatrix} (v_\alpha^2 + v_\beta^2) & 0 & 0 \\ 0 & v_0 v_\alpha & v_0 v_\beta \\ 0 & v_0 v_\beta & -v_0 v_\alpha \end{bmatrix} \begin{bmatrix} p_0^* \\ p^* \\ q^* \end{bmatrix} \tag{4.13}$$

Reference currents $i^*_{\alpha\beta 0}$ are then transformed into $i^*_{abc}$ using the inverse Clarke transformation from Equation 4.4. Figure 4.2 gives an overview of the instantaneous power theory control algorithm. Several methods for separating the average power $\bar{p}$ from the power $p$ exists, where low-pass filters (LPFs) is a common method.

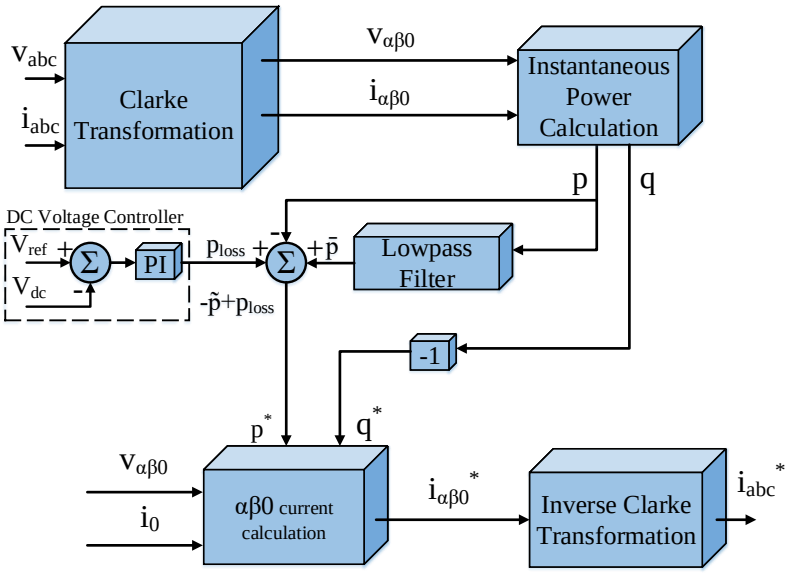


Figure 4.2: Instantaneous power theory overview [7].

During sinusoidal utility voltage conditions, the oscillating powers can be assumed to be caused solely by the harmonic currents from the non-linear load [7]. However, if the shunt APF were to operate under non-sinusoidal utility voltage, the reference currents would not fully compensate the harmonic currents from the non-linear load, because harmonic currents may contribute together with harmonic voltages to produce average active or reactive power. Therefore a positive sequence detector is used to extract the fundamental positive sequence voltage from the voltage waveform and used as input in Figure 4.2, when the compensation goal is sinusoidal source currents.

## 4.2 Positive Sequence Detector

The phase voltages are composed primarily of the fundamental positive sequence component ($V_{1+}$), but may be unbalanced containing negative and zero sequence fundamental components as well as harmonics. A positive sequence detector is necessary in the sinusoidal current control strategy. The positive sequence detector provides the possibility for the shunt APF to compensate for load currents that are not responsible for average active power together with the fundamental positive sequence voltage.

The fundamental positive sequence detector shown in Figure 4.3 is based on the *p-q* theory and determines the fundamental positive sequence from the three-phase utility voltage. The main component is the phase locked loop (PLL) that tracks the fundamental frequency of the voltage waveforms and is explained in Section 4.2.1.

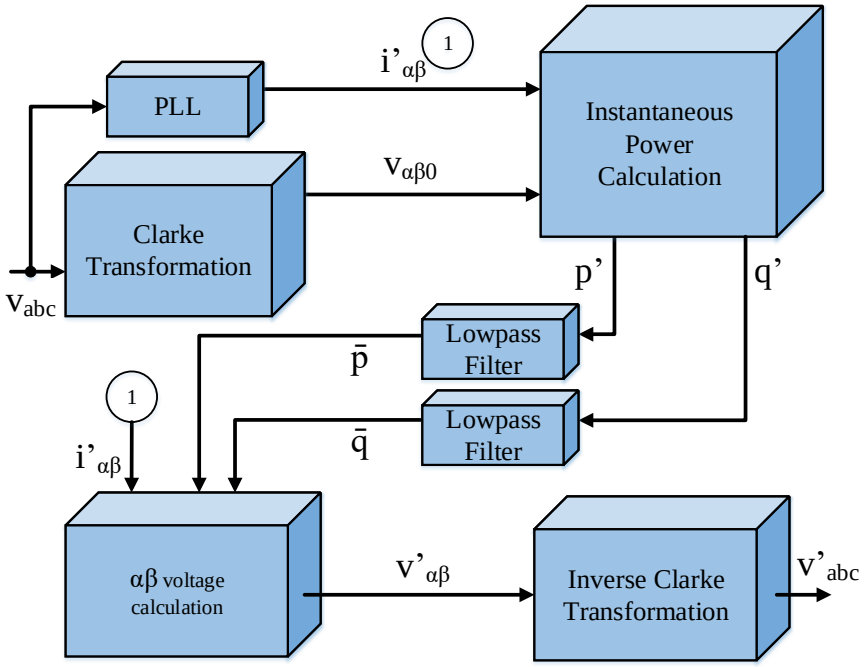


Figure 4.3: Fundamental positive sequence detector scheme [7].

In terms of symmetrical components the currents are given as

$$i_\alpha = \sum_{h=1}^{\infty} \sqrt{3} I_{+h} \sin(\omega_h t + \delta_{+h}) + \sum_{h=1}^{\infty} \sqrt{3} I_{-h} \sin(\omega_h t + \delta_{-h}) \tag{4.14}$$

$$i_\beta = -\sum_{h=1}^{\infty} \sqrt{3} I_{+h} \cos(\omega_h t + \delta_{+h}) + \sum_{h=1}^{\infty} \sqrt{3} I_{-h} \cos(\omega_h t + \delta_{-h}) \tag{4.15}$$

$$i_0 = \sum_{h=1}^{\infty} \sqrt{6} I_{0h} \sin(\omega_h t + \delta_{0h}) \tag{4.16}$$

thus the fundamental positive sequence currents are given as

$$i_\alpha = \sqrt{3} I_{+1} \sin(\omega_1 t + \delta_{+1}) \tag{4.17}$$

$$i_\beta = -\sqrt{3} I_{+1} \cos(\omega_1 t + \delta_{+1}) \tag{4.18}$$

To obtain the fundamental positive sequence voltages using the scheme in Figure 4.3, the amplitude of the auxiliary currents $i'_\alpha$ and $i'_\beta$ nor the phase angle is important and can be chosen arbitarily [7]. Only accurate tracking of $\omega_1 t$ is important, therefore the auxiliary currents reduce to

$$i'_\alpha = \sin(\omega_1 t) \tag{4.19}$$

$$i'_\beta = -\cos(\omega_1 t) \tag{4.20}$$

Recalling from Chapter 3, the average powers are given by

$$\bar{p} = \sum_{h=1}^{\infty} 3 V_{+h} I_{+h} \cos(\phi_{+h} - \delta_{+h}) + \sum_{h=1}^{\infty} 3 V_{-h} I_{-h} \cos(\phi_{-h} - \delta_{-h}) \tag{4.21}$$

$$\bar{q} = \sum_{h=1}^{\infty} 3 V_{+h} I_{+h} \sin(\phi_{+h} - \delta_{+h}) - \sum_{h=1}^{\infty} 3 V_{-h} I_{-h} \sin(\phi_{-h} - \delta_{-h}) \tag{4.22}$$

It can easily be seen from Equations 4.21 and 4.22 that only the fundamental positive sequence voltage $V_+$ contributes to the average values of the fictitious powers $p'$ and $q'$ (calculated in the positive sequence detector, see Figure 4.3), this can be guaranteed because the currents $i'_\alpha$ and $i'_\beta$ are derived from the positive sequence current $I_+$ only. Thus any presence of negative sequence or harmonic voltages and/or currents will result in oscillating powers, which are not included in the inverse Clarke transformation.

The $\alpha\beta$ voltages are calculated from $i'_\alpha$, $i'_\beta$, $\bar{p}'$ and $\bar{q}'$ as

$$\begin{bmatrix} v'_\alpha \\ v'_\beta \end{bmatrix} = \frac{1}{i'^2_\alpha + i'^2_\beta} \begin{bmatrix} i'_\alpha & -i'_\beta \\ i'_\beta & i'_\alpha \end{bmatrix} \begin{bmatrix} \bar{p}' \\ \bar{q}' \end{bmatrix} \tag{4.23}$$

The inverse Clarke transformation is then used on $v'_{\alpha\beta}$ to obtain $v'_{abc}$, which resemble the fundamental positive sequence voltages.

### 4.2.1 Phase Locked Loop

A PLL circuit is commonly used to obtain frequency and/or phase information of the measured waveform. Among many PLL algorithms, the synchronous reference frame (SRF) PLL is among the popular [43]. The three-phase voltage waveforms are transformed into the $\alpha\beta$ frame using the Clarke transformation and then to the SRF ($dq$ frame) using the Park transformation. A block diagram showing the conventional SRF-PLL is shown in Figure 4.4.

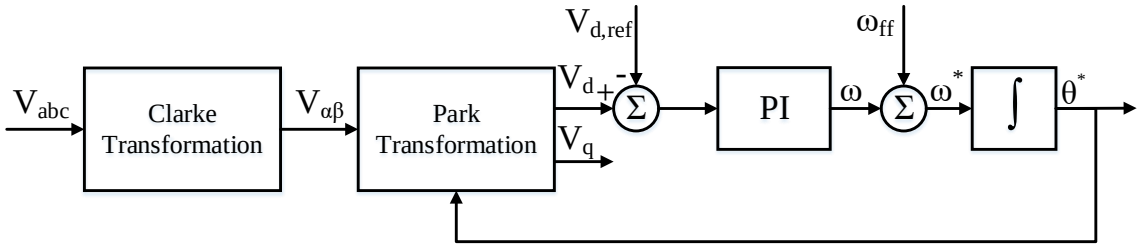


Figure 4.4: Block diagram of the PLL.

The angle $\theta^*$ used in the Park transformation is obtained by integrating the frequency $\omega^*$, generated using a PI controller. If the utility frequency is equal to the frequency $\omega^*$, $V_d$ and $V_q$ appear as DC values depending on $\theta^*$. The initial dynamic response can be improved using a feed forward signal, $\omega_{ff} = 2\pi 50$, seen in Figure 4.4. Similarly, if the frequency change is known a feed forward signal may be used to reduce the tracking error between $\theta^*$ and the actual angle $\theta$ during frequency changes.

Setting the reference value $V_{d,ref}$ equal to zero, will make the PI controller drive the feedback voltage $V_d$ to the reference value $V_{d,ref}$. In other words the PI controller results in a rotating reference frame to which the voltage $V_d$ has the desired reference value $V_{d,ref}$. This gives the ability to lock onto the rotating utility voltage space vector, $V_s$.

The presence of harmonics in the utility voltage will enter the PLL as oscillating signals. The obvious method to eliminate the problem is to use filters, but this reduces the dynamic response. The presence of the integrator in the forward path provides strong filtering properties and the use of filters may be avoided [44].

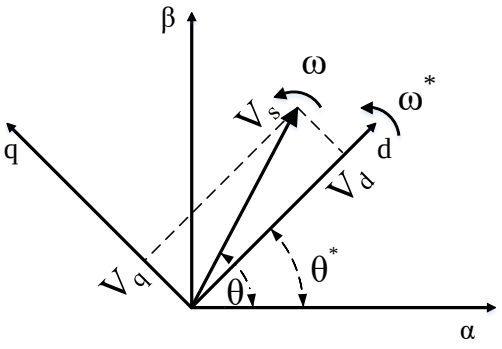


Figure 4.5: Syncronous reference frame and voltage vector.

## 4.3 Hysteresis Current Controller

Among various PWM current control strategies for shunt APFs, the hysteresis current controller (HCC) is a simple, robust and high bandwidth method used for generating the switching patterns for the VSC, the main drawback is its varying switching frequency [45, 46]. The HCC maintain the compensation current within a desired hysteresis band (HB). The HB directly affect the switching frequency, a lower value of $HB$ gives less ripple but higher average switching frequency and vice versa. The switching logic in Figure 4.6 for leg $A$ is given by

If $i_{ca} < (i_{ca,ref} - HB)$ - the upper switch is *off* and the lower switch is *on*.
If $i_{ca} > (i_{ca,ref} + HB)$ - the upper switch is *on* and the lower switch is *off*.

Where $i_{ca}$ and $i_{ca,ref}$ are the line current and reference line current respectively for leg $A$. The current and voltage waveforms for phase $a$ is shown in Figure 4.7, similar waveforms and switching logic also applies to phase $b$ and phase $c$ but shifted in time.

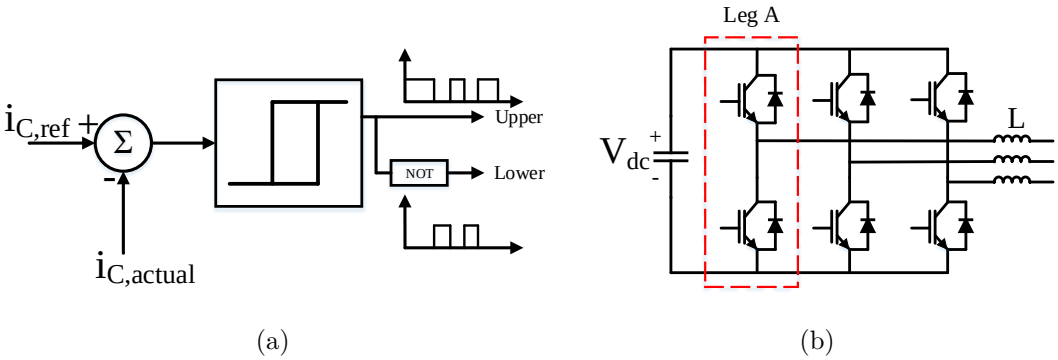


Figure 4.6: (a) Hysteresis current controller. (b) Voltage source converter.

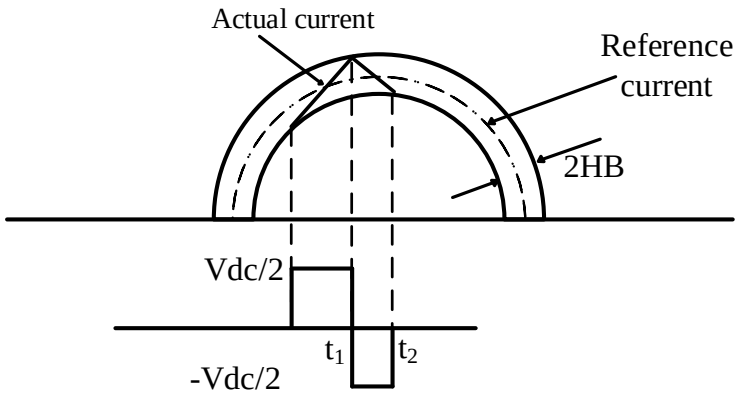


Figure 4.7: Principle of the hysteresis current controller.

Chapter 5

# Simulation Model

Nowadays, simulation has become an important and powerful tool during development and to study the behaviour of various systems. MATLAB/Simulink is used as the simulation platform for studying the shunt active power filter as it offers an environment where complex control algorithms and electrical networks can easily be integrated. An overview of the simulation model is shown in Figure 5.1, the subsystems will be explained in the following sections.

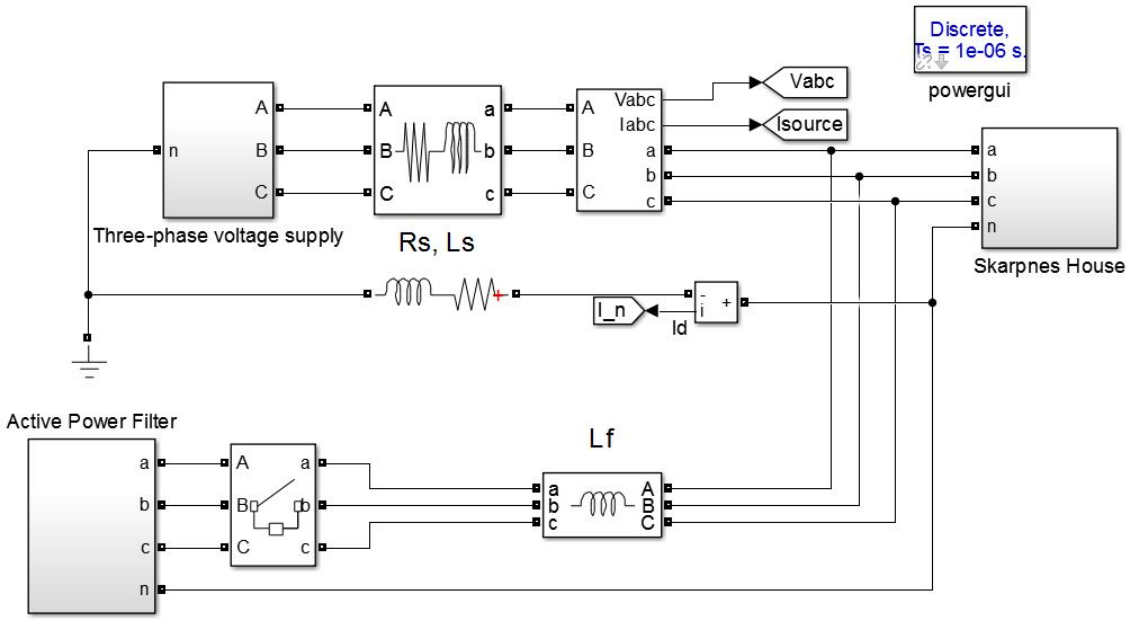


Figure 5.1: Overview of the simulation model.

## 5.1 Supply Modeling

The three-phase voltage source is implemented in MATLAB/Simulink as shown in Figure 5.2, the supply voltage is given by the following expression

$$\begin{bmatrix} v_a \\ v_b \\ v_c \end{bmatrix} = \sqrt{2} \times 230 \begin{bmatrix} \sin(\omega t) \\ \sin(\omega t - 2\pi/3) \\ \sin(\omega t + 2\pi/3) \end{bmatrix} \tag{5.1}$$

At a given time, a voltage disturbance can be added (Figure 5.2b) to the source. The supply voltage is then given by the following expression

$$\begin{bmatrix} v_a \\ v_b \\ v_c \end{bmatrix} = \sqrt{2} \times 230 \begin{bmatrix} \sin(\omega t) \\ \sin(\omega t - 2\pi/3) \\ \sin(\omega t + 2\pi/3) \end{bmatrix} + \begin{bmatrix} V_{-a} \sin(\omega t + \phi_{-a}) \\ V_{-b} \sin(\omega t + \phi_{-b}) \\ V_{-c} \sin(\omega t + \phi_{-c}) \end{bmatrix} + \begin{bmatrix} V_a \sin(h\omega t + \phi_{h,a}) \\ V_b \sin(h\omega t + \phi_{h,b}) \\ V_c \sin(h\omega t + \phi_{h,c}) \end{bmatrix} \tag{5.2}$$

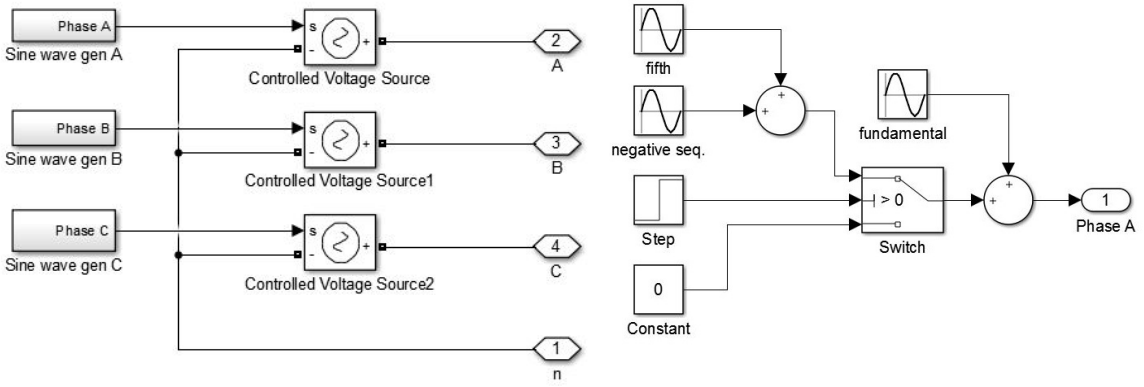


(a) Three-phase voltage source. (b) Sine wave gen A block.

Figure 5.2

Similar sine wave generator blocks in Figure 5.2b are also implemented for phase $B$ and $C$.

## 5.2 Load Modeling

The load data are real measurements obtained from the Skarpnes village through Elspec Investigator. Elspec Investigator had no option to show the phase shift for each harmonic with respect to the fundamental waveform, hence the harmonics are assumed to be in phase with its respected fundamental waveform. The load is implemented in MATLAB/Simulink as parallel current sources with numerical values as in Table 5.1 and 5.2.

Table 5.1: Load data used in the simulation model, harmonics are displayed in percentage of fundamental. From house C6 at 01.10.2015 - 07:30.

| Phase | 50 Hz | $h_3$ | $h_5$ | $h_7$ | $h_9$ | $h_{11}$ | $h_{13}$ | $h_{15}$ |
|---|---|---|---|---|---|---|---|---|
| A | 3.5949 | 8.885% | 11.724% | 9.794% | 6.443% | 3.842% | 0.960% | 0.000% |
| B | 2.5977 | 16.170% | 11.356% | 9.445% | 8.085% | 5.639% | 4.699% | 0.000% |
| C | 4.2711 | 13.837% | 6.183% | 8.547% | 6.443% | 4.464% | 2.858% | 2.556% |

To simulate the scenario when the residence is exporting power, the load data in Table 5.2 is used.

Table 5.2: Load data used in the simulation model, harmonics are displayed in percentage of fundamental. From house C6 at 01.07.2015 - 13:30.

| Phase | 50 Hz | $h_3$ | $h_5$ | $h_7$ | $h_9$ | $h_{11}$ | $h_{13}$ | $h_{15}$ |
|---|---|---|---|---|---|---|---|---|
| A | -7.9093 | 2.489% | 4.141% | 2.226% | 1.543% | 0.309% | 0.873% | 0.309% |
| B | -7.6760 | 6.490% | 7.522% | 5.123% | 3.773% | 1.742% | 1.025% | 0.000% |
| C | -7.1477 | 4.771% | 4.855% | 3.181% | 1.908% | 0.711% | 0.300% | 0.000% |

## 5.3 Shunt Active Power Filter

The inside of the *Active Power Filter* block in Figure 5.1 is shown in Figure 5.3 and includes two subsystems, *reference current calculation* and *PWM hysteresis*. The DC side capacitors was chosen to have the value $C_{apf} = 2\ \mu$F, based on similar active power filters in articles [39, 47, 48] and slightly modified by trial and error to give adequate performance (e.q. energy storage capability and voltage ripple) for this particular system. Each capacitor initial voltage is set to 400V to avoid large start up currents.

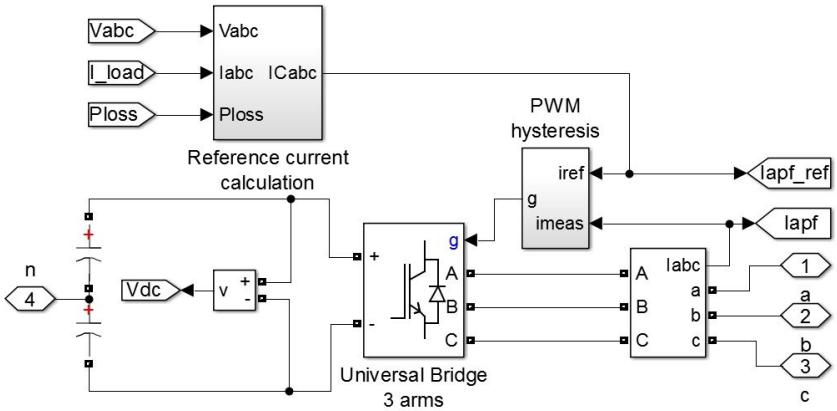


Figure 5.3: Active power filter block.

The inductor, $L_f$ connected between the shunt APF and the PCC (see Figure 5.1) was selected to be 10 mH based on analysis done in [39, 47, 49] and modified slightly to give adequate performance for this particular system. The value of $L_f$ affect the dynamic response of the shunt APF and should be kept small to maintain a fast response. However, a lower value of $L_f$ will also increase the switching frequency in the hysteresis current controller resulting in increased switching losses.

### 5.3.1 DC Voltage Controller

The DC voltage controller is implemented as shown in Figure 5.4, the reference value $Vdc^*$ is set to 800V. For proper operation, the voltage reference should be greater than atleast twice the value of the utility voltage [50]. The PI controller parameters are found by a trial and error approach and are $K_p = 50$ and $K_i = 250$. The feedback signal has oscillations and therefore the PI controller output has oscillations, a low-pass filter is installed before the PI controller with a cut-off frequency of 25 Hz to reduce the oscillations in the input signal to the controller.

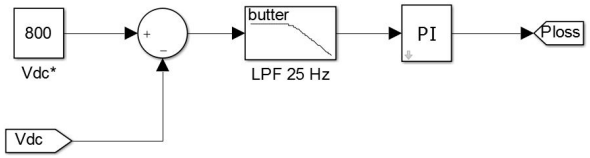


Figure 5.4: DC voltage controller.

### 5.3.2 Hysteresis Controller

A hysteresis controller with hysteresis band, $HB = 0.2$ was used, implemented as in Figure 5.5. The relay blocks to the right compares the input to the specified thresholds, the on/off state of the relay is not affected if the input is between the upper and lower limits.

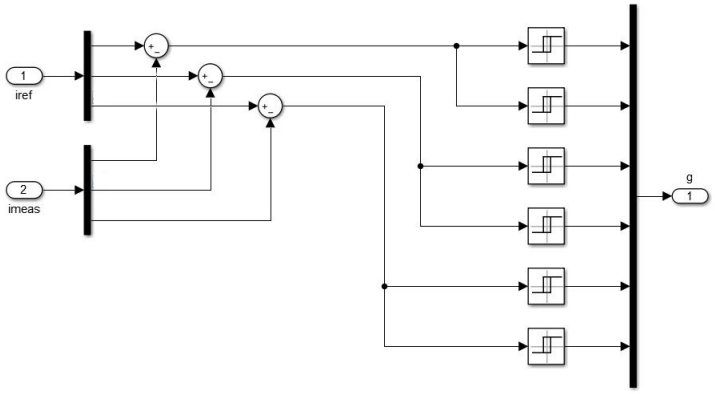


Figure 5.5: Hysteresis controller, PWM hysteresis block.

### 5.3.3 Reference Current Calculation

The reference current calculation block, shown in Figure 5.6, has three main sub-blocks: *Positive sequence detector*, *instantaneous p-q calc* and *Iαβ ref calc*.

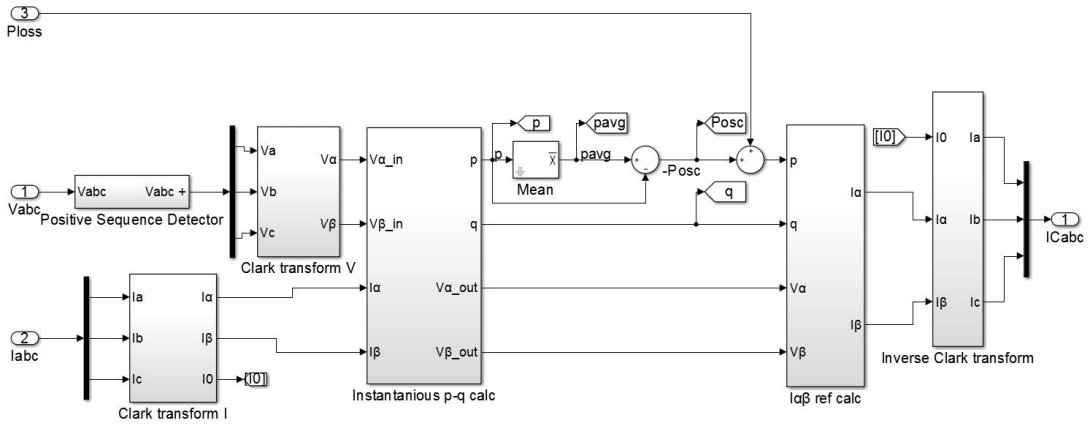


Figure 5.6: Reference current calculation block.

**Instantaneous p-q Calculation Block**

The *instantaneous p-q calc* block is calculating the instantaneous powers $p$ and $q$ using Equation 5.3

$$\begin{bmatrix} p_0 \\ p \\ q \end{bmatrix} = \begin{bmatrix} v_0 & 0 & 0 \\ 0 & v_\alpha & v_\beta \\ 0 & v_\beta & -v_\alpha \end{bmatrix} \begin{bmatrix} i_0 \\ i_\alpha \\ i_\beta \end{bmatrix} \tag{5.3}$$

Frequently, the average value of the instantaneous active power ($p$) is obtained as shown in Figure 5.7 but with a low-pass filter. Depending on the order and cut-off frequency it takes some time to settle and may have overshoot and still an oscillating component in the output. This can of course be adjusted with the cut-off frequency, but a lower cut-off frequency limits the dynamical response.

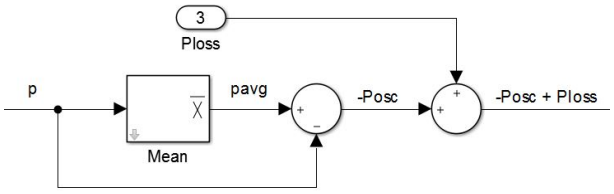


Figure 5.7: Obtaining the average power.

Instead, using a mean block as in Figure 5.7 to calculate the average value, it is possible to exploit symmetries found in the instantaneous power waveforms, at best the calculation of the average value only requires a fraction of the measured waveforms and can be as small as 1/6 but never greater than one cycle [35].

Depending on whether the voltages and/or currents are balanced and the presence of even harmonics the following symmetries exist [35]:

- **1/6 Cycle**
  If the power system has balanced voltages and currents without even harmonics, the instantaneous power waveforms have symmetry equal to 1/6 of the fundamental period.
- **1/3 Cycle**
  If the power system has balanced voltages and currents with even harmonics, the instantaneous power waveforms have symmetry equal to 1/3 of the fundamental period.
- **1/2 Cycle**
  If the power system has unbalanced voltages and/or currents without even harmonics, the instantaneous power waveforms have symmetry equal to 1/2 of the fundamental period.
- **1 Cycle**
  If the power system has unbalanced voltages and/or currents with even harmonics the instantaneous power waveforms have symmetry equal to the fundamental frequency period.

As an example, the instantaneous active power waveform from an unbalanced system without even harmonics is shown in Figure 5.8. The figure shows the waveform repeat itself twice during one fundamental cycle period, i.e. only half a fundamental cycle is required to calculate the average value.

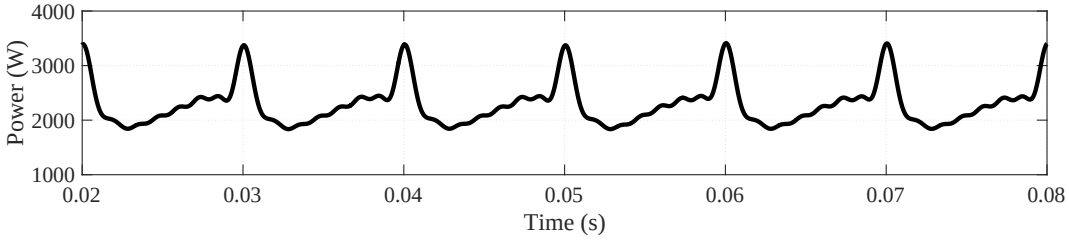


Figure 5.8: Instantaneous real power in an unbalanced system without even harmonics.

A comparison between a second-order butterworth low-pass filter with a cut-off frequency equal to 25 Hz and a moving average filter exploiting symmetries to obtain the average value of the instantaneous active power is shown in Figure 5.9.

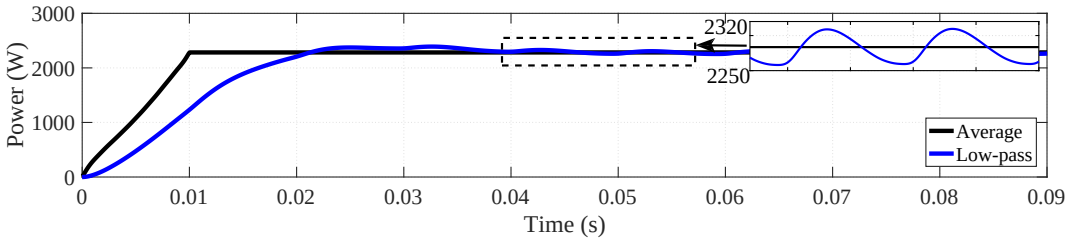


Figure 5.9: Average active power in an unbalanced system without even harmonics.

**I$\alpha\beta$ Reference Calculation**

The *I$\alpha\beta$ reference calc* block is calculating the reference currents in the $\alpha\beta 0$ frame as

$$\begin{bmatrix} i_0^* \\ i_\alpha^* \\ i_\beta^* \end{bmatrix} = \frac{1}{v_0(v_\alpha^2 + v_\beta^2)} \begin{bmatrix} (v_\alpha^2 + v_\beta^2) & 0 & 0 \\ 0 & v_0 v_\alpha & v_0 v_\beta \\ 0 & v_0 v_\beta & -v_0 v_\alpha \end{bmatrix} \begin{bmatrix} p_0^* \\ p^* \\ q^* \end{bmatrix} \tag{5.4}$$

Then the currents are transformed to $i_{abc}^*$ using the inverse Clarke transformation.

$$\begin{bmatrix} i_a^* \\ i_b^* \\ i_c^* \end{bmatrix} = \sqrt{\frac{2}{3}} \begin{bmatrix} \frac{1}{\sqrt{2}} & 1 & 0 \\ \frac{1}{\sqrt{2}} & -\frac{1}{2} & \frac{\sqrt{3}}{2} \\ \frac{1}{\sqrt{2}} & -\frac{1}{2} & -\frac{\sqrt{3}}{2} \end{bmatrix} \begin{bmatrix} i_0^* \\ i_\alpha^* \\ i_\beta^* \end{bmatrix} \tag{5.5}$$

**Positive Sequence Detector**

The *Positive Sequence Detector* block is implemented based on Chapter 4, Section 4.2 and shown in Figure 5.10. The utility voltage is transformed using the Clarke transformation, then the fictitious instantaneous powers $p'$ and $q'$ are calculated inside the *p-q calc* block as

$$\begin{bmatrix} p' \\ q' \end{bmatrix} = \begin{bmatrix} v_\alpha & v_\beta \\ v_\beta & -v_\alpha \end{bmatrix} \begin{bmatrix} i'_\alpha \\ i'_\beta \end{bmatrix} \tag{5.6}$$

Using a mean block and exploiting symmetries the average values of $p'$ and $q'$ are obtained, then used in Equation 5.7 for calculating the instantaneous voltages $v'_\alpha$ and $v'_\beta$ in the $V_{\alpha\beta}$ *pos. calc* block as

$$\begin{bmatrix} v'_\alpha \\ v'_\beta \end{bmatrix} = \frac{1}{i'^2_\alpha + i'^2_\beta} \begin{bmatrix} i'_\alpha & -i'_\beta \\ i'_\beta & i'_\alpha \end{bmatrix} \begin{bmatrix} \bar{p}' \\ \bar{q}' \end{bmatrix} \tag{5.7}$$

The auxiliary currents $i'^2_\alpha$ and $i'^2_\beta$ are obtained from the SRF-PLL block. Using the inverse Clarke transformation on $v'_\alpha$ and $v'_\beta$, the instantaneous positive fundamental voltages, $V_{+abc}$ are obtained as

$$\begin{bmatrix} v'_a \\ v'_b \\ v'_c \end{bmatrix} = \begin{bmatrix} 1 & 0 \\ -\frac{1}{2} & \frac{\sqrt{3}}{2} \\ -\frac{1}{2} & -\frac{\sqrt{3}}{2} \end{bmatrix} \begin{bmatrix} v'_\alpha \\ v'_\beta \end{bmatrix} \tag{5.8}$$

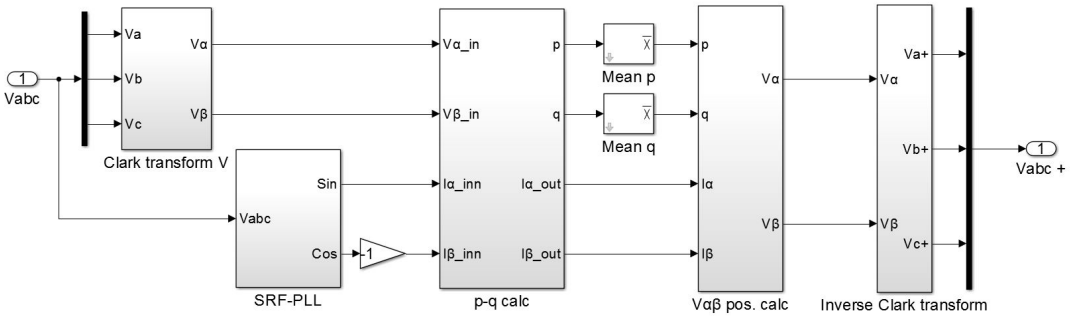


Figure 5.10: Positive sequence detector.

**Synchronous Reference Frame Phase Locked Loop**

The *SRF-PLL* block is implemented as shown in Figure 5.11 based on Subsection 4.2.1. First the *abc* voltages are transformed using the Clarke and Park transformation

$$\begin{bmatrix} v_d \\ v_q \\ v_0 \end{bmatrix} = \frac{2}{3} \begin{bmatrix} \cos(\omega_s t) & \cos(\omega_s t - 120°) & \cos(\omega_s t + 120°) \\ -\sin(\omega_s t) & -\sin(\omega_s t - 120°) & -\sin(\omega_s t + 120°) \\ 1/2 & 1/2 & 1/2 \end{bmatrix} \begin{bmatrix} v_a \\ v_b \\ v_c \end{bmatrix} \tag{5.9}$$

The PI controller parameters were found by trial and error and was selected as $k_p = 0.1$ and $k_i = 100$. The angle, $\theta$ is used to create the auxiliary currents $i'_\alpha$ and $i'_\beta$ (Equations 4.19 and 4.20) used in the positive sequence detector.

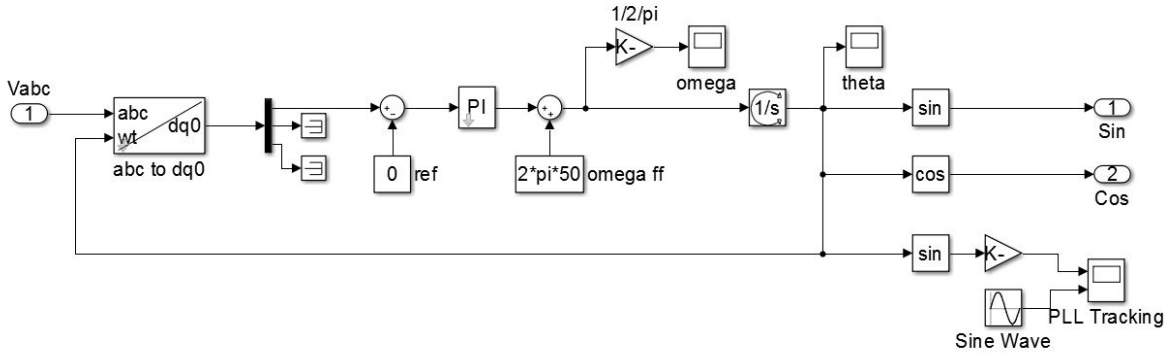


Figure 5.11: Synchronous reference frame phase locked loop.

Chapter 6

# Results and Discussion

This chapter presents a number of simulations that have been performed to observe the behaviour of the shunt APF under various loading and utility voltage conditions. The shunt APF is activated at time $t = 0.02$s in all five cases, below is a description of each case.

- **Case 1** shows the simulation results during sinusoidal utility voltage, load currents from Table 5.1 are used. At $t = 0.1$s an increase in load is activated.
- **Case 2** shows the simulation results during distorted and unbalanced utility voltage, load currents from Table 5.1 are used.
- **Case 3** shows the simulation results during sinusoidal utility voltage and when the residence is exporting power to the grid. Current profile from Table 5.2 is used.
- **Case 4** is similar to Case 3, but distorted and unbalanced utility voltage is included.
- **Case 5** shows the simulation results during sinusoidal utility voltage, load currents from Table 5.1 are used. The source impedance is increased to observe the effects on a weaker grid.

The system parameters used in the simulation model are listed in Table 6.1, where $f_s$, $R_s$, $L_s$, $C_{apf}$ and $L_f$ are system frequency, source resistance, source inductance, capacitance of the capacitors used in the shunt APF and inductance of the inductors connected between the shunt APF and PCC respectively. Refer to Figure 5.1 for a schematic, and as mentioned in Chapter 5 the values for $C_{apf}$ and $L_f$ was chosen based on relevant articles and then modified slightly to give an adequate performance.

Table 6.1: System parameters.

| $f_s$ | $R_s$ | $L_s$ | $C_{apf}$ | $L_f$ |
|---|---|---|---|---|
| 50 Hz | 0.1 Ω | 0.01 mH | 2000 $\mu$F | 10 mH |

## 6.1 Case 1 - Sinusoidal Utility Voltage

This section presents the simulation results for Case 1,the results will be discussed at the end of this section. At $t = 0.02$s the shunt APF is activated and at $t = 0.1$s the fundamental current is doubled in all phases, the third harmonic is doubled in phase $B$ and the fifth harmonic is doubled in phase $C$. The rest remains unchanged with respect to Table 5.1. In Case 1 there is no need for a positive sequence detector as the utility voltages are purely sinusoidal and balanced.

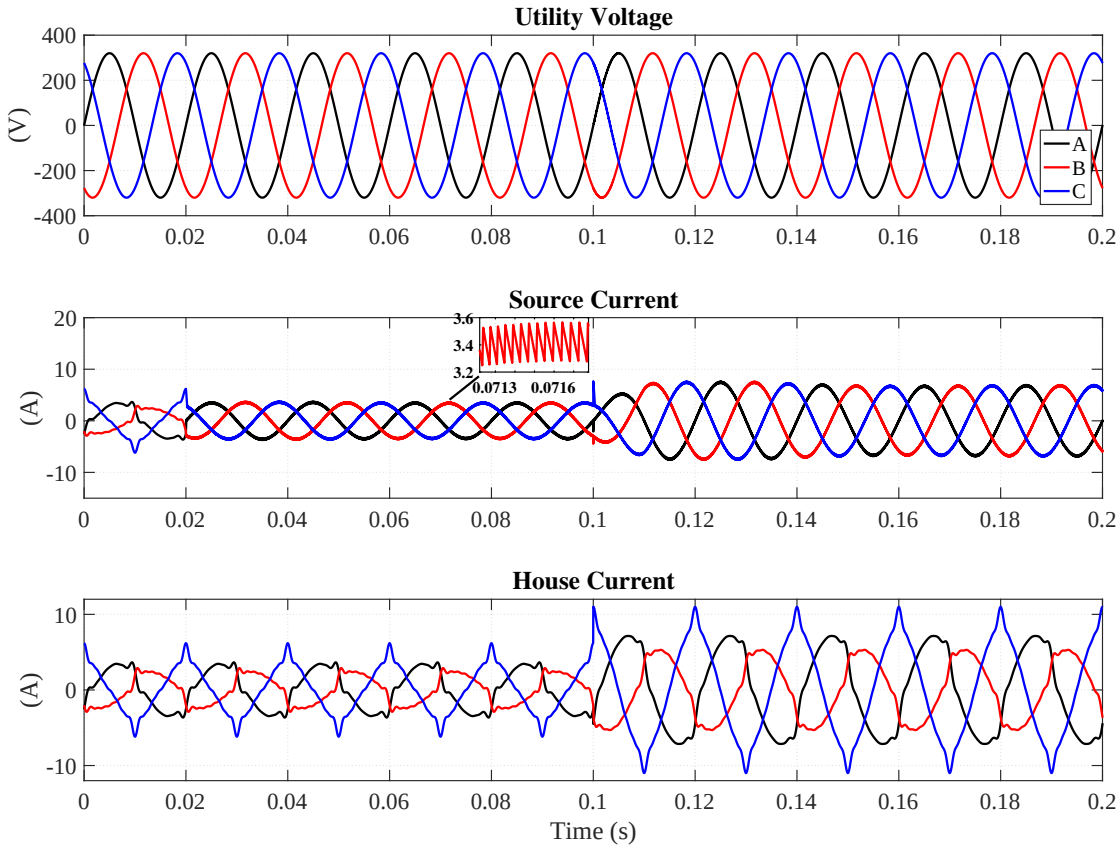


Figure 6.1: Utility voltage, source currents and house currents.

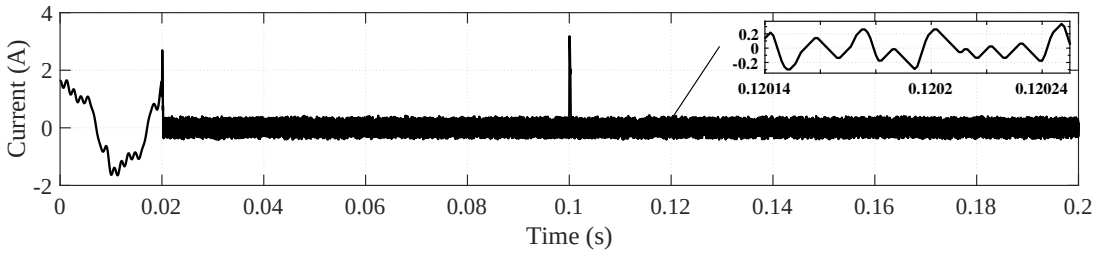


Figure 6.2: Neutral Current.

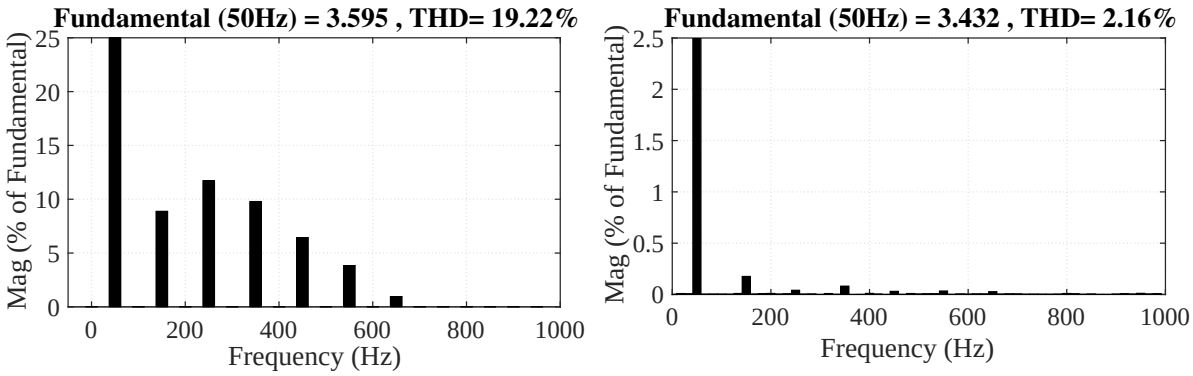


(a) Before compensation.

(b) After compensation.

Figure 6.3: THD in the source current for phase $A$, before and after compensation.

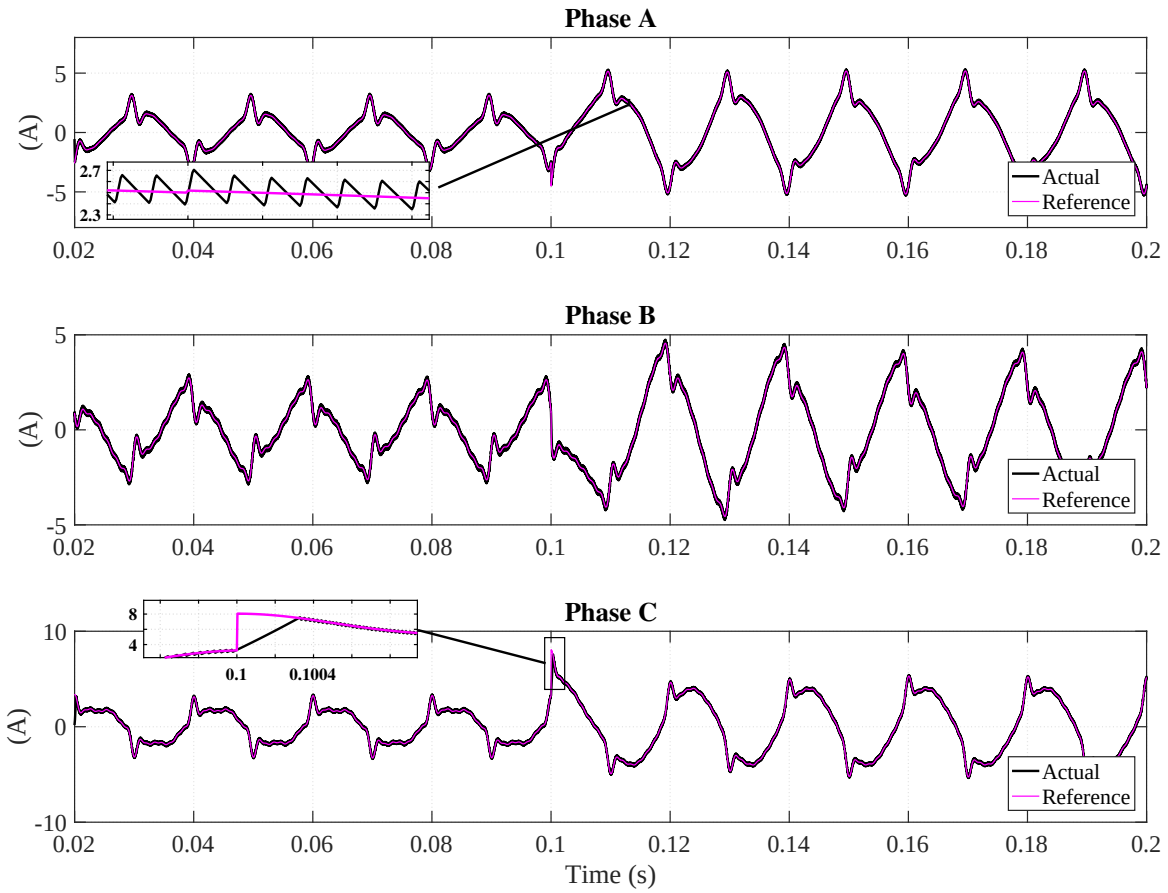


Figure 6.4: Reference and actual compensating currents from the shunt APF.

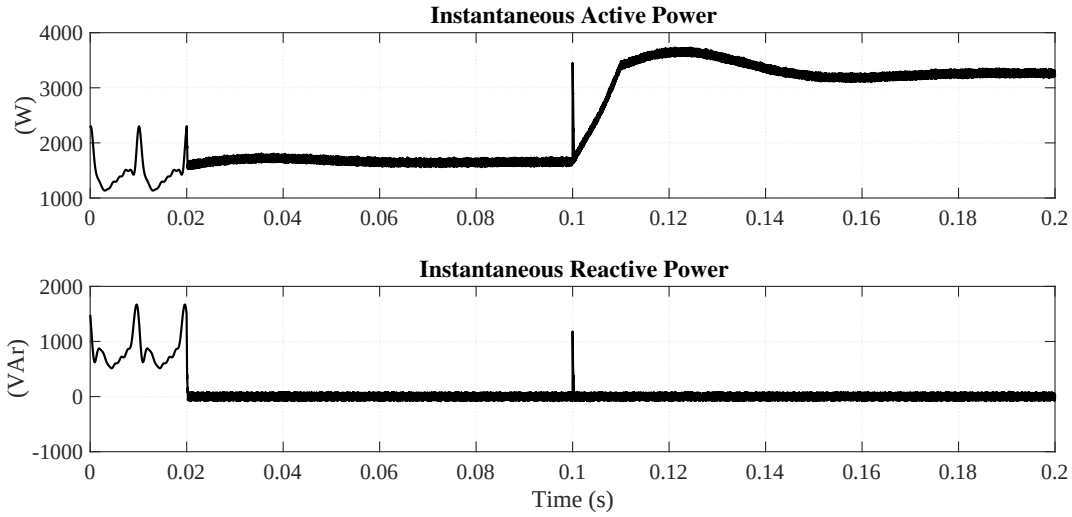


Figure 6.5: Instantaneous active and reactive source power.

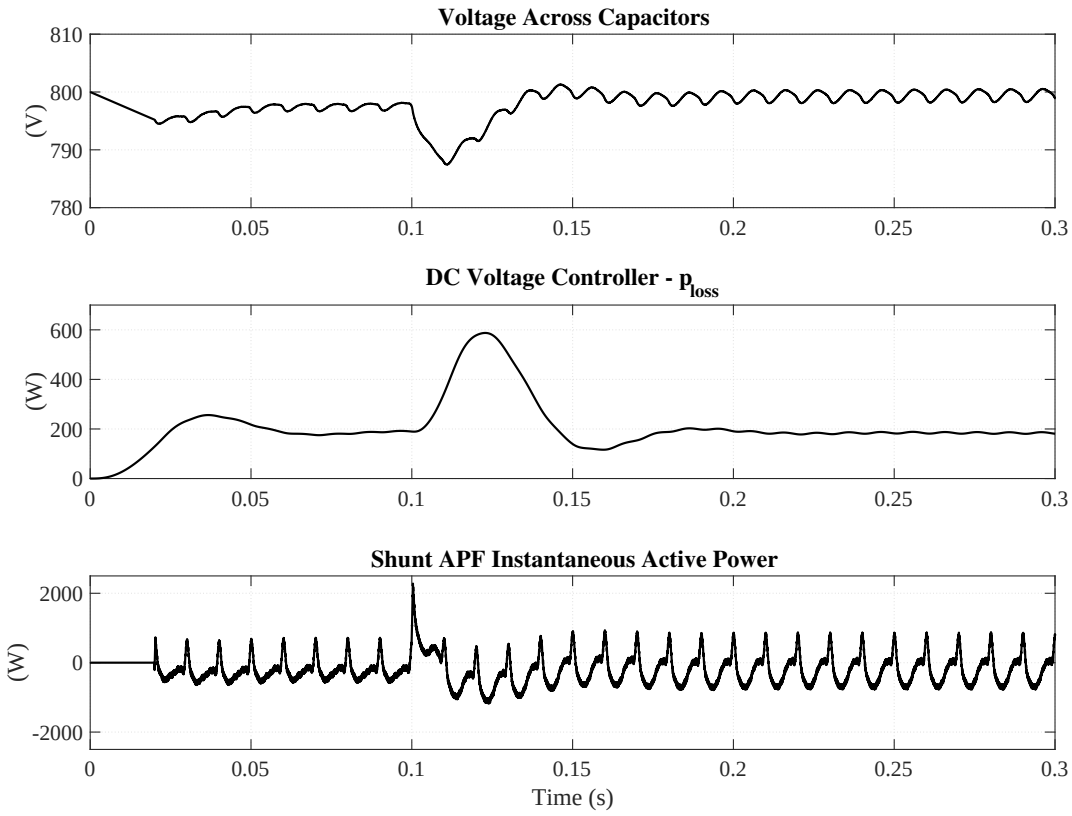


Figure 6.6: Voltage across the capacitors, $P_{loss}$ signal and the shunt APF instantaneous active power.

### 6.1.1 Discussion based on Case 1

Figure 6.1 shows the utility voltage, source currents and house currents respectively. The shunt APF is turned on at $t = 0.02$s and the source currents become sinusoidal, balanced and in-phase with its respective phase voltage i.e unity power factor. The THD of the phase $A$ current before and after compensation can be seen in Figure 6.3, before compensation the THD is equal to 19.22% and after compensation equal to 2.16%, similar plots for phase $B$ and $C$ can be found in Appendix C. The frequency spectrum plots showing the THD etc. is taken before the load change, but similar values of THD are present after the load change in steady state. Most of the harmonic currents are compensated, but high frequency components have been introduced in the source currents, which can be seen in Figure 6.1, where a zoomed plot of the source current is showing high frequency ripple with a peak to peak value of approximately 0.3A. The magnitude can be reduced by lowering the hysteresis band, $HB$ but as a result the switching frequency will increase. Similarly the switching frequency can be lowered by increasing $HB$, but this will increase the peak to peak value of the ripple. An overview of the high frequency spectrum can be seen in Appendix C, Figure C.1, showing the majority to be within the range 20-50kHz.

The neutral current in Figure 6.2 is reduced after compensation, what remains is the high frequency ripple current with a maximum peak to peak value of approximately 0.4A.

The instantaneous active and reactive powers supplied by the source are shown in Figure 6.5. After compensation at $t = 0.02$s, only average active power is supplied by the source. The reactive power and oscillating active power demanded by the house is now compensated by the shunt APF. However, due to the switching ripple in the compensating currents (Figure 6.4), the instantaneous powers supplied by the source also have high frequency, low magnitude ripples.

At $t = 0.1$s, when the increase in load is activated, a spike in the source currents can be observed. As a consequence, spikes can be seen in the neutral current and instantaneous power plots. The shunt APF is not able to instantaneously compensate the instantaneous step in the load currents (last plot, Figure 6.4). Apart from the spikes, the source currents remain sinusoidal, balanced and in-phase with its respective phase voltage. The voltage across the capacitors in the shunt APF drops due to the load change, seen in the first plot in Figure 6.6. During transients the shunt APF is supplying the load with average and oscillating instantaneous active power for a short period of time, seen in the last plot in Figure 6.6. The DC voltage controller responds to the load change by increasing the $p_{loss}$ signal (second plot, Figure 6.6) so that the DC voltage is forced back to the reference value in steady state.

## 6.2 Case 2 - Distorted and Unbalanced Utility Voltage

Case 2 studies how the shunt APF is operating under distorted and unbalanced utility voltage, the results will be discussed at the end of this section. At $t = 0.05$s a voltage disturbance, composed of a negative sequence fundamental component and a fifth harmonic component is added. The utility voltage can be expressed as

$$\begin{bmatrix} v_a \\ v_b \\ v_c \end{bmatrix} = \sqrt{2} \cdot 230 \begin{bmatrix} \sin(\omega t) \\ \sin(\omega t - 2\pi/3) \\ \sin(\omega t + 2\pi/3) \end{bmatrix} + \begin{bmatrix} 40\sin(\omega t) \\ 40\sin(\omega t + 2\pi/3) \\ 20\sin(\omega t - 2\pi/3) \end{bmatrix} + \begin{bmatrix} 30\sin(5\omega t) \\ 40\sin(5\omega t + 2\pi/3) \\ 30\sin(5\omega t - 2\pi/3) \end{bmatrix} \quad (6.1)$$

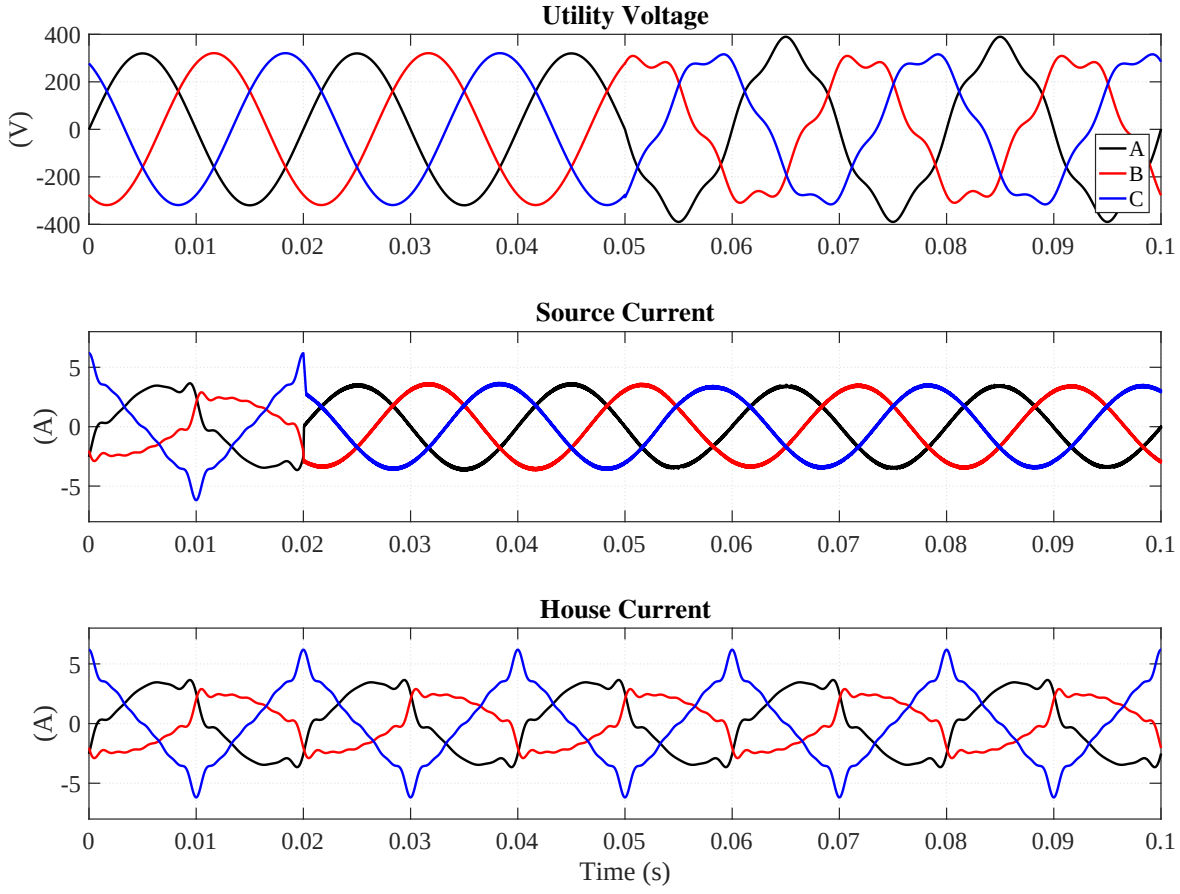


Figure 6.7: Utility voltage, source currents and house currents.

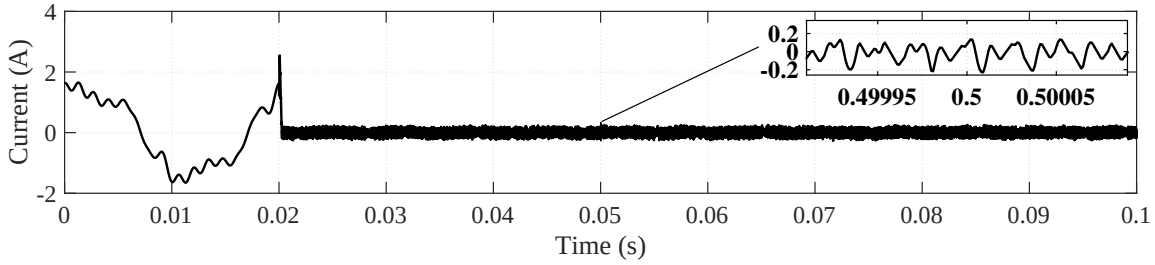


Figure 6.8: Neutral Current.

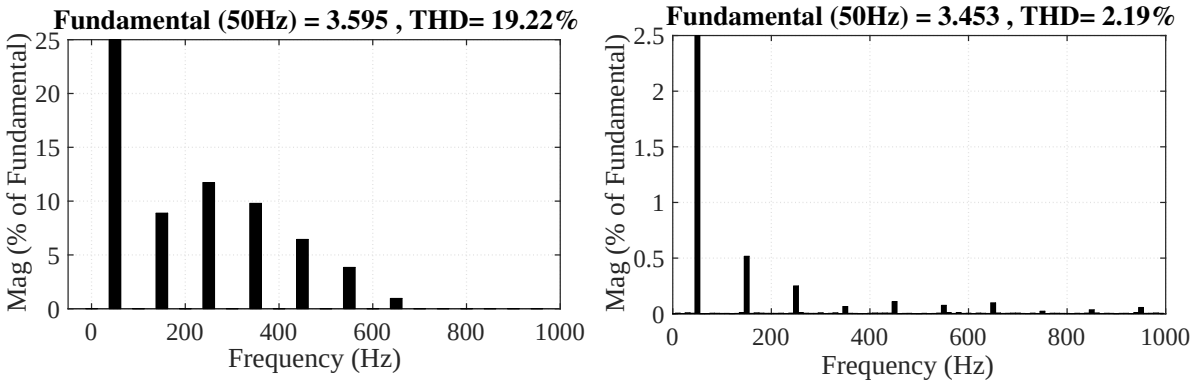


(a) Before compensation.

(b) After compensation.

Figure 6.9: THD in the source current for phase $A$, before and after compensation.

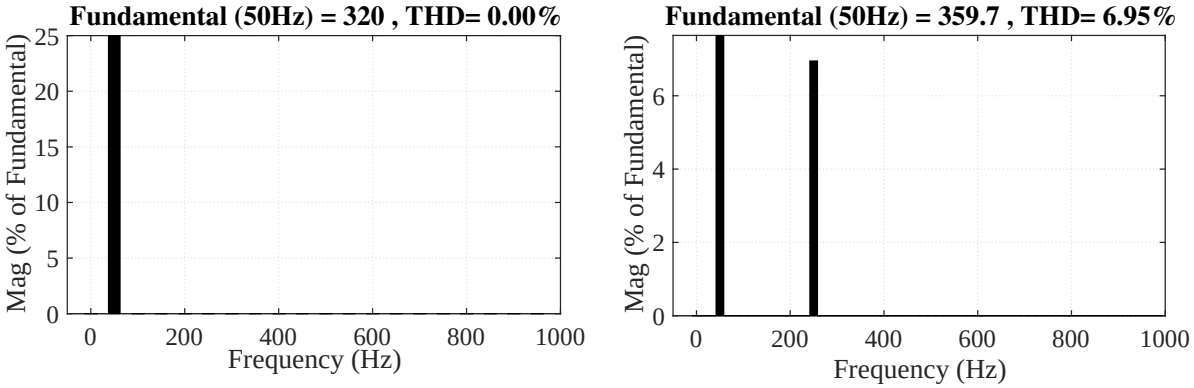


(a) Before

(b) After

Figure 6.10: THD in the utility voltage for phase $A$, before and after the disturbance.

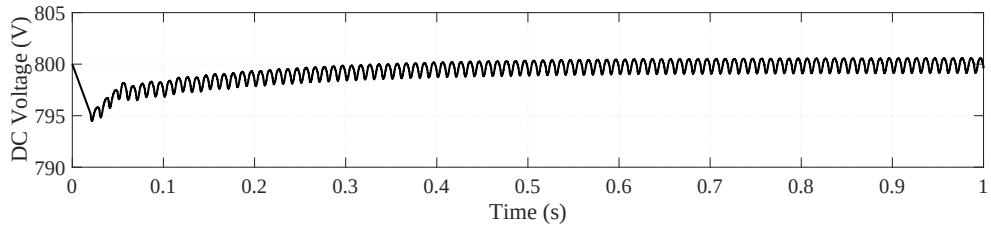


Figure 6.11: Voltage across the capacitors.

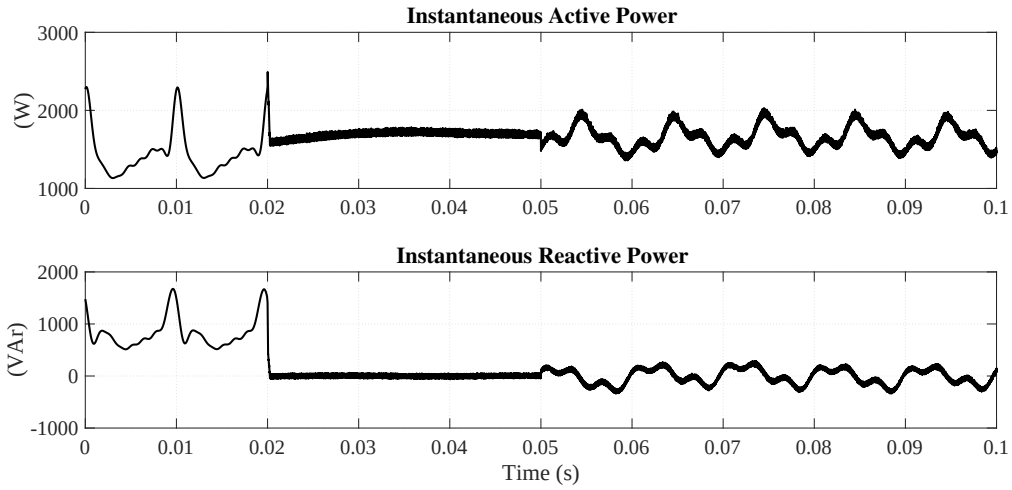


Figure 6.12: Instantaneous active and reactive source power when the compensation goal is sinusoidal source currents.

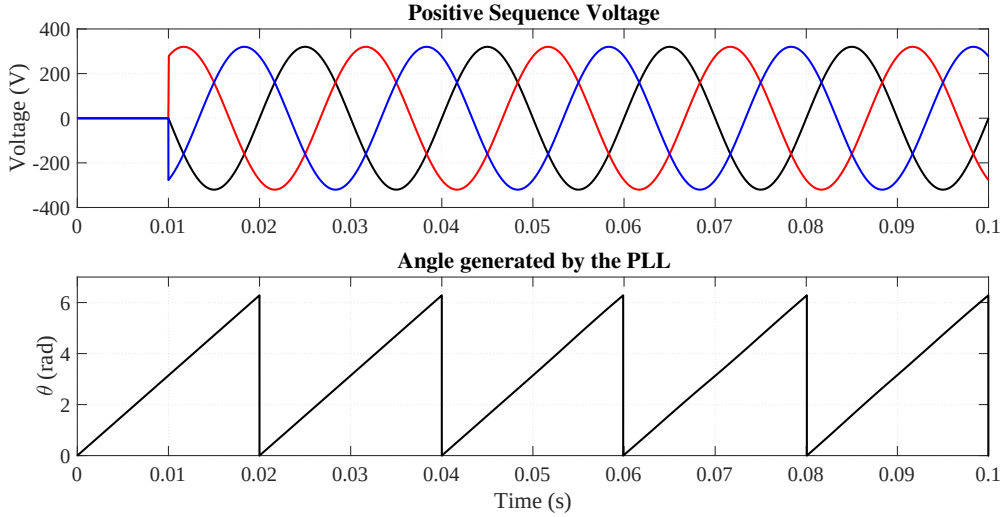


Figure 6.13: Positive sequence voltage detected by the positive sequence detector and angle $\theta$ generated by the PLL.

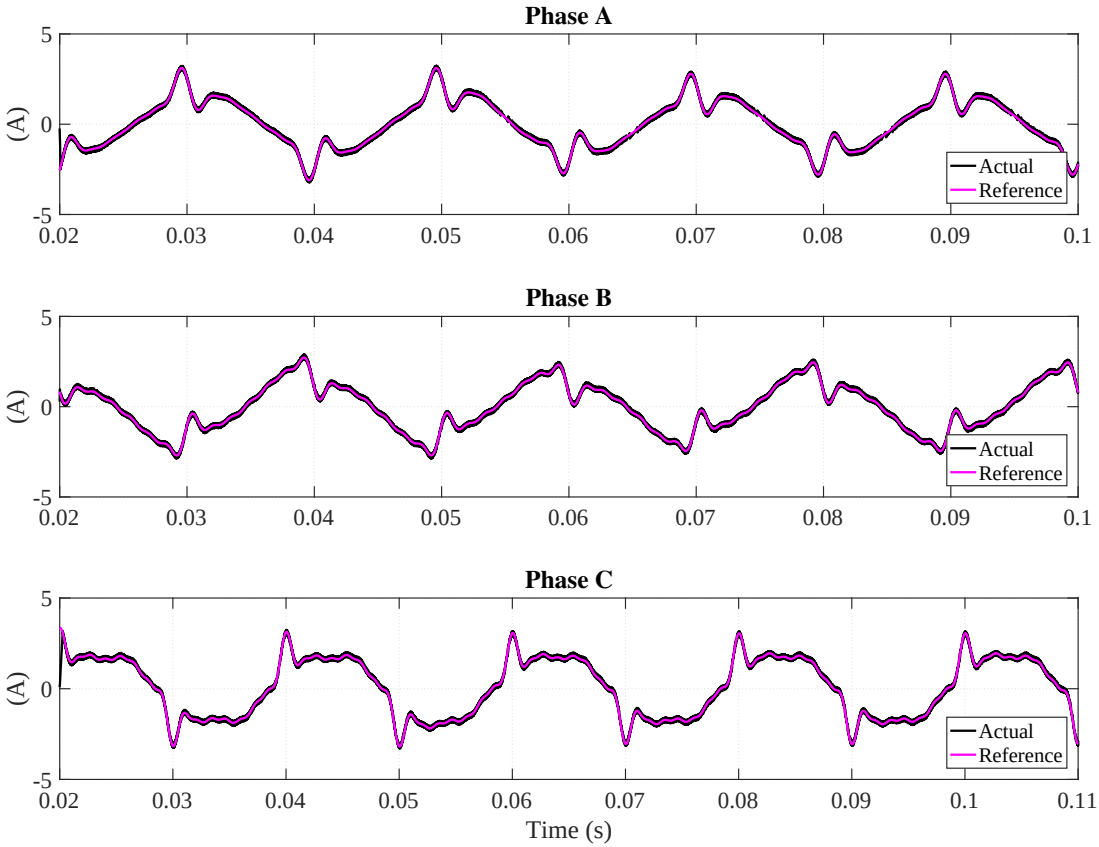


Figure 6.14: Reference and actual compensating currents supplied by the shunt APF, when the compensation goal is sinusoidal source currents.

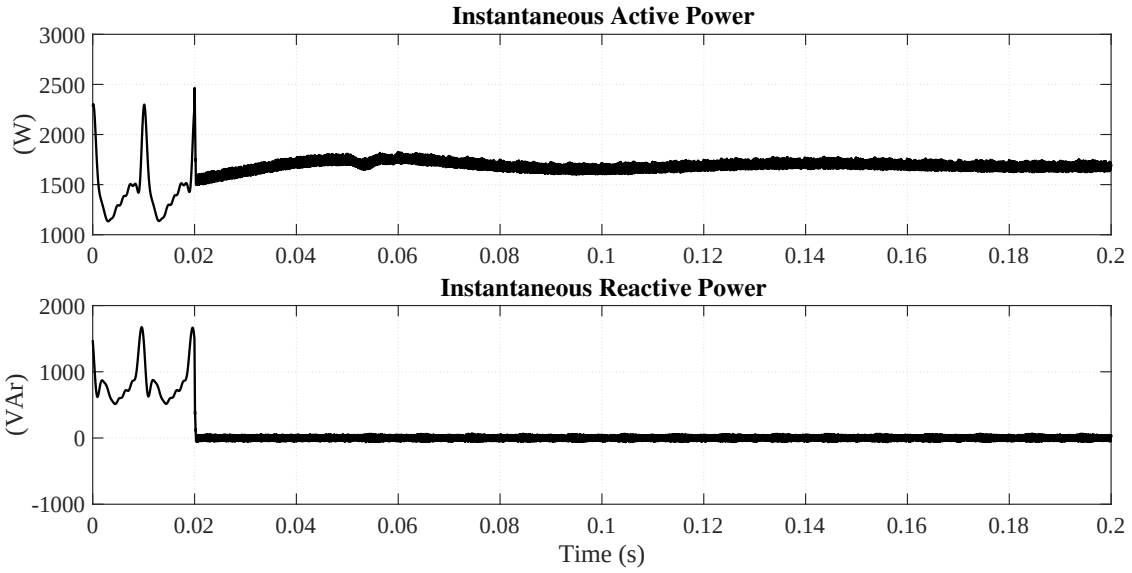


Figure 6.15: Instantaneous active and reactive source power when the compensation goal is constant source active power.

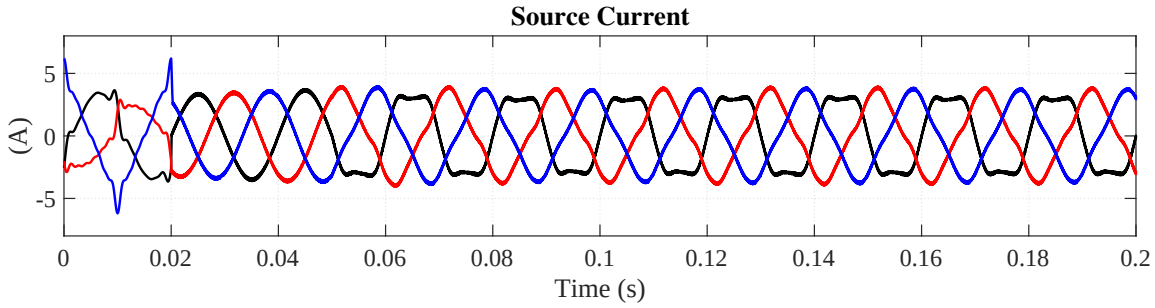


Figure 6.16: Source currents when the compensation goal is constant source power.

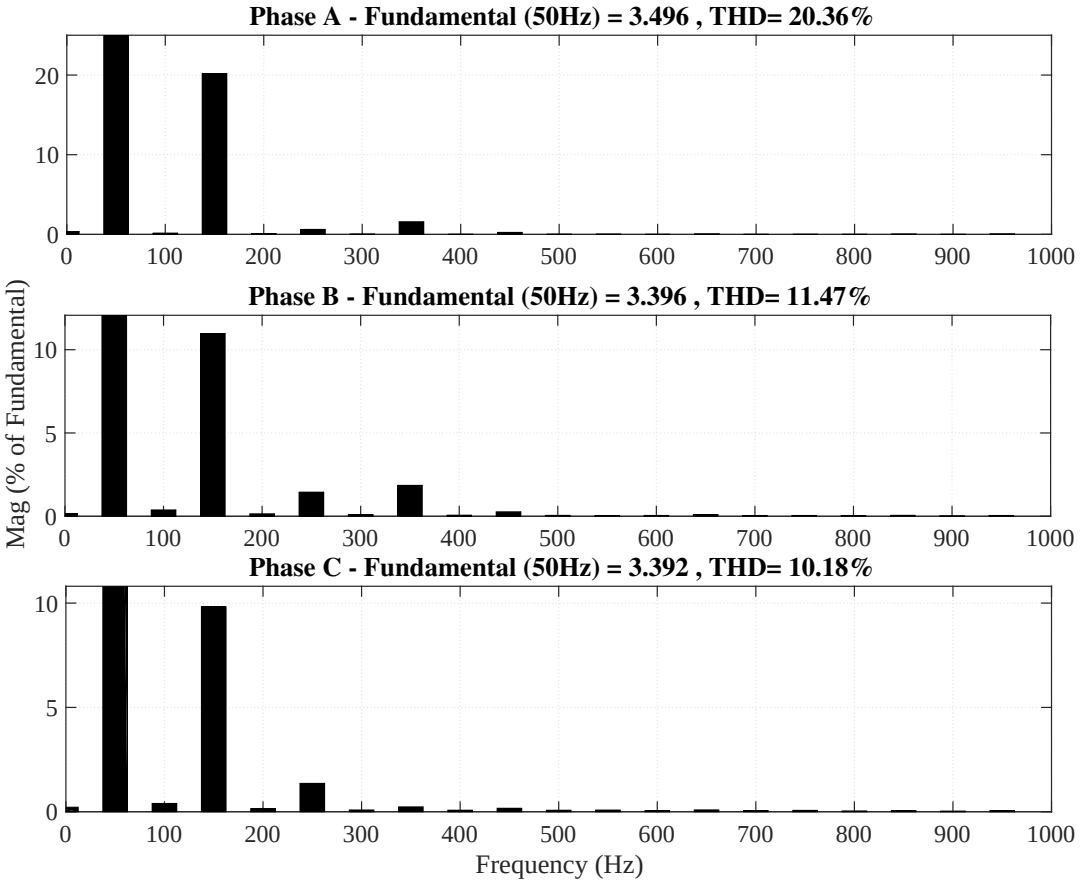


Figure 6.17: THD in the source currents after compensation, when the compensation goal is constant source power.

### 6.2.1 Discussion based on Case 2

Figure 6.7 shows the utility voltage, source currents and house currents respectively. Before $t = 0.05$s, Case 2 is identical to Case 1. At $t = 0.05$ and beyond, when the utility voltage is distorted and unbalanced, the source currents remains sinusoidal and it appears to be no change in spite of the disturbance in the utility voltage. The positive sequence detector is able to detect the fundamental positive sequence (first plot, Figure 6.13) during distorted and unbalanced utility voltage. The PLL output (last plot, Figure 6.13) is also able to track the angle $\theta$ during distorted and unbalanced waveforms.

As a result of the presence of distorted and unbalanced utility voltage, the shunt APF can no longer both compensate to achieve sinusoidal source currents and constant source power (Chapter 3). A decision between the two compensation goals has to be made. Figure 6.12 shows the instantaneous source powers when sinusoidal currents are the compensation goal, the instantaneous powers are no longer constant. Nevertheless, the currents are sinusoidal and the THD is reduced to 2.24% in phase $A$ down from 19.22% (Figure 6.10), similar plots for phase $B$ and $C$ can be seen in Appendix C, Figures C.5 and C.6.

If the compensation goal is to supply constant power from the source, i.e. removing the positive sequence detector, the source currents can no longer remain sinusoidal as shown in the plots in Figure 6.15. Figure 6.17 shows source currents that now contain third harmonics in all phases and a THD value above 10%.

High frequency, low magnitude ripples are still present after the shunt APF is activated and have the same characteristics as shown in the Figures in Case 1.

A comparison between a moving average and low pass filter is shown in Appendix C, Figure C.4.

## 6.3 Case 3 - Exporting Power

Case 3 studies how the shunt APF operates when the residence is exporting power under sinusoidal and balanced utility voltage. The results will be discussed at the end of this section.

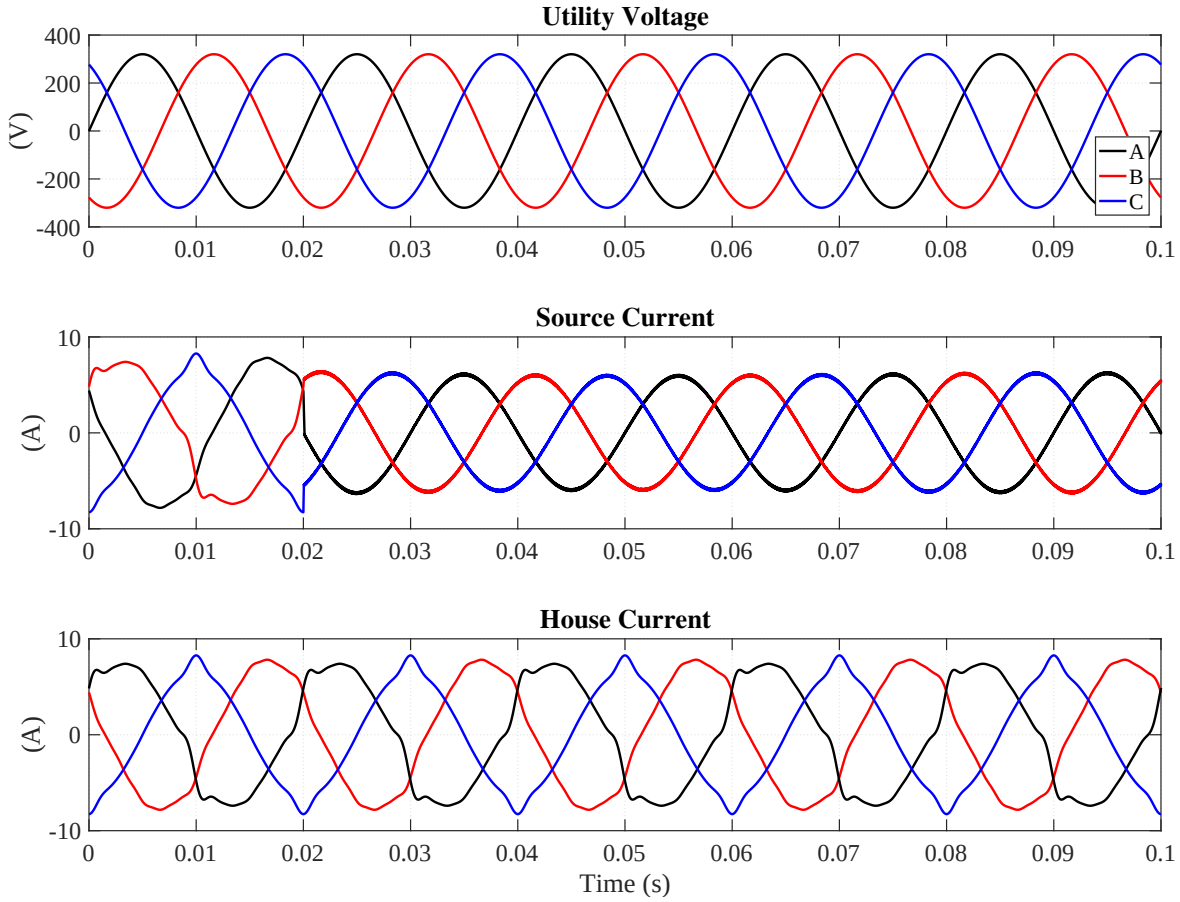


Figure 6.18: Utility voltage, source currents and house currents.

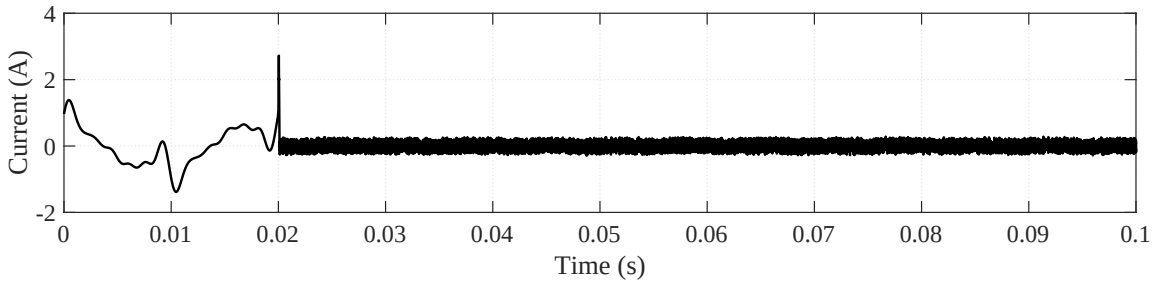


Figure 6.19: Neutral Current.

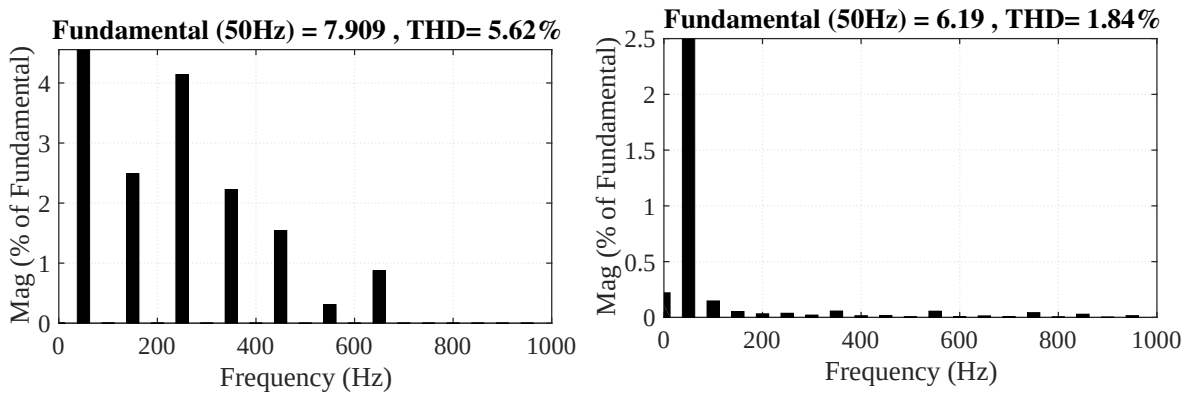


(a) Before compensation.

(b) After compensation.

Figure 6.20: THD in the source current for phase $A$, before and after compensation.

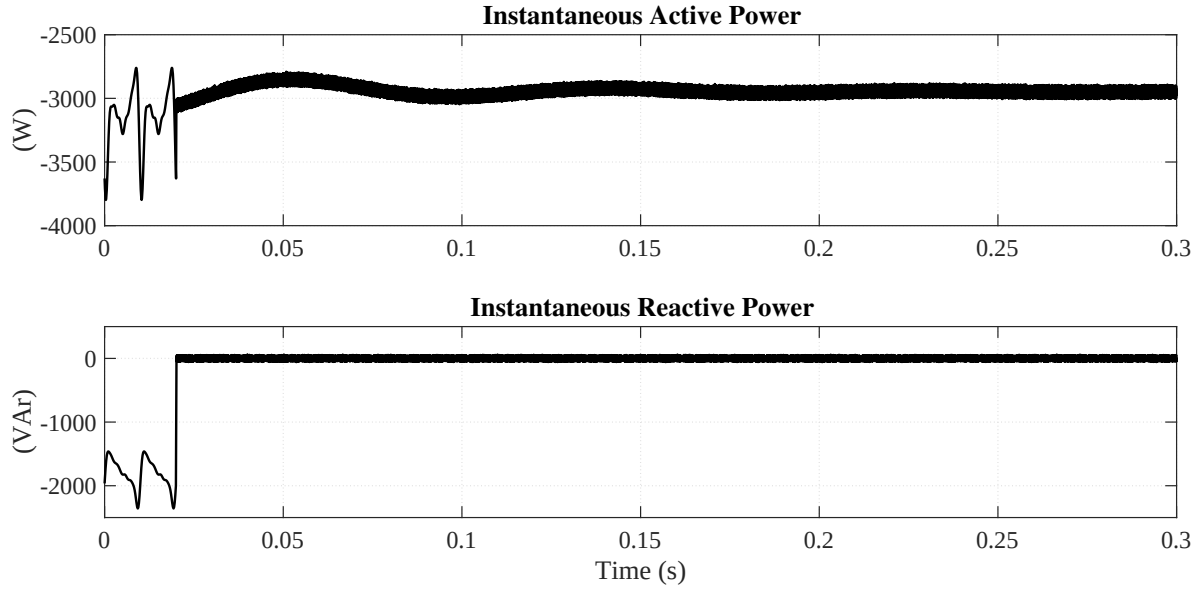


Figure 6.21: Instantaneous active and reactive source power, compensating for oscillating active power and both the average and oscillating reactive power.

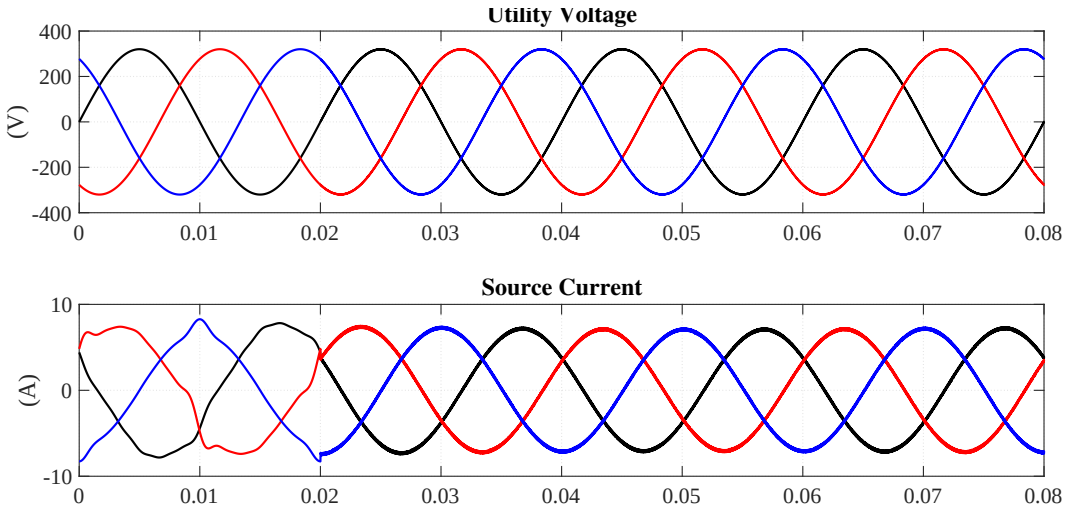


Figure 6.22: Utility voltage and source currents, not compensating for average reactive power.

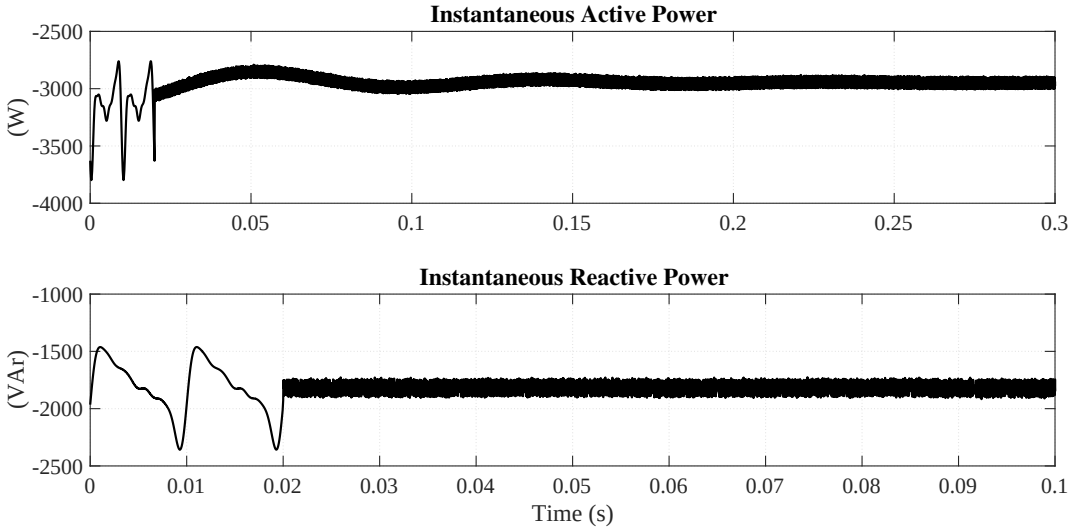


Figure 6.23: Instantaneous active and reactive source power, not compensating for average reactive power.

### 6.3.1 Discussion based on Case 3

Figure 6.18 shows the utility voltage, source currents and load currents respectively. After activating the shunt APF at $t = 0.02$ the source currents becomes sinusoidal and balanced, with a THD in phase $A$ of 1.84% and is operating at unity power factor. THD plots for phase $B$ and $C$ and compensating currents can be seen in Appendix C, Figures C.7, C.8 and C.9 respectively.

The instantaneous source powers are shown in Figure 6.21, only the average value of the instantaneous active power is exported to the grid, and the instantaneous reactive power is zero after compensation.

If the residence was to export reactive power to the grid, the shunt APF will prevent the residence from doing so. To solve this, the compensating algorithm has to be slightly modified so the shunt APF is only compensating for the oscillating part of the instantaneous reactive power ($\tilde{q}$) and not the average part of instantaneous reactive power ($\bar{q}$). The instantaneous reactive power when the shunt APF is only compensating for the oscillating part of the instantaneous reactive power is shown in Figure 6.23, the system is no longer operating at unity power factor (Figure 6.22) and the average instantaneous reactive power is no longer zero. The instantaneous active power remains unaffected.

## 6.4 Case 4 - Exporting Power and Distorted and Unbalanced Utility Voltage

In Case 4, Case 3 is extended to include distorted and unbalanced utility voltage..

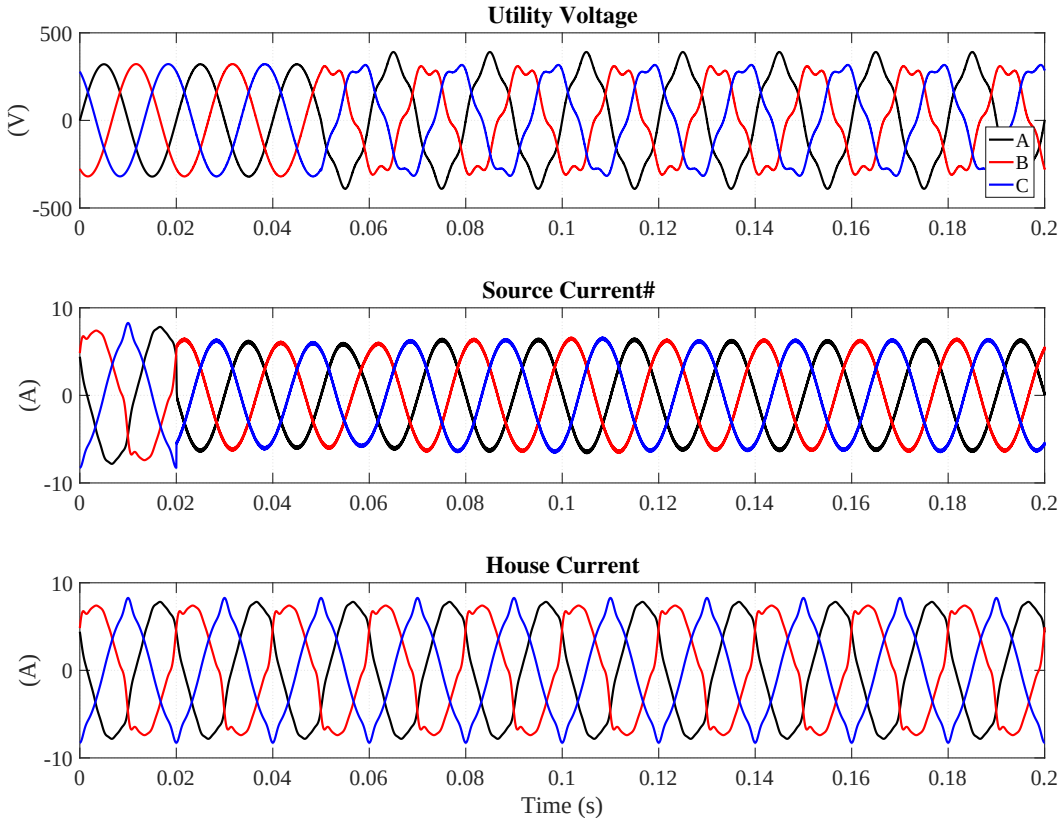


Figure 6.24: Utility voltage, source currents and house currents. Compensation goal: Sinusoidal source currents and zero average reactive power.

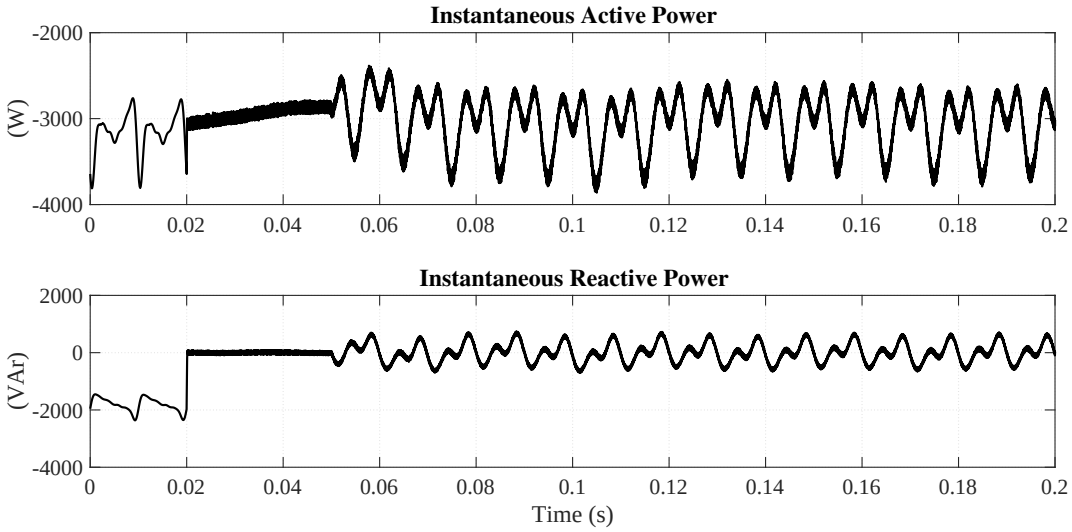


Figure 6.25: Instantaneous active and reactive source power. Compensation goal: Sinusoidal source currents and zero average reactive power.

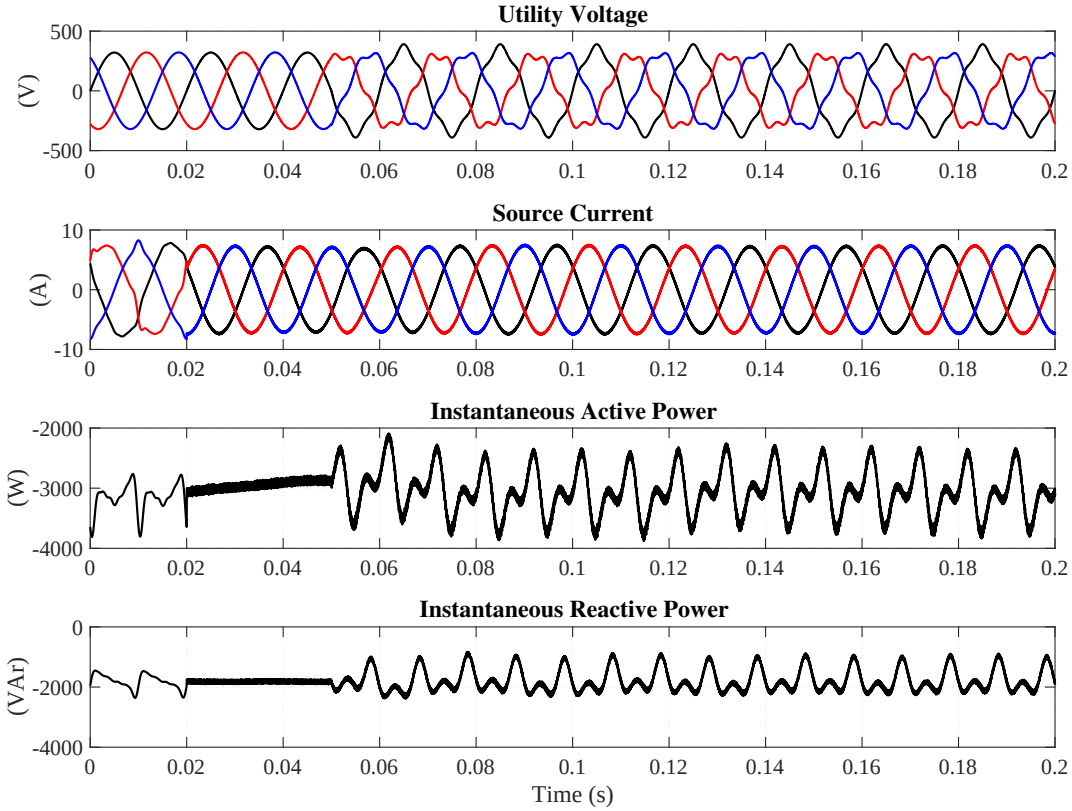


Figure 6.26: Utility voltage, source current, instantaneous active and reactive source power. Compensation goal: Sinusoidal source currents and non-zero average reactive power.

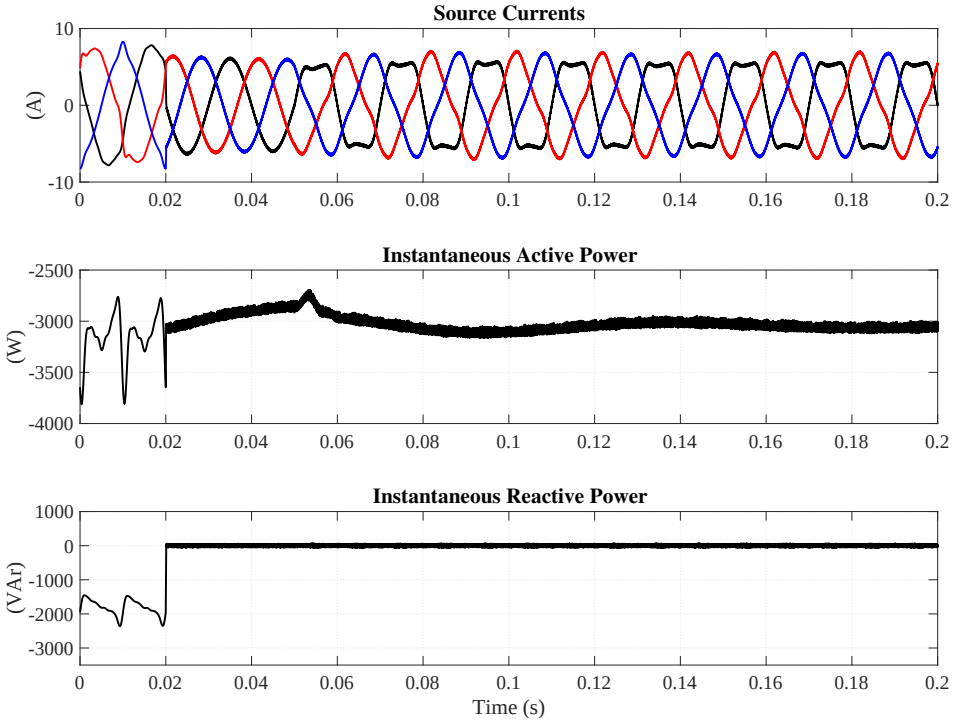


Figure 6.27: Source currents, instantaneous active and reactive source power. Compensation goal: Constant source active power and zero reactive power.

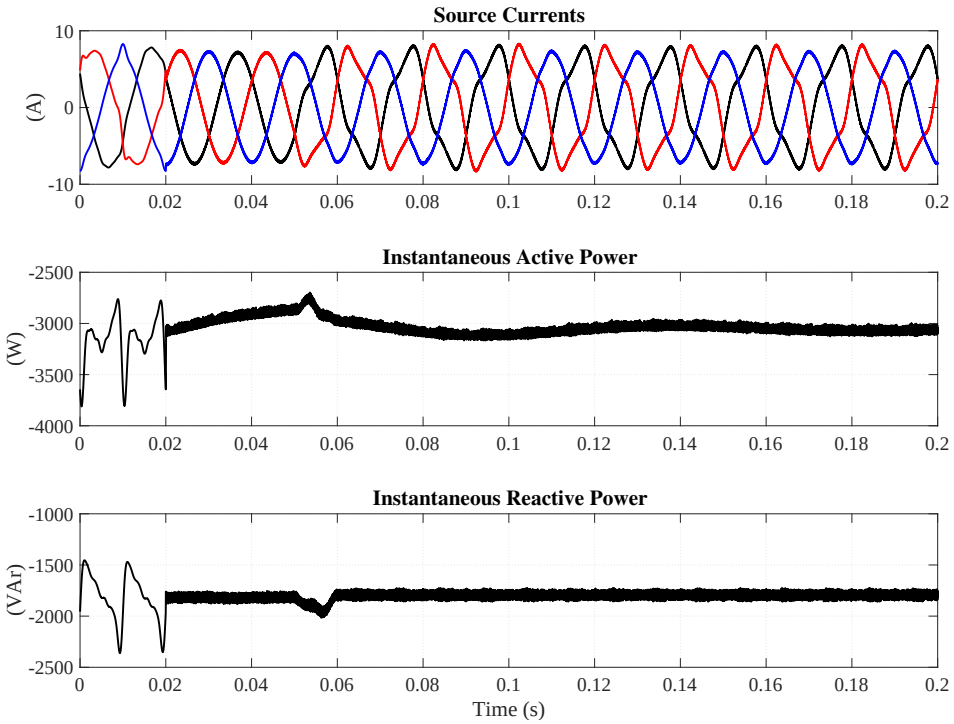


Figure 6.28: Source currents, instantaneous active and reactive source power. Compensation goal: Constant source active power and constant non-zero average reactive power.

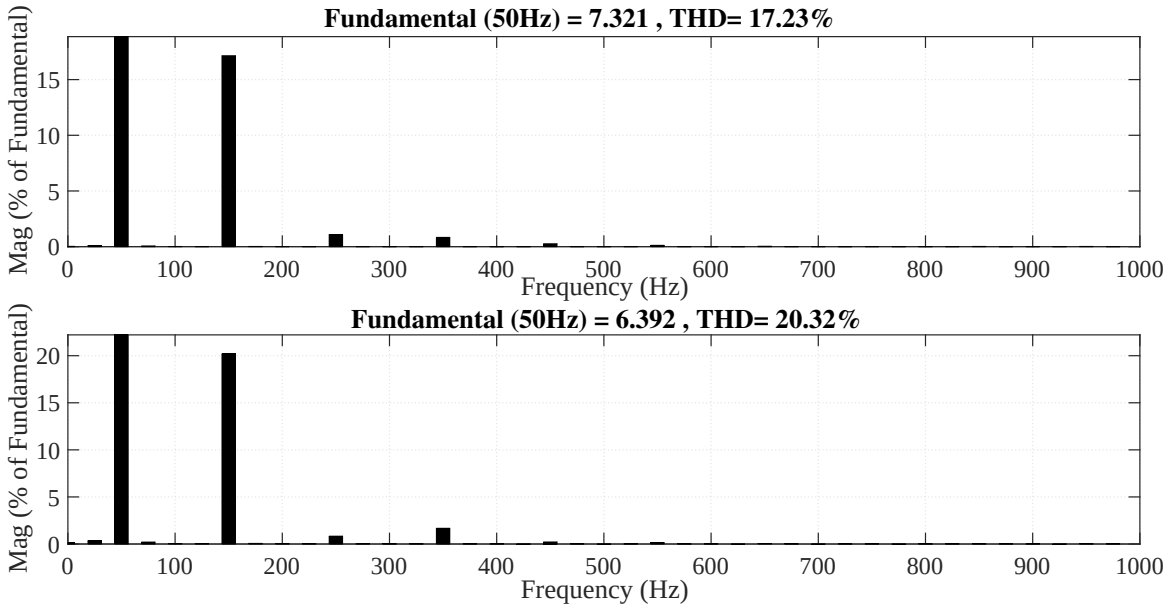


Figure 6.29: THD after compensation in phase $A$ for Figures 6.27 and 6.28 respectively.

### 6.4.1 Discussion based on Case 4

Figure 6.24 shows the utility voltage, source currents and house currents respectively during power export, when the compensation goal is sinusoidal currents and zero average value of the reactive power. The source currents become sinusoidal and have the same amount of high frequency, low magnitude ripples as previous cases. Because of the presence of distorted and unbalanced utility voltage, the instantaneous source powers in Figure 6.25 are no longer constant.

In Figure 6.26 the utility voltage, source currents, instantaneous active and reactive powers are shown respectively. The compensation goal is sinusoidal source currents, but export of reactive power to the grid (notice non-zero average value of the instantaneous reactive power). As a result the source currents are no longer in phase with the utility voltage.

In Figure 6.27 the source currents, instantaneous active and reactive powers are shown respectively, when the compensation goal is constant source active power and full reactive power compensation. The source currents are no longer sinusoidal and has a THD above 5%, see first plot in Figure 6.29.

In Figure 6.28 the source currents, instantaneous active and reactive powers are shown respectively, when the compensation goal is constant source active power but export of constant reactive power to the grid. The source currents are no longer sinusoidal and has a THD above 5%, see last plot in Figure 6.29.

## 6.5 Case 5 - Increasing System Impedance

Case 5 studies the effect of the shunt APF when it is connected to a weaker grid. Therefore the source impedance is increased to $R_s = 1\,\Omega$ and $L_s = 0.5$ mH, the rest of the parameters in Table 6.1 remain unchanged.

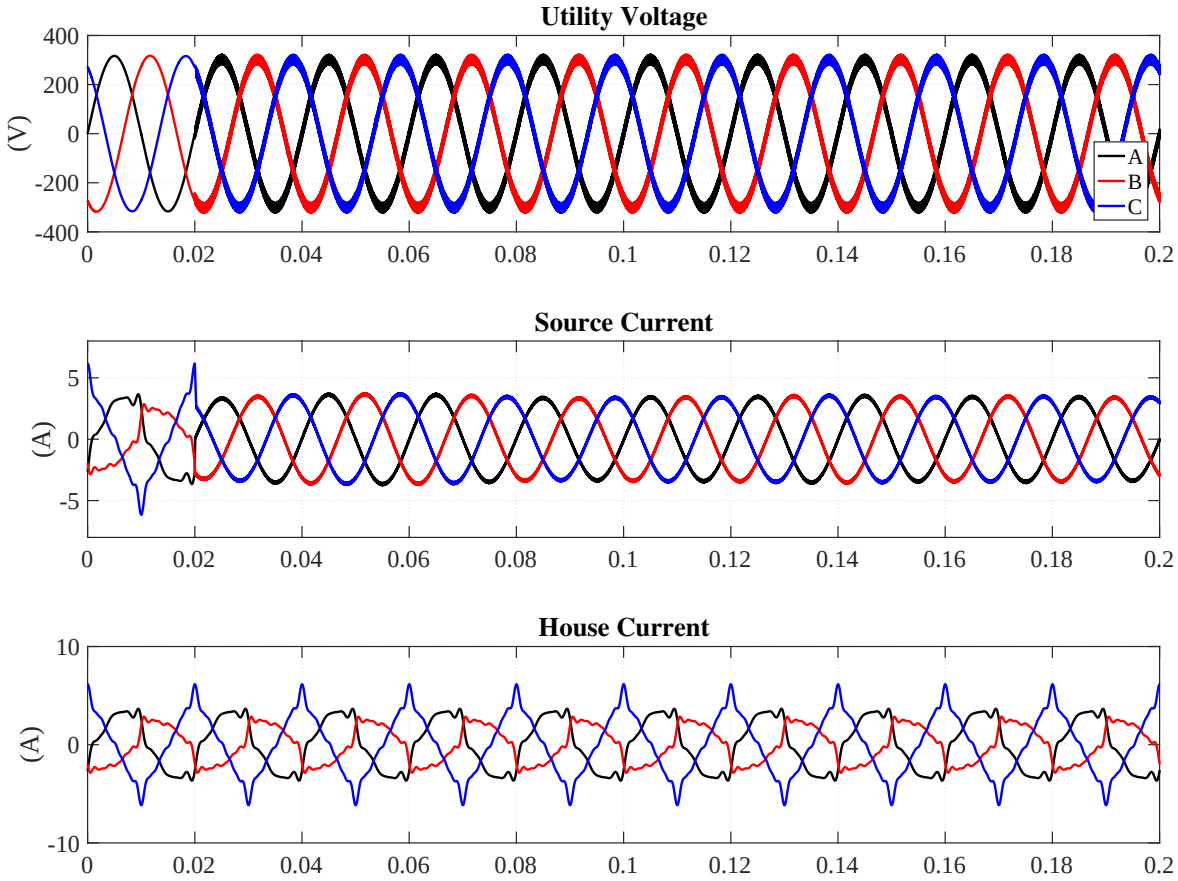


Figure 6.30: Utility voltage, source currents and house currents.

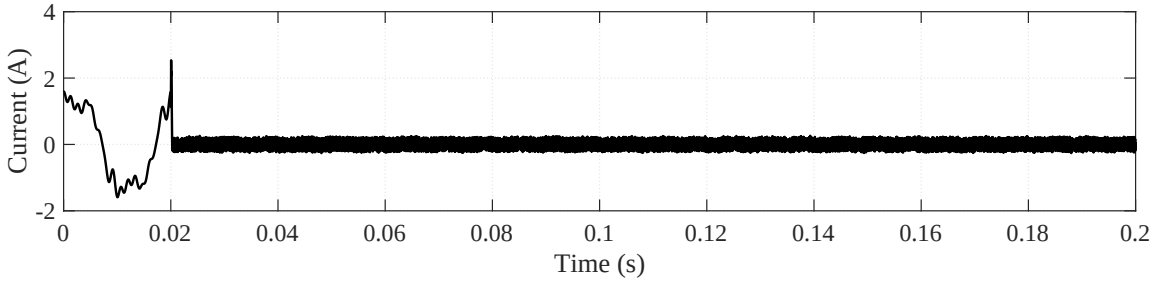


Figure 6.31: Neutral Current.

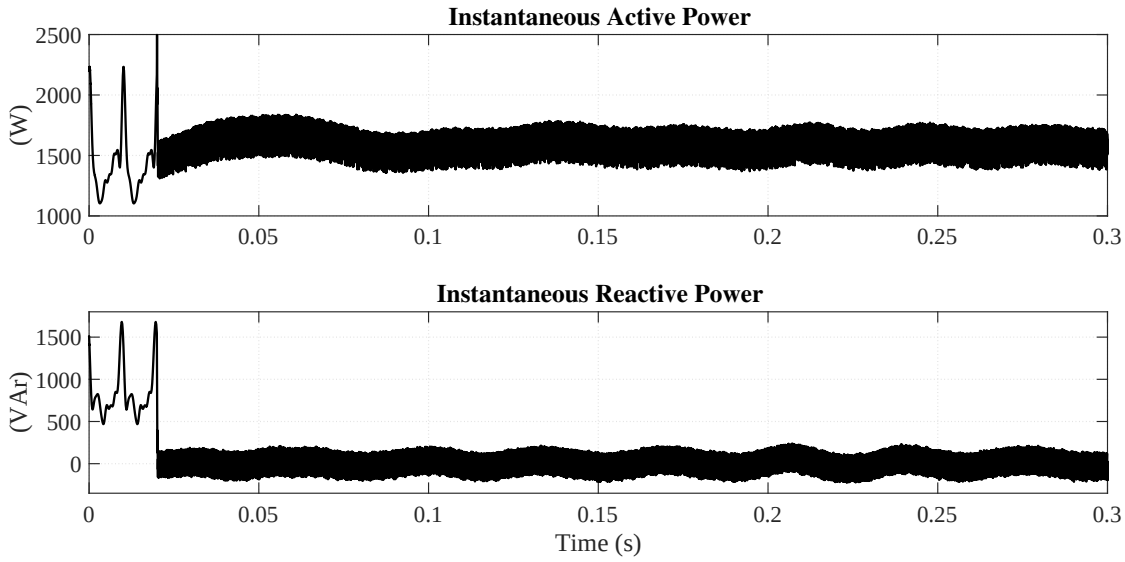


Figure 6.32: Instantaneous active and reactive source power.

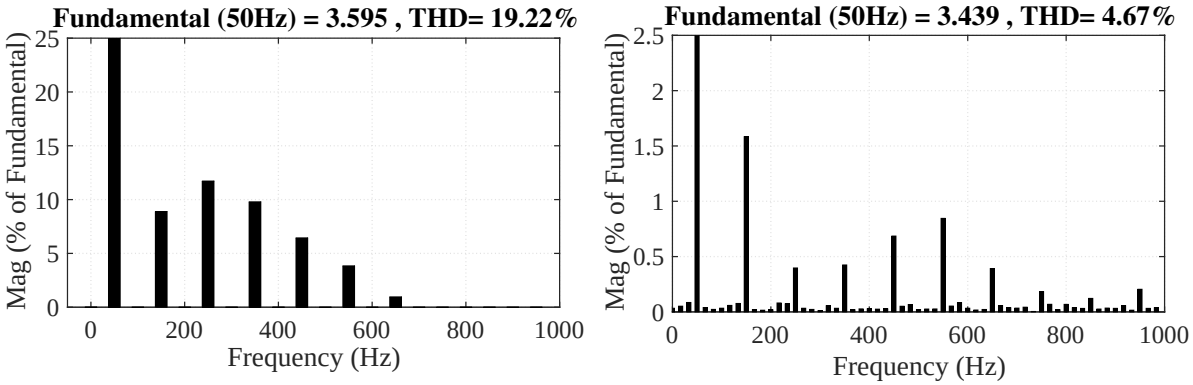


(a) Before compensation.

(b) After compensation.

Figure 6.33: THD in source current for phase $A$, before and after compensation.

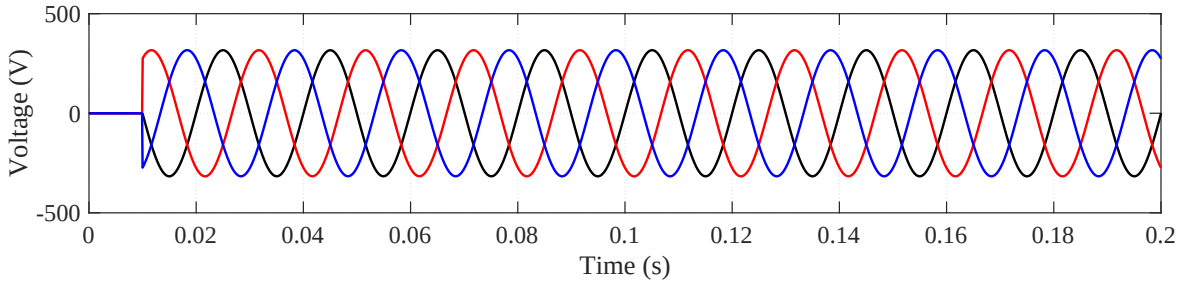


Figure 6.34: Positive sequence voltage detected by the positive sequence detector.

### 6.5.1 Discussion based on Case 5

The utility voltage, source currents and house currents can be seen in Figure 6.30 respectively. The effect of the increased source impedance can be seen in the utility voltage. The high frequency ripple currents are now responsible for high frequency ripple in the utility voltage.

The THD in the source current in phase $A$ after compensation is 4.67% (Figure 6.33), which is approximately 2-3% higher than the previous cases. The shunt APF is able to compensate and achieve sinusoidal source currents with approximately the same amount of high frequency ripples as in the previous cases.

The instantaneous active and reactive source power in Figure 6.32 have now a higher peak to peak ripple magnitude and oscillations. The positive sequence detector is able to detect the fundamental positive sequence component (Figure 6.34).

Chapter 7

# Conclusion

A simulation model for a three-phase, four-wire shunt APF using the instantaneous power theory as the control algorithm was implemented in MATLAB/Simulink studying the operation of the shunt APF under various conditions using load data from Skarpnes.

The shunt APF with a hysteresis current controller was able to almost instantaneously compensate for the harmonic currents, reactive power and neutral current during all five test cases.

- **Case 1** The source currents became sinusoidal and the THD was reduced below 5%. Neutral current and reactive power were successfully compensated and constant active power supplied by the source was achieved.
- **Case 2** Having to chose between sinusoidal source currents or constant powers, as both are not possible during distorted and/or unbalanced utility voltage. Choosing sinusoidal source currents, the harmonic currents were successfully compensated and the source current became sinusoidal, the THD was reduced below 5%. The average value of the instantaneous reactive power was compensated, but oscillations in both the active and reactive instantaneous powers appeared during the voltage disturbance. If the compensation goal was constant powers, the source currents could not remain sinusoidal and as a result the THD was above 10%.
- **Case 3** The residence was able to supply sinusoidal currents with a THD value below 5% and at unity power factor. If however, reactive power had to be exported, the control algorithm had to be slightly modified, so the shunt APF did not compensate for the average value of the instantaneous reactive power.
- **Case 4** Similar to Case 3, but under distorted and unbalanced utility voltage. The residence was able to supply sinusoidal currents with low distortion, but with the voltage disturbance the powers could no longer remain constant. If constant powers was the goal, the source currents could no longer remain sinusoidal. As in Case 3, the compensation algorithm had to be slightly modified depending on whether reactive power were to be exported or not.

- **Case 5** With an increased impedance, the high frequency ripple was responsible for high frequency ripple in the utility voltage waveforms. Nevertheless, sinusoidal source currents were achieved, but the instantaneous powers now had a higher peak to peak ripple magnitude.

The neutral current remains the same in all cases as in Case 1, because the zero-sequence powers were always compensated.

Based on this study, the simulations have shown that the shunt APF can be used in zero energy buildings for harmonic currents, reactive power and neutral current compensation. However, due to the low energy demand of a zero energy building, several buildings could be compensated with one shunt APF as the ripple stays approximately the same whether the load is one or five buildings.

## 7.1 Future Work

Based on the work done in this thesis, future work may include:

- Other control algorithms than the instantaneous power theory can be implemented and tested.
- Implementing different PWM techniques and design of a LC/LCL output filter in order to reduce the current ripples.
- Build an experimental setup and/or a hardware-in-the-loop model to study the effect of sampling frequency and physical limitation such as switching frequency etc.

# Bibliography


[1] J. Arrillaga and N. R. Watson, *Power system harmonics*. John Wiley & Sons, 2004.

[2] D. Hansen, "Ieee 519 misapplications—point of common coupling issues," in *Power and Energy Society General Meeting-Conversion and Delivery of Electrical Energy in the 21st Century, 2008 IEEE*. IEEE, 2008, pp. 1–3.

[3] H. Özkaya, "Parallel active filter design, control, and implementation," Ph.D. dissertation, Citeseer, 2007.

[4] ABB. Technical note: Reducing harmonics caused by variable speed drives. [Online]. Available: https://library.e.abb.com/public/afa9690deb15a092c125744f003cb018/TD2_Reducing_harmonics_EN_revD_LR.pdf

[5] IEEE Std 519-1992, "IEEE Recommended Practices and Requirements for Harmonic Control in Electrical Power Systems," 1992.

[6] ABB. (2017) Power quality filters. [Online]. Available: http://new.abb.com/high-voltage/capacitors/lv/power-quality-filters

[7] H. Akagi, E. H. Watanabe, and M. Aredes, *Instantaneous Power Theory and Applications to Power Conditioning*. John Wiley & Sons, 2007, vol. 31.

[8] Norges Forskningsråd. (2013-2017) Electricity usage in smart village skarpnes. [Online]. Available: https://www.forskningsradet.no/prosjektbanken/#!/project/226139/no

[9] P. Torcellini, S. Pless, M. Deru, and D. Crawley, "Zero energy buildings: a critical look at the definition," *National Renewable Energy Laboratory and Department of Energy, US*, 2006.

[10] C. Sankaran, *Power Quality*. CRC Press Inc, 2001, chapter 1, pages 12-34.

[11] J. Niitsoo, P. Taklaja, I. Palu, and J. Klüss, "Power quality issues concerning photovoltaic generation and electrical vehicle loads in distribution grids," *Smart Grid and Renewable Energy*, vol. 6, no. 06, p. 164, 2015.

[12] J. C. Smith, G. Hensley, and L. Ray, "Ieee recommended practice for monitoring electric power quality," *IEEE Std*, pp. 1159–1995, 1995.

[13] N. Shah, "Harmonics in power systems causes, effects and control," *Whitepaper design engineering low-voltage drives*, 2013.

[14] Y. Liu and G. Heydt, "Power system even harmonics and power quality indices," *Electric Power Components and Systems*, vol. 33, no. 8, pp. 833–844, 2005.

[15] C. L. Fortescue, "Method of symmetrical co-ordinates applied to the solution of polyphase networks," *Transactions of the American Institute of Electrical Engineers*, vol. 37, no. 2, pp. 1027–1140, 1918.

[16] M. H. Ali, *Wind energy systems: solutions for power quality and stabilization.* CRC Press, 2012, chapter 3, pages 71.

[17] E. Fuchs and M. A. Masoum, *Power quality in power systems and electrical machines.* Academic press, 2011.

[18] IEEE Std 1124-2003, "IEEE Guide for Analysis and Definition of DC Side Harmonic Performance of HVDC Transmission Systems," 2003.

[19] Y. Zhang, M.-C. Cheng, and P. Pillay, "Magnetic characteristics and excess eddy current losses," in *Industry Applications Society Annual Meeting, 2009. IAS 2009. IEEE.* IEEE, 2009, pp. 1–5.

[20] X. Li, W. Xu, and T. Ding, "Damped high passive filter–a new filtering scheme for multipulse rectifier systems," *IEEE Transactions on Power Delivery*, 2016.

[21] M. El-Habrouk, M. Darwish, and P. Mehta, "Active power filters: A review," *IEE Proceedings-Electric Power Applications*, vol. 147, no. 5, pp. 403–413, 2000.

[22] M. H. Rashid, *Power electronics handbook: devices, circuits and applications.* Academic press, 2010.

[23] H. Fujita and H. Akagi, "The unified power quality conditioner: the integration of series-and shunt-active filters," *IEEE transactions on power electronics*, vol. 13, no. 2, pp. 315–322, 1998.

[24] M. Routimo, M. Salo, and H. Tuusa, "Comparison of voltage-source and current-source shunt active power filters," *IEEE Transactions on Power Electronics*, vol. 22, no. 2, pp. 636–643, 2007.

[25] A. VanderMeulen and J. Maurin, "Current source inverter vs. voltage source inverter topology," *Technical Data TD02004004E, Eaton*, 2010.

[26] C. A. Quinn and N. Mohan, "Active filtering of harmonic currents in three-phase, four-wire systems with three-phase and single-phase nonlinear loads," in *Applied Power Electronics Conference and Exposition, 1992. APEC'92. Conference Proceedings 1992., Seventh Annual.* IEEE, 1992, pp. 829–836.

[27] Emerson Industrial Automation. Harmonic distortion and variable frequency drives. [Online]. Available: http://www.emersonindustrial.com/en-EN/documentcenter/ControlTechniques/Brochures/CTA/HVACR/WHP_HarmonicMitigation.pdf

[28] T. S. Key and J.-S. Lai, "Comparison of standards and power supply design options for limiting harmonic distortion in power systems," *IEEE Transactions on Industry Applications*, vol. 29, no. 4, pp. 688–695, 1993.

[29] A. Emanuel, "Apparent and reactive powers in three-phase systems: In search of a physical meaning and a better resolution," *International Transactions on Electrical Energy Systems*, vol. 3, no. 1, pp. 7–14, 1993.

[30] Z. Hanzelka and J. Milanovic, "Power electronics in smart electrical energy networks," 2008.

[31] C. Budeanu, "Puissances réactives et fictives. institut romain de i'energte. bucharest," *Romania*, 1927.

[32] L. S. Czarnecki, "What is wrong with the budeanu concept of reactive and distortion power and why it should be abandoned," *IEEE Transactions on Instrumentation and measurement*, vol. 1001, no. 3, pp. 834–837, 1987.

[33] S. Fryze, "Wirk-, blind-und scheinleistung in elektrischen stromkreisen mit nichtsinusförmigem verlauf von strom und spannung," *Elektrotechnische Zeitschrift*, vol. 25, no. 569-599, p. 33, 1932.

[34] H. Akagi, Y. Kanazawa, and A. Nabae, "Generalized theory of the instantaneous reactive power in three-phase circuits," in *IPEC*, vol. 83. Tokyo, 1983, pp. 1375–1386.

[35] J. L. Afonso, M. S. Freitas, and J. S. Martins, "pq theory power components calculations," in *Industrial Electronics, 2003. ISIE'03. 2003 IEEE International Symposium on*, vol. 1. IEEE, 2003, pp. 385–390.

[36] V. Mahajan, P. Agarwal, and H. O. Gupta, "Simulation of instantaneous power theory for active power filter," in *Power, Control and Embedded Systems (ICPCES), 2012 2nd International Conference on*. IEEE, 2012, pp. 1–4.

[37] Y. S. Prabhu, A. Dharme, and D. Talange, "A three phase shunt active power filter based on instantaneous reactive power theory," in *India Conference (INDICON), 2014 Annual IEEE*. IEEE, 2014, pp. 1–5.

[38] B. Pragathi and G. Bharathi, "Control of shunt active filter based on instantaneous power theory," in *International Journal of Engineering Research and Technology*, vol. 1, no. 6 (August-2012). ESRSA Publications, 2012.

[39] M. Aredes, J. Hafner, and K. Heumann, "Three-phase four-wire shunt active filter control strategies," *IEEE Transactions on Power Electronics*, vol. 12, no. 2, pp. 311–318, 1997.

[40] H. Usman, H. Hizam, and M. A. M. Radzi, "Simulation of single-phase shunt active power filter with fuzzy logic controller for power quality improvement," in *Clean Energy and Technology (CEAT), 2013 IEEE Conference on.* IEEE, 2013, pp. 353–357.

[41] C.-Y. Hsu and H.-Y. Wu, "A new single-phase active power filter with reduced energy-storage capacity," *IEE Proceedings-Electric Power Applications*, vol. 143, no. 1, pp. 25–30, 1996.

[42] M. Kumar, "Power quality in power distribution systems," 2014.

[43] K. Young and R. Dougal, "Srf-pll with dynamic center frequency for improved phase detection," in *Clean Electrical Power, 2009 International Conference on.* IEEE, 2009, pp. 212–216.

[44] V. Kaura and V. Blasko, "Operation of a phase locked loop system under distorted utility conditions," *IEEE Transactions on Industry applications*, vol. 33, no. 1, pp. 58–63, 1997.

[45] M. Kale and E. Ozdemir, "An adaptive hysteresis band current controller for shunt active power filter," *Electric power systems research*, vol. 73, no. 2, pp. 113–119, 2005.

[46] H. Vahedi, A. Sheikholeslami, M. Tavakoli Bina, and M. Vahedi, "Review and simulation of fixed and adaptive hysteresis current control considering switching losses and high-frequency harmonics," *Advances in Power Electronics, Hindawi Publishing Corporation*, vol. 2011, 2011.

[47] C. Rejil, M. Anzari, and K. R. Arun, "Design and simulation of three phase shunt active power filter using srf theory," *Advance in Electronic and Electric Engineering*, vol. 3, no. 6, pp. 651–660, 2013.

[48] Y. Tang, P. C. Loh, P. Wang, F. H. Choo, F. Gao, and F. Blaabjerg, "Generalized design of high performance shunt active power filter with output lcl filter," *IEEE Transactions on Industrial Electronics*, vol. 59, no. 3, pp. 1443–1452, 2012.

[49] S. K. Jain and P. Agarwal, "Design simulation and experimental investigations, on a shunt active power filter for harmonics, and reactive power compensation," *Electric Power Components and Systems*, vol. 31, no. 7, pp. 671–692, 2003.

[50] T. M. Undeland, W. P. Robbins, and N. Mohan, "Power electronics: converters, applications, and design," 2003.

# Appendices

Appendix A

# Data Acquisition

Figure A.1 gives an overview of the Elspec and ABB data acquisition system installed at Skarpnes.

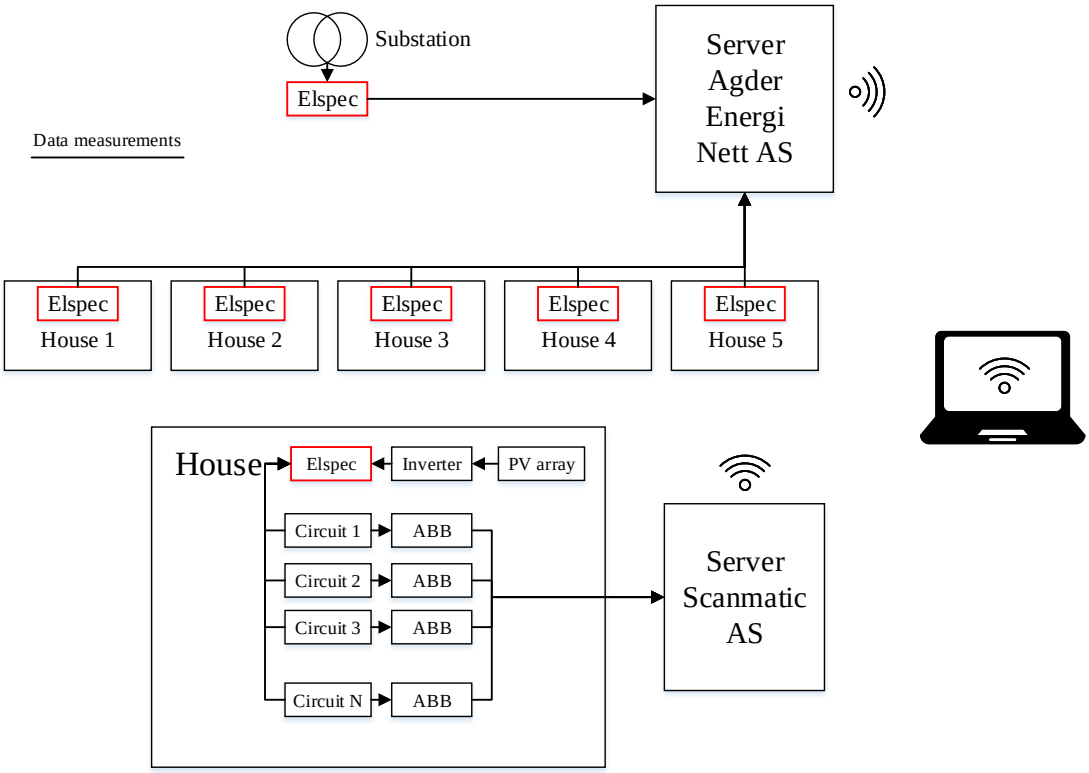


Figure A.1: System overview of data acquisition.

All five houses and the local substation have an Elspec G4420 Blacbox Power Quality Analyser installed. The device measures the current and voltage waveforms at a very high resolution, based on those measurements several parameters such as total harmonic distortion, rms values, real-time waveforms, active and reactive power can be obtained

and studied. All these parameters and more are available and can be viewed in the Elspec Investigator software. Figure A.2 shows the user interface for the Elspec Investigator.

Due to the high cost of the Elspec equipment, each circuit inside each house is not equipped with a power analyser from Elspec. Instead cheaper measurement devices from ABB, installed and managed by Scanmatic AS are used, but measures at a much lower resolution. Thus looking at waveforms and harmonics are only possible with the measurements from the Elspec equipment. However, the measurements from the ABB equipment may be useful to see if any particular appliances are causing any problems.

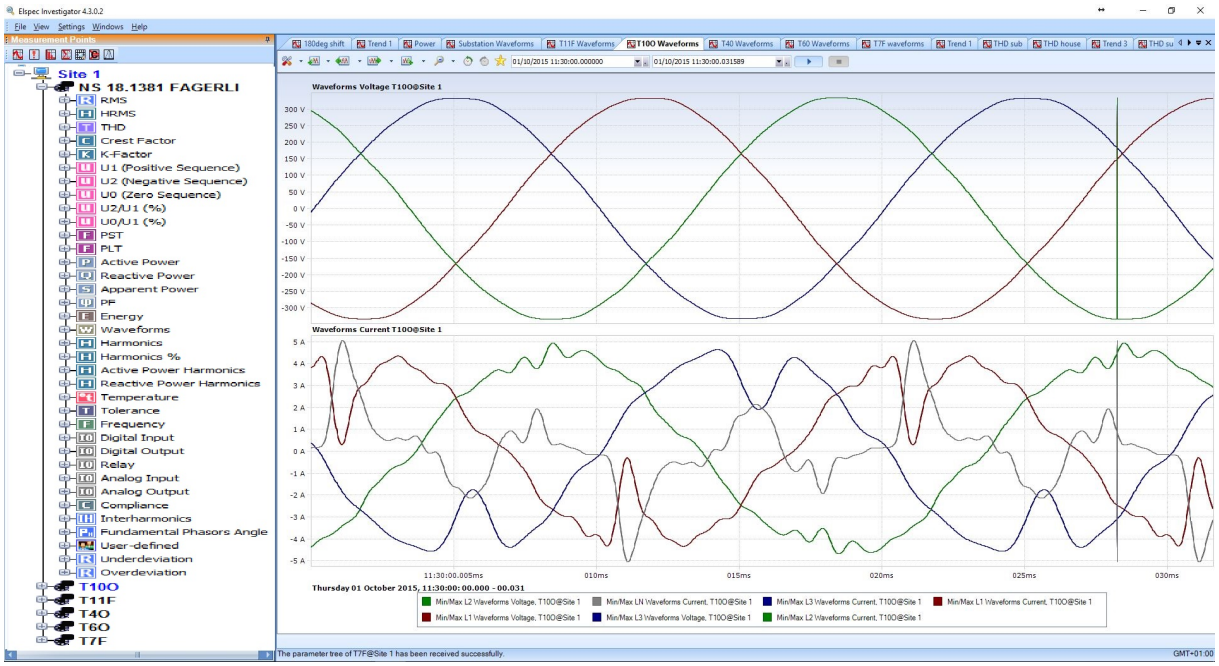


Figure A.2: Elspec Investigator interface.

Appendix B

# Load Parameters

Load parameters exracted from Elspec Investigator for Skarpnes used in the Simulation.

```
%%%%% Load parameters used in simulation Case 1,2 and 5 %%%%%

%%parameters
clear all;
clc;
%%%%%%%%%%%%%%%%%%%%%%%%%%%%%%%%%%%%%%%%
% Phase A %
L1_fund = 3.5949;
L1_h3   = L1_fund*8.885/100;
L1_h5   = L1_fund*11.724/100;
L1_h7   = L1_fund*9.794/100;
L1_h9   = L1_fund*6.443/100;
L1_h11  = L1_fund*3.842/100;
L1_h13  = L1_fund*0.960/100;
L1_h15  = L1_fund*0/100;

% Phase shifts (deg) %
Theta1_fund = -30;
Theta1_h3   = -30;
Theta1_h5   = -30;
Theta1_h7   = -30;
Theta1_h9   = -30;
Theta1_h11  = -30;
Theta1_h13  = -30;
Theta1_h15  = -30;

%%%%%%%%%%%%%%%%%%%%%%%%%%%%%%%%%%%%%%%%
% Phase B %
L2_fund = 2.5977;
L2_h3   = L2_fund*16.170/100;
L2_h5   = L2_fund*11.356/100;
L2_h7   = L2_fund*9.445/100;
L2_h9   = L2_fund*8.085/100;
L2_h11  = L2_fund*5.639/100;
```

```
L2_h13  = L2_fund*4.699/100;
L2_h15  = L2_fund*0/100;

% Phase shifts (deg) %
Theta2_fund = -120-30;
Theta2_h3   = -120-30;
Theta2_h5   = -120-30;
Theta2_h7   = -120-30;
Theta2_h9   = -120-30;
Theta2_h11  = -120-30;
Theta2_h13  = -120-30;
Theta2_h15  = -120-30;


%%%%%%%%%%%%%%%%%%%%%%%%%%%%%%%%%%%%%%
% Phase C %
L3_fund = 4.2711;
L3_h3   = L3_fund*13.837/100;
L3_h5   = L3_fund*6.183/100;
L3_h7   = L3_fund*8.574/100;
L3_h9   = L3_fund*6.443/100;
L3_h11  = L3_fund*4.464/100;
L3_h13  = L3_fund*2.858/100;
L3_h15  = L3_fund*2.556/100;



% Phase shifts (deg) %
Theta3_fund = 120-30;
Theta3_h3   = 120-30;
Theta3_h5   = 120-30;
Theta3_h7   = 120-30;
Theta3_h9   = 120-30;
Theta3_h11  = 120-30;
Theta3_h13  = 120-30;
Theta3_h15  = 120-30;

% Hysteresis Band PWM Controller %
H_band  =  .2;
H_upper =   H_band/2;%H_band/2;
H_lower =  -H_band/2;%H_band/2;
```

```
%%%% Load parameters used in simulation Case 3 and 4 %%%%


%%parameters
clear all;
clc;
%%%%%%%%%%%%%%%%%%%%%%%%%%%%%%%%%%%%%%
% Phase A %
L1_fund = -7.91;
L1_h3   = L1_fund*2.489/100;
```

```
L1_h5   = L1_fund*4.141/100;
L1_h7   = L1_fund*2.226/100;
L1_h9   = L1_fund*1.543/100;
L1_h11  = L1_fund*0.309/100;
L1_h13  = L1_fund*0.873/100;
L1_h15  = L1_fund*0/100;

% Phase shifts (deg) %
Theta1_fund = -30;
Theta1_h3   = -30;
Theta1_h5   = -30;
Theta1_h7   = -30;
Theta1_h9   = -30;
Theta1_h11  = -30;
Theta1_h13  = -30;
Theta1_h15  = -30;

%%%%%%%%%%%%%%%%%%%%%%%%%%%%%%%%%%%%%%%%
% Phase B %
L2_fund = -7.6760;
L2_h3   = L2_fund*6.490/100;
L2_h5   = L2_fund*7.552/100;
L2_h7   = L2_fund*5.123/100;
L2_h9   = L2_fund*3.773/100;
L2_h11  = L2_fund*1.742/100;
L2_h13  = L2_fund*1.025/100;
L2_h15  = L2_fund*0/100;

% Phase shifts (deg) %
Theta2_fund = -120-30;
Theta2_h3   = -120-30;
Theta2_h5   = -120-30;
Theta2_h7   = -120-30;
Theta2_h9   = -120-30;
Theta2_h11  = -120-30;
Theta2_h13  = -120-30;
Theta2_h15  = -120-30;


%%%%%%%%%%%%%%%%%%%%%%%%%%%%%%%%%%%%%%%%
% Phase C %
L3_fund = -7.1477;
L3_h3   = L3_fund*4.771/100;
L3_h5   = L3_fund*4.855/100;
L3_h7   = L3_fund*3.181/100;
L3_h9   = L3_fund*1.908/100;
L3_h11  = L3_fund*0.711/100;
L3_h13  = L3_fund*0.300/100;
L3_h15  = L3_fund*0/100;



% Phase shifts (deg) %
```

```
64 Theta3_fund = 120-30;
65 Theta3_h3   = 120-30;
66 Theta3_h5   = 120-30;
67 Theta3_h7   = 120-30;
68 Theta3_h9   = 120-30;
69 Theta3_h11  = 120-30;
70 Theta3_h13  = 120-30;
71 Theta3_h15  = 120-30;
72
73 % Hysteresis Band PWM Controller %
74 H_band  =  .2;
75 H_upper =   H_band/2;%H_band/2;
76 H_lower =  -H_band/2;%H_band/2;
```

Appendix C

# Simulation Results

### Case 1

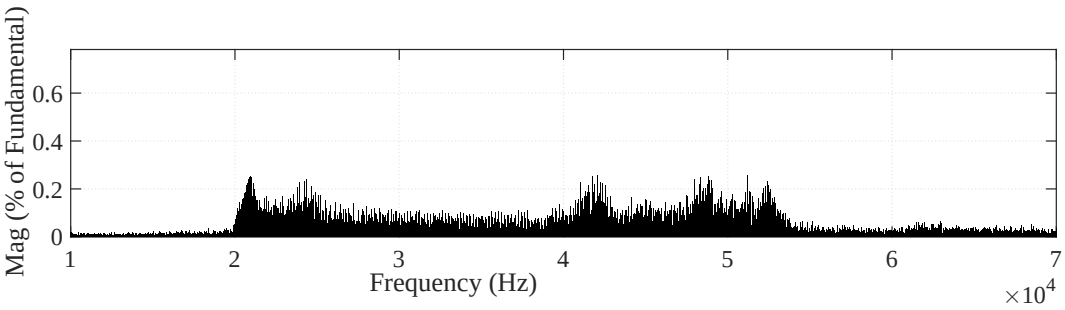


Figure C.1: High frequency spectrum of the source current.

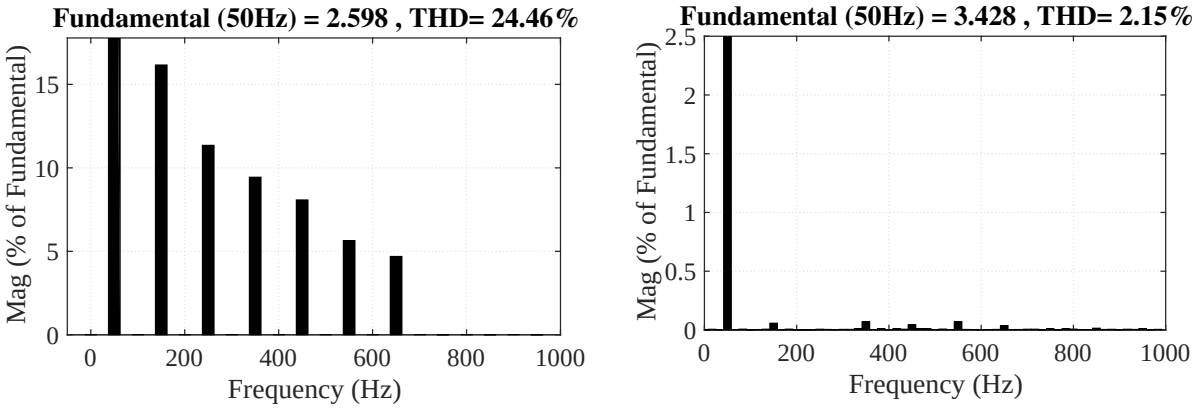


(a) THD before compensation.

(b) THD after compensation.

Figure C.2: THD in the source current in phase B, before and after compensation.

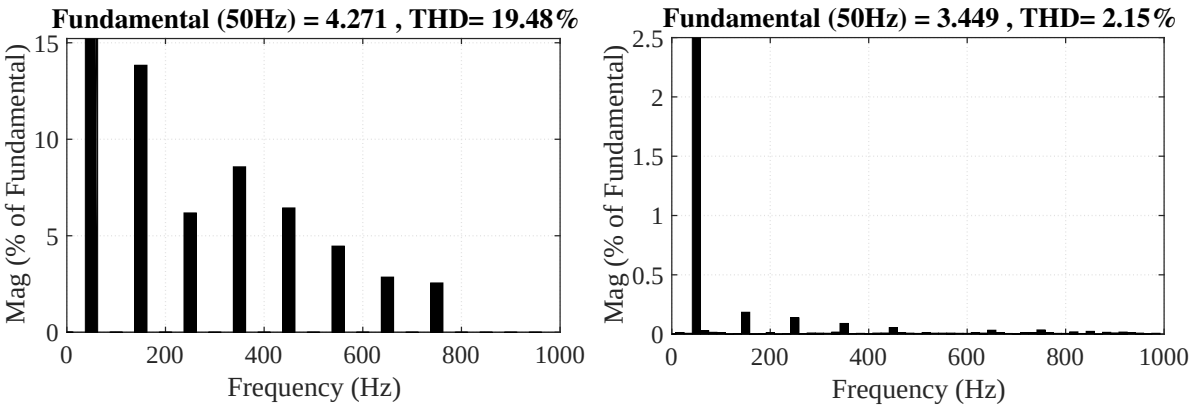


(a) THD before compensation.

(b) THD after compensation.

Figure C.3: THD in the source current in phase C, before and after compensation.

**Case 2**

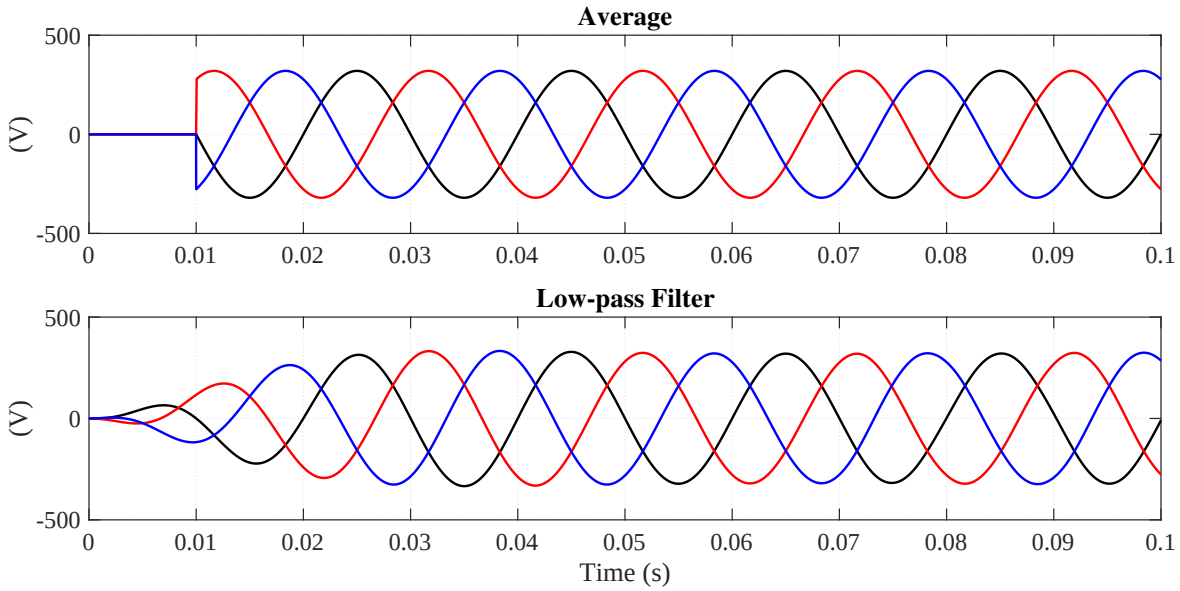


Figure C.4: Positive sequence detector using moving average and low-pass filter.

**Case 3**

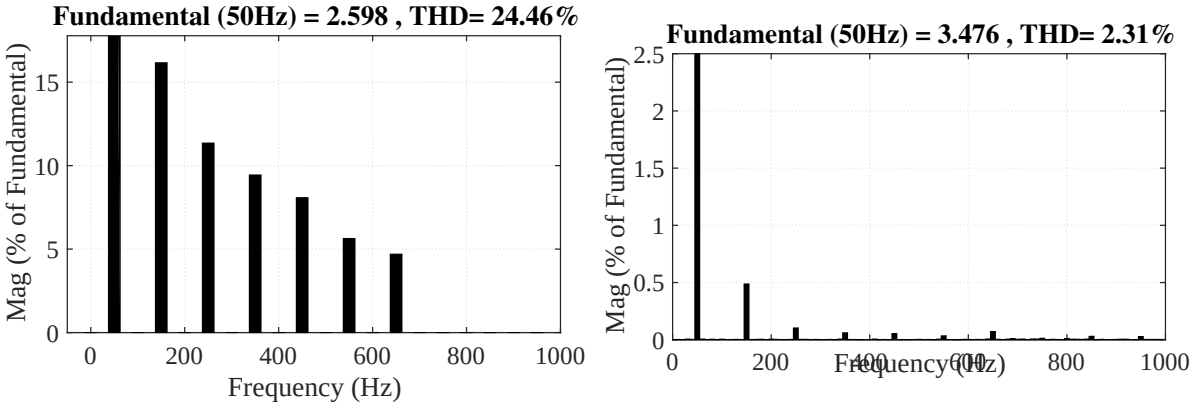


(a) Before compensation. (b) After compensation.

Figure C.5: THD in the source current in phase $B$, before and after compensation.

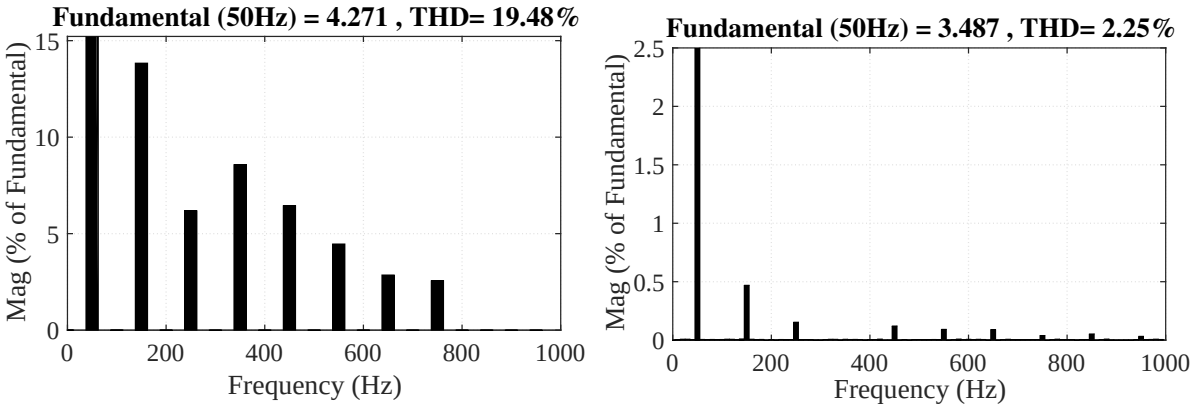


(a) Before compensation. (b) After compensation.

Figure C.6: THD in the source current in phase $C$, before and after compensation.

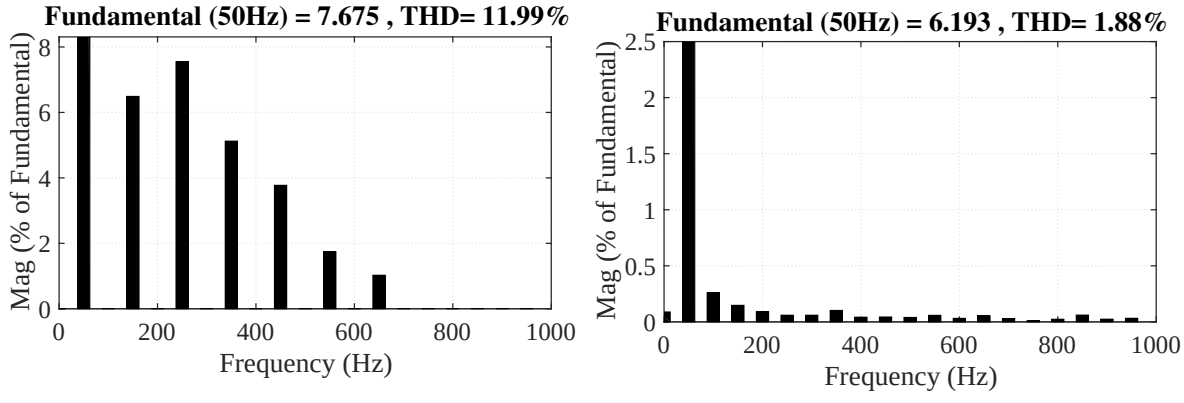


(a) Before compensation. (b) After compensation.

Figure C.7: THD in the source current in phase $B$, before and after compensation.

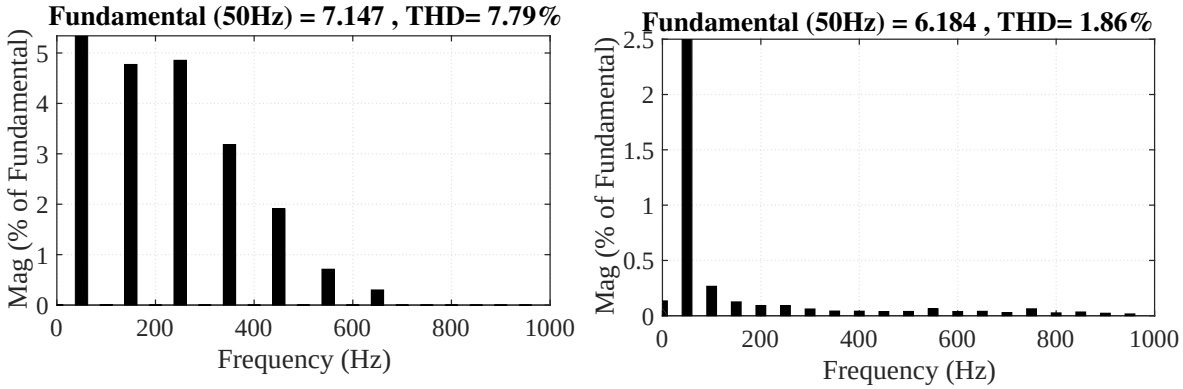


(a) Before compensation.

(b) After compensation.

Figure C.8: THD in the source current in phase $C$, before and after compensation.

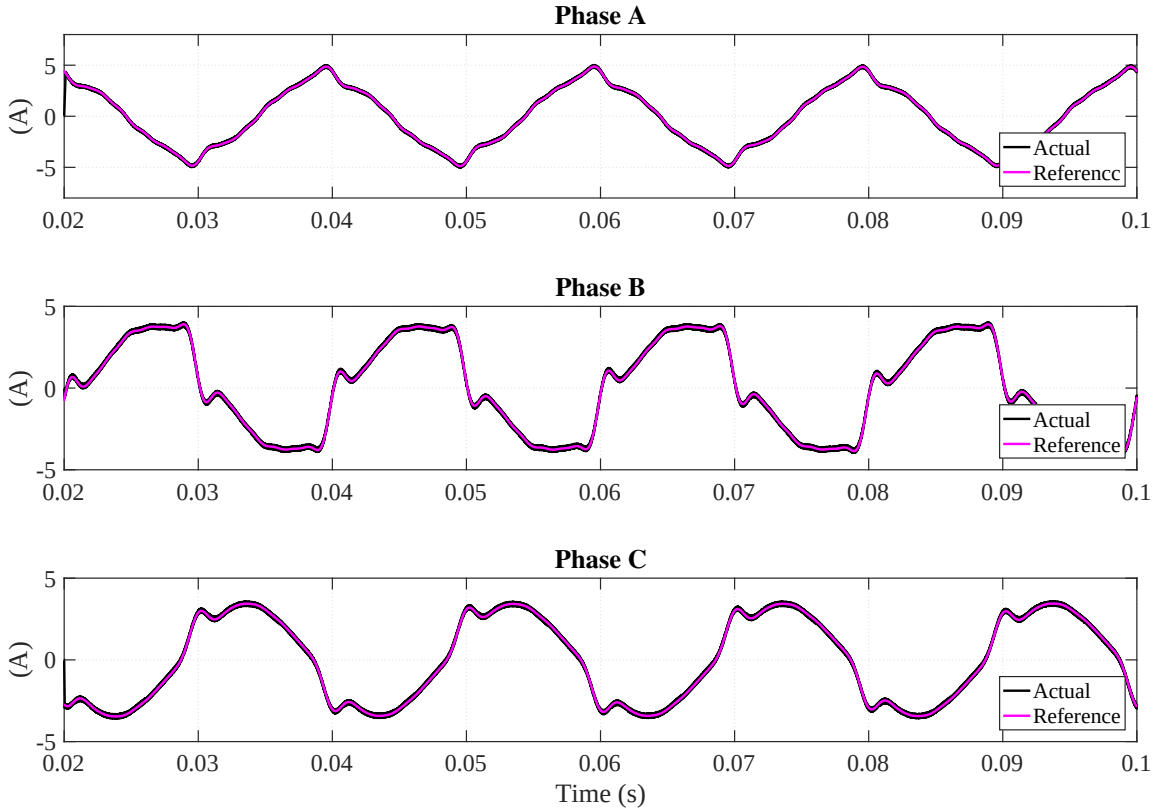


Figure C.9: Actual and reference currents from the shunt APF for Case 3.